

Selected magnetic and gravity anomalies in the Eastern
Transvaal and their possible relation to the
Rustenburg Layered Suite.

by

MARIA PETRONELLA BLOM

Submitted in partial fulfilment of the requirements
for the degree of

MAGISTER SCIENTIAE

in the Faculty of Science,
University of Pretoria, Pretoria.

May, 1988

ABSTRACT

The total field aeromagnetic map of the eastern Transvaal reveals two major magnetic anomalies situated to the east of the known Bushveld Complex perimeter, namely the Wanhoop and Mooiland anomalies. The Bouguer gravity anomaly map of the same area depicts positive anomalies coinciding with the locality of the Wanhoop and Mooiland magnetic anomalies. The wider extent of the gravity anomalies however indicates that the dense rock units associated with the magnetic rock units causing the Wanhoop and Mooiland anomalies are also present to the south of the magnetic rock units.

A quantitative interpretation of the Wanhoop anomaly indicates that it is caused by a combination of a major westward dipping sheet-like unit, 200-500 metres deep and approximately 1 000 metres thick and a thinner sheet which underlies the former one. Results from an investigation of the palaeomagnetic properties of the gabbros, norites and magnetite gabbros of the Rustenburg Layered Suite offered the possibility of correlating the magnetic bodies associated with the Wanhoop anomaly with units in the Rustenburg Layered Suite. Based on this correlation the Wanhoop magnetic bodies possibly cooled through its Curie point at the same time as the main zone of the Rustenburg Layered Suite, thereby attaining the direction of magnetization of the reversed magnetic polarity zone, i.e. declination = 30° and inclination = 58° . The intensity of magnetization of the Wanhoop bodies is of the order of $4\,000 \times 10^{-3} \text{ Am}^{-1}$ which is many times greater than the average magnetization of locally occurring main zone rocks; and is in fact as large as that of the black gabbro of the main zone. The non-magnetic high density rocks inferred from the gravity anomaly and which extend beyond the Wanhoop magnetic bodies towards Dullstroom, is approximately 1 000 metres deep and have a maximum thickness of 500 metres, assuming a density of $3\,100 \text{ kg/m}^3$ against the $2\,780 \text{ kg/m}^3$ of the surrounding rocks of the Transvaal Sequence.

The Mooiland magnetic anomaly is caused by a normally magnetized, sill-like body, 1 400 metres deep, which has a susceptibility of 0,25 SI units and a thickness of approximately 500 metres. The high susceptibility contrast used in the two-dimensional magnetic modelling process is indicative of a high percentage magnetite present in the body, similar to that of the upper zone of the Rustenburg Layered Suite. Another similarity between the Mooiland body and the Rustenburg Layered Suite is that according to the best fitting geophysical models only the upper unit of the gravitational model is magnetic. The gravitational model consists of a 2 500 metres thick sill-like body, dipping to the south, which has a density contrast of 410 kg/m³ with respect to the Archaean granites.

SAMEVATTING

Die totale veld lugmagnetiese kaart van die Oos-Transvaal vertoon twee prominente magnetiese anomalieë, die Wanhoop en Mooiland anomalieë, wat oos van die rand van die Bosveldkompleks voorkom. Die Bougueranomaliëkaart van dieselfde area toon positiewe anomalieë wat ooreenstem met die posisie van die Wanhoop en Mooiland magnetiese anomalieë. Die wyer strekking van die gravitasie anomalieë dui egter daarop dat die hoë digtheid gesteentes geassosieer met die Wanhoop en Mooiland magnetiese anomalieë ook verder suid van die magnetiese gesteentes voorkom.

'n Kwantitatiewe interpretasie van die Wanhoop anomalie dui daarop dat dit veroorsaak word deur 'n groot plaatvormige liggaam wat weswaarts hel; 200-500 meter diep en ongeveer 1 000 meter dik, wat 'n dunner plaat oorlê. Resultate van 'n paleomagnetiese ondersoek op die gabbro's, noriete en magnetietgabbro's van die Gelaagde Suite Rustenburg het die moontlikheid daargestel om die magnetiese liggame geassosieer met die Wanhoop anomalie te korreleer met eenhede in die Gelaagde Suite Rustenburg. Gebaseer op hierdie korrelasie het die Wanhoop magnetiese liggame waarskynlik afgekoel deur die Curie temperatuur van die gesteentes, op dieselfde tydstep as die hoofone van die Gelaagde Suite Rustenburg, om sodoende die rigting van magnetisasie van die omgekeerde polariteitsone te verkry, nl. deklinasie = 30° en inklinasie = 58° . Die intensiteit van magnetisasie van die Wanhoop liggame is in die orde van $4\,000 \times 10^{-3} \text{ Am}^{-1}$, wat baie hoër is as die gemiddelde magnetisasie van hoofone gesteentes wat plaaslik voorkom, maar wel so hoog is soos die van die swart gabbro's van die hoofone. Die nie-magnetiese, hoë digtheid gesteentes afgelei uit die gravitasie anomalie, wat verby die Wanhoop liggame uitstrek in die rigting van Dullstroom, is ongeveer 1 000 meter diep en 500 meter dik indien 'n digtheid van $3\,100 \text{ kg/m}^3$ aanvaar word in teenstelling met $2\,780 \text{ kg/m}^3$ van die omliggende gesteentes van die Opeenvolging Transvaal.

Die Mooiland magnetiese anomalie word veroorsaak deur 'n normaal gemagnetiseerde, plaatvormige liggaam; 1 400 meter diep, 'n susseptibiliteit van 0,25 SI eenhede en 'n dikte van ongeveer 500 meter. Die hoë susseptibiliteitskontras wat gebruik is in die twee-dimensionele magnetiese modelleringsproses, dui op 'n hoë persentasie magnetiet wat in die liggaam teenwoordig is, soortgelyk aan die van die bosone van die Gelaagde Suite Rustenburg. 'n Verdere ooreenkoms tussen die Mooiland liggaam en die Gelaagde Suite Rustenburg is dat volgens die geofisiese modelle wat die beste passing gegee het, is slegs die boonste eenheid van die gravitasie-model magneties. Die gravitasie-model bestaan uit 'n plaatvormige liggaam wat 2 500 meter dik is, suidwaarts hel en 'n digtheidskontras van 410 kg/m^3 met betrekking tot die Argeiese graniet bereik.

CONTENTS

	<u>PAGE</u>
1. INTRODUCTION	1
2. GEOLOGY	3
2.1 Archaean rock types	3
2.2 Transvaal Sequence	3
2.3 Intrusives	5
3. PHYSICAL PROPERTIES OF THE DIFFERENT ROCK TYPES	8
3.1 Densities	8
3.2 Magnetic properties	9
3.2.1 Magnetization of the Rustenburg Layered Suite	13
3.2.1.1 Field and laboratory procedures	13
3.2.1.2 Treatment and presentation of data	16
3.2.1.3 Interpretation and discussion of data	18
4. QUALITATIVE INTERPRETATION	55
4.1 Total field aeromagnetic map	55
4.2 The gravity anomaly maps	57
4.3 The Wanhoop anomaly	62
4.4 The Mooiland anomaly	68
5. QUANTITATIVE INTERPRETATION	71
5.1 The Wanhoop anomaly	71
5.2 The Mooiland anomaly	81
6. DISCUSSION AND CONCLUSIONS	89
ACKNOWLEDGEMENTS	92
REFERENCES	93

LIST OF TABLES AND FIGURES IN THE TEXT

<u>TABLES</u>	<u>PAGE</u>
Table 3.1 Average densities for all the major rock formations in the area	8
Table 3.2 Summary of magnetic measurements on rock samples	19
Table 3.3 Magnetization directions of sites after alternating field demagnetization	23
Table 3.4 Summary of induced and remanent intensity of magne- tization for each subzone of the Rustenburg Layered Suite	47
Table 3.5 Magnetization directions of sites in the reversed polarity zone (MPZB)	49
Table 3.6 Magnetization directions of sites in the normal polarity zone MPZC/1 (subzone C of the main zone)	49
Table 3.7 Magnetization directions of sites in the normal polarity zone MPZC/2 (upper zone)	51
Table 4.1 Flight specifications for the aeromagnetic surveys of the area between 29°-31° longitude and 24°-26° latitude	56
 <u>FIGURES</u>	
Fig. 2.1 Simplified geological map of the eastern Transvaal	4

	<u>PAGE</u>
Fig. 3.1	Simplified lithostratigraphic column of the Rustenburg Layered Suite in the eastern Bushveld Complex, showing the magnetic polarity zones and sampling sites 11
Fig. 3.2	Histogram plots of NRM intensities of specimens from the (a) critical zone, (b) main zone and (c) upper zone 12
Fig. 3.3	Geological map of the Draaikraal-Roossenekal area showing the location of the sampling sites and their stratigraphical positions 14
Fig. 3.4	Stereographic projection (equal angle) of NRM directions of sites 20
Fig. 3.5	Intensities of magnetization along the lithostratigraphic column of the Rustenburg Layered Suite 21
Fig. 3.6	Stereographic projection of magnetization directions of sites after bulk alternating field demagnetization 24
Fig. 3.7	Königsberger ratios of sites calculated before (Q_1) and after (Q_2) bulk alternating field demagnetization 25
Fig. 3.8	Anisotropy data along the lithostratigraphic column of the Rustenburg Layered Suite 26
Fig. 3.9	(a) Sample and site mean directions, and (b) histograms of the logarithmic susceptibility and intensity of magnetization after bulk AF demagnetization of sites B, D, F and K situated in subzone A of the main zone ... 28

	<u>PAGE</u>
Fig. 3.10	Magnetic anisotropy data for site F 29
Fig. 3.11	Magnetic anisotropy data for site D 30
Fig. 3.12	Magnetic anisotropy data for site K 31
Fig. 3.13	(a) Stereographic projections, (b) intensity decay curve and (c+d) Zijdeveld plots for specimen E3b submitted to AF demagnetization 33
Fig. 3.14	(a) Sample and site mean directions, and (b) histograms of the logarithmic susceptibility and intensity of magnetization after bulk AF demagnetization of sites C, E and I situated in subzone C of the main zone 34
Fig. 3.15	Magnetic anisotropy data for site C 35
Fig. 3.16	Magnetic anisotropy data for site I 36
Fig. 3.17	(a) Stereographic projections, (b) intensity decay curve and (c+d) Zijdeveld plots for specimen N1b submitted to AF demagnetization 38
Fig. 3.18	Magnetic anisotropy data for site H 39
Fig. 3.19	(a) Stereographic projections, (b) intensity decay curve and (c+d) Zijdeveld plots for specimen M6c submitted to AF demagnetization 40

Fig. 3.20	(a) Stereographic projections, (b) intensity decay curve and (c+d) Zijdeveld plots for specimen M2c submitted to thermal demagnetization	41
Fig. 3.21	(a) Sample and site mean directions, and (b) histograms of the logarithmic susceptibility and intensity of magnetization after bulk AF demagnetization of sites G, L and N situated in subzone B of the upper zone	42
Fig. 3.22	Magnetic anisotropy data for site G	43
Fig. 3.23	(a) Sample and site mean directions, and (b) histograms of the logarithmic susceptibility and intensity of magnetization after bulk AF demagnetization of site J situated in subzone C of the upper zone	45
Fig. 3.24	Magnetic anisotropy data for site J	46
Fig. 3.25	Stereographic projection of magnetization directions of sites in the reversed polarity zone (MPZB) in the main zone of the Rustenburg Layered Suite	48
Fig. 3.26	Stereographic projection of magnetization directions of sites in the normal polarity zone MPZC/1 (subzone C of the main zone) of the Rustenburg Layered Suite	50
Fig. 3.27	Stereographic projection of magnetization directions of sites in the normal polarity zone MPZC/2 (upper zone) of the Rustenburg Layered Suite	52

	<u>PAGE</u>
Fig. 4.1	Locality map of the aeromagnetic surveys used in the compilation of the colour coded aeromagnetic map of the eastern Transvaal 56
Fig. 4.2	Location map of the Dullstroom-Lydenburg area showing the outline of the Wanhoop magnetic anomaly and the positions of the magnetic profiles 58
Fig. 4.3	Location map of the Mooiland magnetic anomaly showing the outline of the anomaly and the position of the magnetic profile 59
Fig. 4.4	Colour coded Bouguer gravity anomaly map of the area between latitudes 25°S and 26°S and longitudes 30°E and 31°E 61
Fig. 4.5	Ground magnetic profile from the Wanhoop area 63
Fig. 4.6	Regional Bouguer anomaly map of the area showing the station locations and the positions of the gravity profiles 64
Fig. 4.7	Gravity station positions from the detailed gravity survey across the Wanhoop body 65
Fig. 4.8	Two-dimensional terrain corrections for three selected gravity stations situated in areas of severe topographical relief 67

	<u>PAGE</u>
Fig. 4.9	Terrain corrected Bouguer anomaly map superimposed on a simplified geological map, showing the outline of the Wanhoop magnetic anomaly and the position of the gravity profile 69
Fig. 5.1	Digital aeromagnetic data from the Barberton - Pilgrim's Rest survey. The shaded area on each flight-line indicates the position of the Wanhoop negative magnetic anomaly 72
Fig. 5.2	Log-energy spectrum of flight-line 2280 from the Barberton - Pilgrim's Rest survey 73
Fig. 5.3	Two-dimensional magnetic modelling of profiles AA', BB', CC', and DD' across the Wanhoop magnetic anomaly. The contact between the Rustenburg Layered Suite and the Transvaal Sequence is indicated on each profile 75
Fig. 5.4	Aerial extent of the Wanhoop magnetic bodies as determined from two-dimensional modelling 77
Fig. 5.5	Two-dimensional gravity and magnetic modelling of profile XX' across the Wanhoop bodies 78
Fig. 5.6	Two-dimensional gravity modelling of profile BB' across the major Wanhoop body, using different intensities of magnetization and body shapes 80
Fig. 5.7	Two-dimensional magnetic modelling of profile AA' across the Mooiland magnetic anomaly 82

Fig. 5.8	Station complete Bouguer anomaly and true complete Bouguer anomaly (on the reference plane) along profiles (a) YY' and (b) XX' on the two-dimensional topographical surface in the Mooiland area	85
Fig. 5.9	Two-dimensional modelling of the residual gravity anomalies along profiles (a + b) XX' and (c) YY' across the Mooiland gravity anomaly	86

MAPS IN FOLDER

Map 1	Colour coded aeromagnetic map of the eastern Transvaal between latitudes 24°S and 26°S and longitudes 29°E and 31°E.
Map 2	Simplified geological map of the eastern Transvaal (overlay).
Map 3	Isostatic gravity anomaly map of the eastern Transvaal (overlay).

1. INTRODUCTION

Satellite intrusions of sill-, dyke- and plug-like mafic and ultramafic Bushveld rocks outside the known perimeter of the Bushveld Complex have been mentioned in the literature by amongst others Coertze (1969), Sharpe (1982) and Walraven (1987). Similar intrusions are also known to exist in the vicinity of other layered intrusions e.g. the Great Dyke in Zimbabwe (Robertson and Van Breemen, 1969) and the Sudbury Basin in Ontario, Canada (Morris, 1982).

Geophysical surveys across the Bushveld Complex have been conducted for many years. These include regional gravity surveys, ground and aeromagnetic surveys, palaeomagnetic studies, deep DC resistivity soundings and seismic reflection studies (Hattingh, 1980, 1983; Molyneux and Klinkert, 1978; Meyer and De Beer, 1987; De Beer, Meyer and Hattingh, 1987; Du Plessis and Levitt, 1987). The aim of these surveys was to gain more information on the structural relationships of the Bushveld Complex.

A study of the aeromagnetic and gravity data of the eastern Transvaal revealed a significant negative magnetic anomaly coinciding with an aerielly larger gravity high that is situated to the east of the Bushveld Complex margin. In view of the nearness of these anomalies to the Rustenburg Layered Suite, it was tempting to speculate on the possibility that the body relates (compositionally or in terms of age) to one of the known zones of the Rustenburg Layered Suite. The presence of another gravity and magnetic anomaly in the Nelspruit District, which cuts across the strike directions of the Transvaal Sequence, initiated the thought that annexes of the Rustenburg Layered Suite might exist beyond the eastern margin of the Bushveld Complex, within the Transvaal basin. The discovery of new annexes or extensions of the Rustenburg Layered Suite could have economical implications and may lead to a better understanding of the genesis of the Bushveld Complex.

To investigate the possible relation of the causative bodies of the above-mentioned anomalies to the Rustenburg Layered Suite, two-dimensional geophysical modelling was performed. The combination of gravity and magnetic data combined with surface and borehole geology provided constraints on the deduced structure of the geological models.

2. GEOLOGY

The principal rock types in the area consist of lavas, tuffs, sediments, mafic and ultramafic rocks of the Barberton Sequence, Archaean granite gneiss, sediments and lavas of the Transvaal Sequence, mafic and ultramafic rocks of the Rustenburg Layered Suite and the Uitkomst Suite as well as pre-, syn- and post Bushveld sills.

2.1 Archaean rock types

The base of the Barberton Sequence is formed by the Onverwacht Group consisting of lavas and tuffs as well as cherts (SACS, 1980). Mafic and ultramafic rocks which intruded the Onverwacht Group are associated with the Tjarkastad and Geluk Subgroups. The sedimentary Fig Tree Group overlies the Onverwacht Group. The uppermost sedimentary unit of the Barberton Sequence is the Moodies Group. De Beer et al. (1988) determined the minimum depth extent for the Onverwacht Group as 4,7 km and 3,2 to 3,7 km for the minimum depth extent of the combination of the Moodies and Fig Tree groups. Fig. 2.1 shows the outcrop patterns of the Barberton Sequence as well as suboutcrops intersected by boreholes.

The Barberton Greenstone Belt is surrounded and sometimes intruded by plutons of leucocratic orthogneiss and undeformed granitoid rocks (Anhaeusser et al., 1983), which dominates the surface geology (Fig. 2.1).

2.2 Transvaal Sequence

The basement upon which the rocks of the Transvaal Sequence were deposited varies greatly in character and in age. Palaeohills have been mapped in the granitic areas and some greenstone belts were carved into broad valleys (Button, 1986).

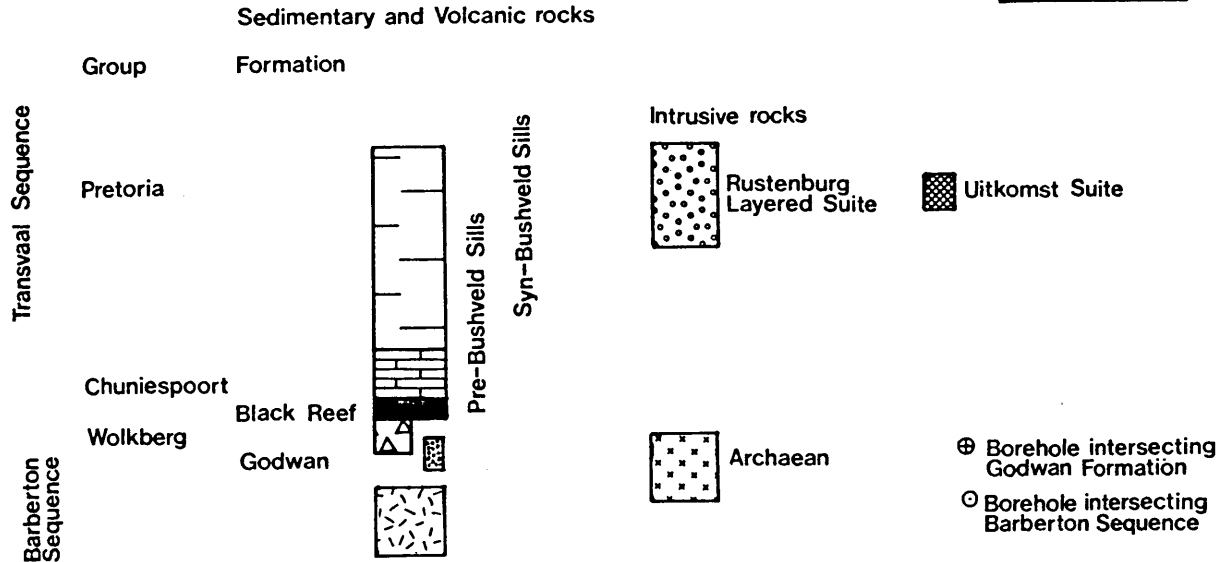
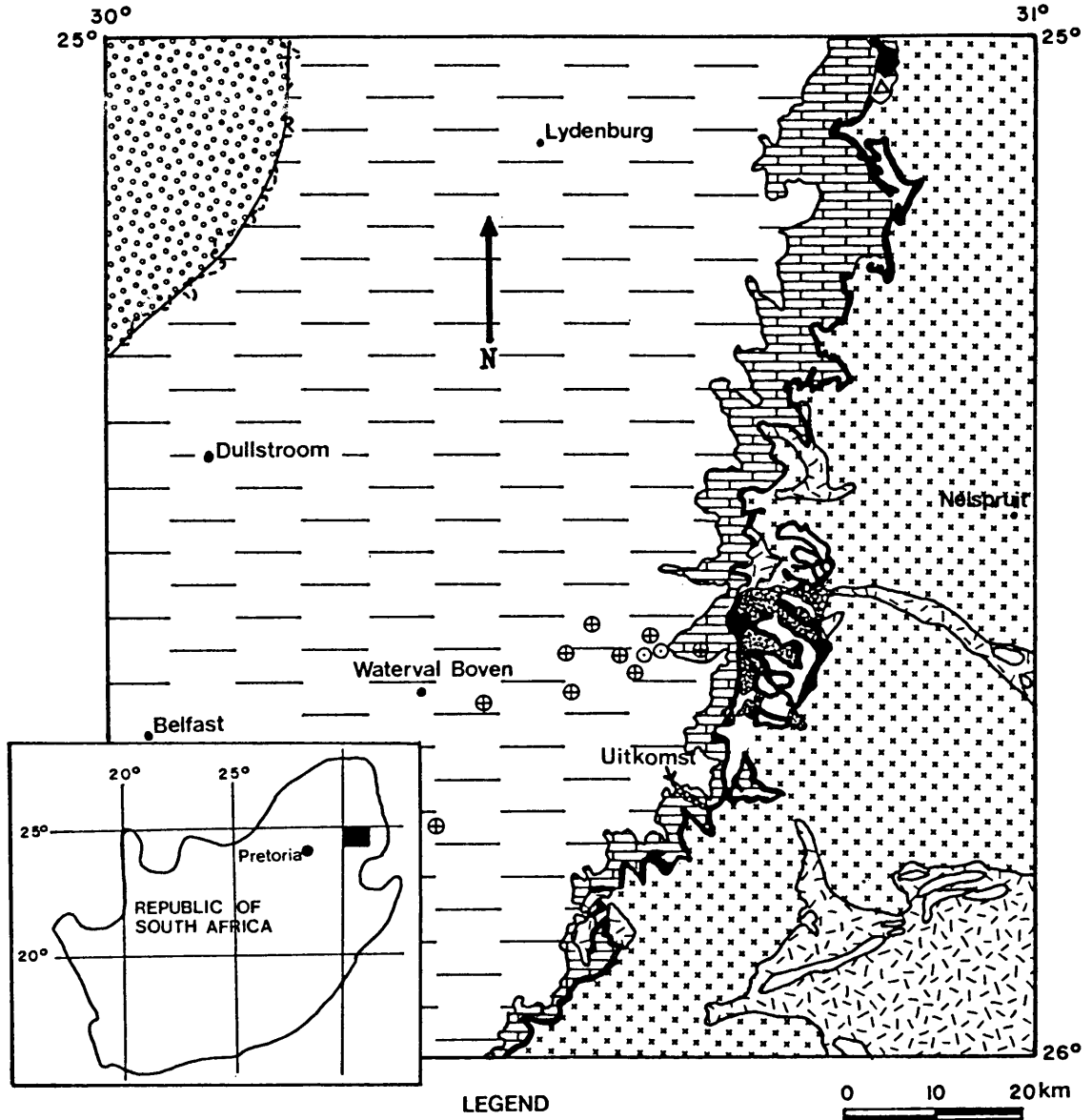


Fig. 2.1 Simplified geological map of the eastern Transvaal.

The oldest rocks which rest unconformably on the Archaean basement are those of the Godwan Formation. This formation's age is uncertain as it is presently correlated with either the Dominion Group, Nsuzze Group of the Pongola Sequence, Ventersdorp Supergroup and the upper part of the Witwatersrand Supergroup. Three members are recognised, namely a lower sedimentary member, approximately 120 metres thick, a volcanic member consisting of lava and tuff with a thickness of 420 metres and a 900 metres thick upper sedimentary member which consists of quartzite with several bands of shale and tuff. Suboutcrops of this formation have been intersected by boreholes as shown in Fig. 2.1.

The Godwan Formation is followed by the Wolkberg Group which has a maximum thickness of 2 000 metres. The distribution of stratigraphic units within the Wolkberg Group is strongly influenced by palaeotopography (Button, 1986). Minor outcrops of this volcanic and clastic unit are found in the northern part of the study area (Fig. 2.1).

The Black Reef Quartzite is very widely developed and grades upward to the third major unit viz the Chuniespoort Group, composed dominantly of chemical sediments. The clastic sediments and volcanics of the Pretoria Group follow on a basin-wide unconformity that cuts across the chemical sediments. According to Sharpe (1982), the thickness of this stratified pile has been greatly increased by numerous types of sills.

The rocks of the Transvaal Sequence strike roughly north-south, with dips varying between 5° and 10° to the west, although slight increases in dip in the vicinity of the Bushveld Complex are common (Button, 1976).

2.3 Intrusives

The mafic rocks of the Rustenburg Layered Suite (age 2050 ± 22 Ma, Von Gruenewaldt et al., 1985) outcrop in the north-eastern part of the area, where they dip gently to the west (Hunter, 1975). The sequence comprises a variety of rock types ranging from dunites, pyroxenites, harzburgites, anorthosite, gabbros, norites to magnetite gabbros and diorites.

Von Gruenewaldt et al. (1980) described the informal zonal subdivision of the Rustenburg Layered Suite into lower, critical, main and upper zones after the convention of SACS. Sharpe (1986) gives a detailed discussion on the emplacement history of the Bushveld Complex and evidence for multiple parental magmas to the Bushveld Complex.

Another complex which is intrusive into the Transvaal Sequence, is the Uitkomst Suite (age 2 025 Ma, Kenyon et al., 1986). It is a layered succession of ultramafic and mafic rocks that bears considerable resemblance to the Rustenburg Layered Suite. The complex has a narrow sill-like structure with maximum horizontal dimension of 5,2 by 1,1 km with a maximum thickness close to 300 metres.

The ultramafic chromite zone of the Uitkomst Suite contains numerous thick chromitite seams with the uppermost seam being 5 to 10 m thick. Calculations made on data listed by Harmer and Sharpe (1985) and Kenyon et al. (1986) have shown that at least 300 metres of ultramafic (UM) parental magma or 1 400 m of boninitic (B1) parental magma were required to form such thick chromite seams. These thicknesses are much larger than the maximum thickness of the Uitkomst complex, which could possibly indicate that the complex extends westwards under the cover of rocks of the Transvaal Sequence.

Extensive investigations of sills intruded into the Transvaal strata by Sharpe (1982, 1984, 1986) have allowed the sills to be subdivided into three main groups, namely pre-Bushveld, syn-Bushveld and Waterberg sills. All the sill groups, with the exception of the Waterberg Suite, are connected with the "Bushveld event".

The pre-Bushveld sills are characterised by amphibolitic assemblages, are common south of Lydenburg, down past Waterval Boven (Fig. 2.1), and are particularly prominent in the Daspoort quartzite and lower Silverton Formations of the Pretoria Group.

The gabbroic and pyroxenite sills, which form the syn-Bushveld group, were emplaced above the Machadodorp volcanics. These sills show an upward increase in frequency towards the margin of the Bushveld Complex.

Most of the dykes that cut the Transvaal Sequence in the area investigated are olivine-dolerites of Karoo age. Concentrations of dykes are found close to the occurrence of doleritic sills with similar petrography which show that many of the dykes are possibly of Waterberg age (Sharpe, 1984).

3. PHYSICAL PROPERTIES OF THE DIFFERENT ROCK TYPES

For the purpose of interpreting the gravity and magnetic anomalies, an accurate knowledge of the densities and magnetic properties of the various formations and rock types in the area of interest is essential.

3.1 Densities

Density determinations for gravity interpretations quoted by Smit and Maree (1966), Hattingh (1980) and De Beer et al. (1988) were used in the investigation. They are indicated in Table 3.1.

TABLE 3.1. AVERAGE DENSITIES FOR ALL THE MAJOR ROCK FORMATIONS IN THE AREA

Stratigraphy	Density (kg/m ³)
Rustenburg Layered Suite	3080
Transvaal Sequence	2780
Godwan Formation	2930
Onverwacht Group	2860
Archaean Granite	2670

A weighted mean density, based on the relative volumetric abundances of the different constituent rock types as deduced from the stratigraphy of the Transvaal Sequence, was calculated at 2780 kg/m³. This mean density takes into account the lower density of the quartzites and shales and the higher densities of the dolomite (2870 kg/m³), andesite (2820 kg/m³), pyroxenite sills (3100 kg/m³) and gabbroic sills (2950 kg/m³).

The mean density of the lower, critical and upper zones of the Rustenburg Layered Suite is estimated as 3100 kg/m³, whereas the main zone has an

estimated density of 2950 kg/m^3 . The mean weighted density of the Rustenburg Layered Suite was calculated as 3080 kg/m^3 .

Borehole data proved the presence of Godwan Formation and Barberton Sequence (Fig. 2.1) underneath the Transvaal rocks at a distance of approximately 20 km from the margin of the basin. To determine their contribution to the gravity anomalies, knowledge of their geophysical properties was essential. The only density data available on the Godwan Formation is that of Smit and Maree (1966). The lava and tuff of the Volcanic Member are the only dense rocks in this formation and their average density is 2930 kg/m^3 . The average density of the Onverwacht Group is considered to be 2860 kg/m^3 (De Beer et al., 1988).

3.2 Magnetic properties

The analysis of a magnetic anomaly involves the consideration of the shape, size and total magnetization characteristics of the rock mass causing the anomaly. The total magnetization of a rock sample is the vector sum of two components, namely the induced and remanent magnetization. In the interpretation of magnetic anomalies it is important that the intensity and direction of each vector is known.

The main assumptions of previous workers who felt that the possible presence of remanent magnetization could be ignored in the interpretation of magnetic surveys were that (a) the remanent intensity of magnetization was small compared to the induced and/or (b) the directions of remanent magnetization were random throughout the rock formation under study, or were along the present direction of the earth's magnetic field. Another main assumption of many workers was that acceptance of induced magnetization was forced upon them due to lack of remanent data.

The importance of remanent magnetization is appreciated by geophysicists, and a number of articles have been published in which evidence is given to support this contention (Green, 1960; Girdler and Peter, 1960; Hood, 1961; Books, 1962; Bath, 1962; Hays and Scharon, 1963).

Palaeomagnetic studies of the Transvaal Sequence (Briden, 1976) and the Barberton Sequence (Layer, 1986) have established directions of magnetization, but not intensity of magnetization and susceptibilities of the different rock types.

Molyneux and Klinkert (1978) assumed that the magnetization of the mafic rocks of the Rustenburg Layered Suite is essentially induced, because a good agreement was found between the observed and calculated magnetic anomalies over areas where the structures are known. However, the study of the palaeomagnetism of the Rustenburg Layered Suite by Hattingh (1983) has established the following (Fig. 3.1 & 3.2).

1. Although a resemblance exists, there is no close relation between either the zonal or lithostratigraphic subdivision and the observed palaeomagnetic polarity pattern.
2. The mafic rocks can be subdivided into three magnetic polarity zones, namely MPZA, MPZB and MPZC. MPZA and MPZC have normal magnetization directions while MPZB has a reversed magnetization direction (Fig. 3.1).
3. The positions of the boundaries between polarity zones were regarded as approximate as more sampling sites will be necessary to locate the exact positions.
4. The mean intensity of natural remanent magnetization (NRM) of all the specimens from the critical, main and upper zones are $27 \times 10^{-3} \text{ Am}^{-1}$, $3395 \times 10^{-3} \text{ Am}^{-1}$ and $6070 \times 10^{-3} \text{ Am}^{-1}$ respectively.

Despite Hattingh's intensive study, more data were required on the susceptibility, anisotropy and intensity of magnetization to calculate the magnetization of the Rustenburg Layered Suite and therefore a palaeomagnetic investigation was undertaken in the area shown in Fig. 3.3. Data from this

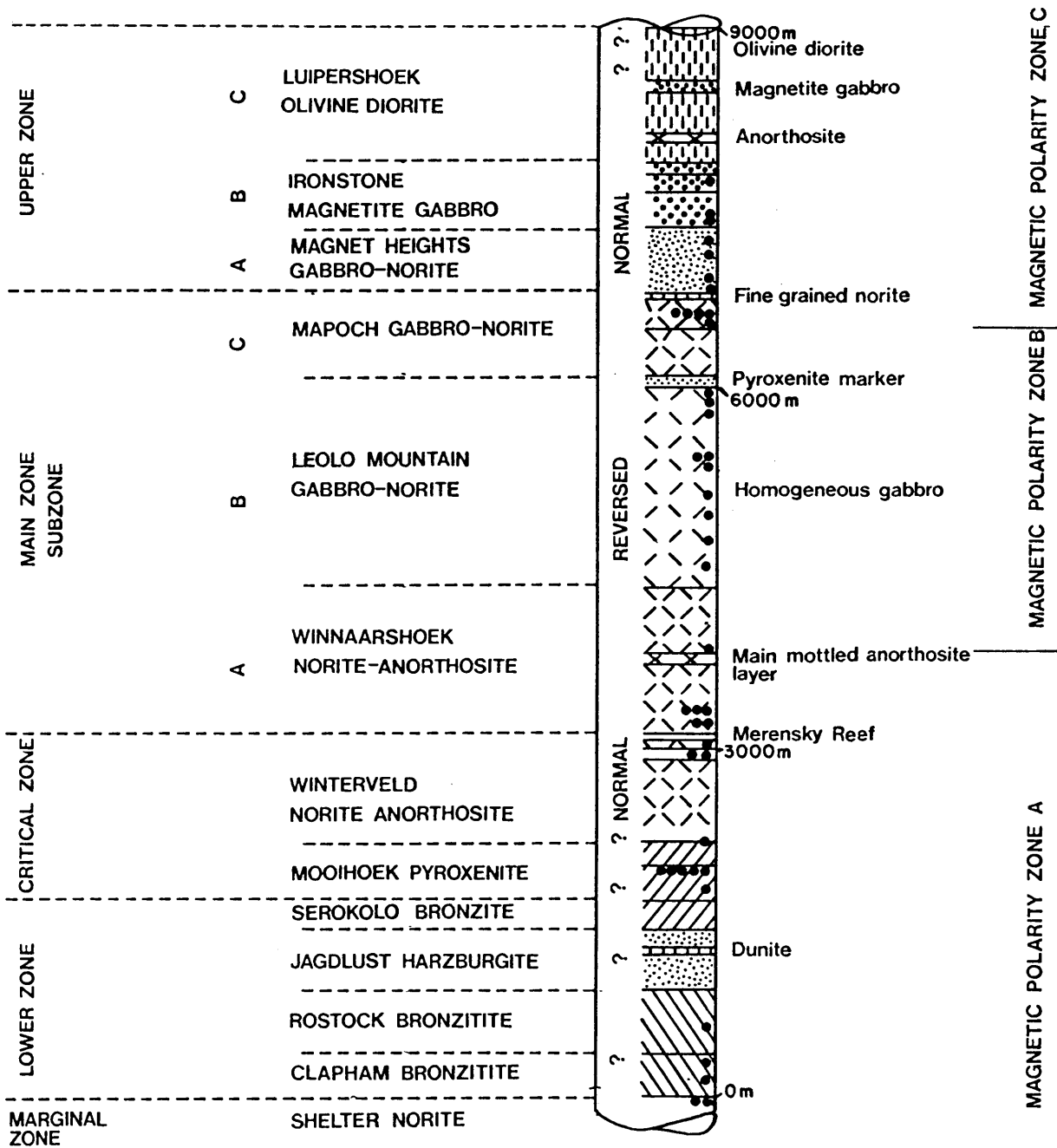


Fig. 3.1 Simplified lithostratigraphic column of the Rustenburg Layered Suite in the eastern Bushveld Complex, showing the magnetic polarity zones and sampling sites. From Hattingh (1983).

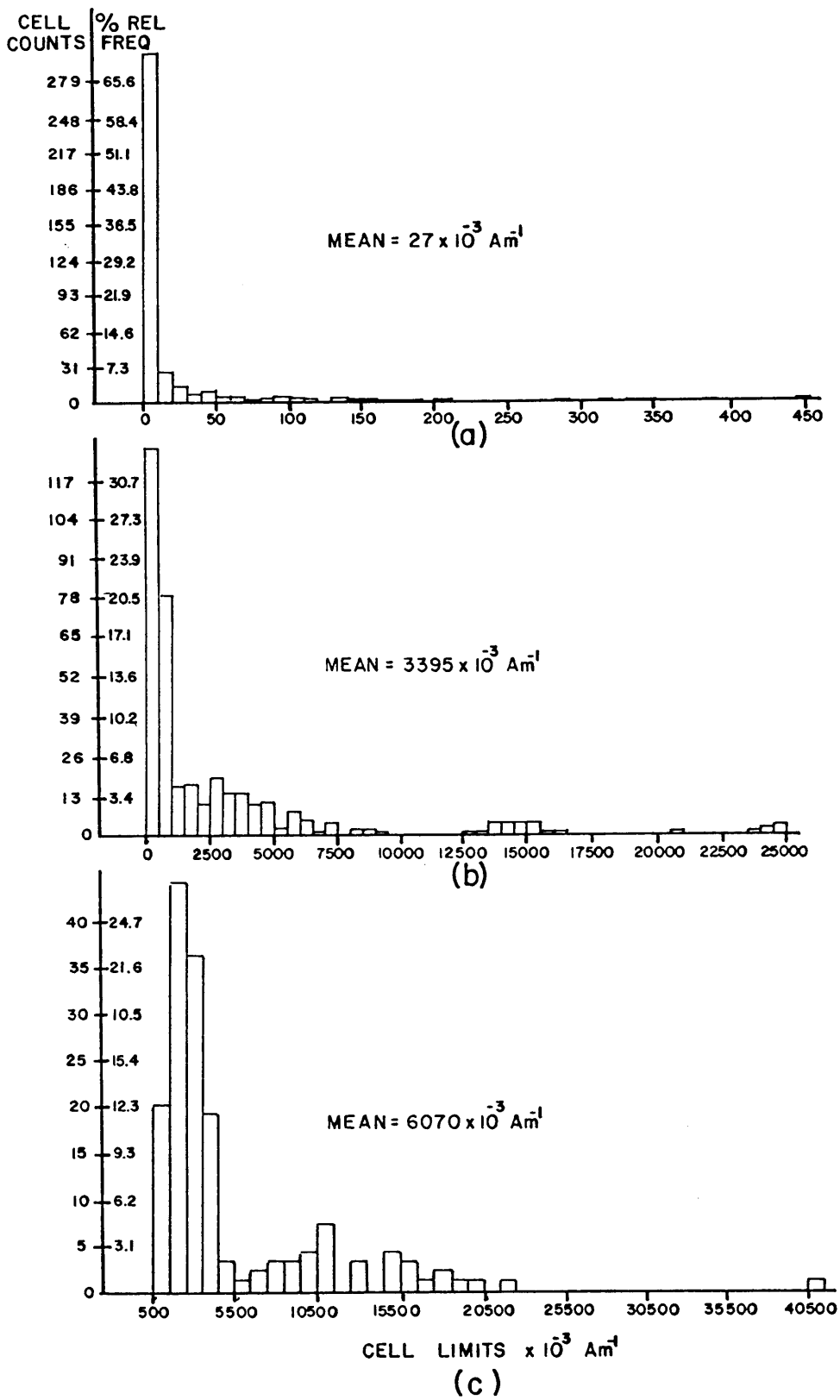


Fig. 3.2 Histogram plots of NRM intensities of specimens from the (a) critical zone, (b) main zone and (c) upper zone. From Hattingh (1983).

study and data from Hattingh (1983) were used in combination to calculate the magnetization vector for each subzone of the Rustenburg Layered Suite.

3.2.1 Magnetization of the Rustenburg Layered Suite

3.2.1.1 Field and laboratory procedures

A collection of rock samples for remanence and susceptibility measurements were made at locations shown in Fig.3.3. The position of the sampling sites in the stratigraphic columns of the layered sequence is also shown in Fig. 3.3.

A petrol driven, portable core drill which produced samples 25 mm in diameter and up to 200 mm in length, was used for sampling. Orientation of core samples, with a precision of 1° (Gough, 1967), was done with a sun compass (Creer and Sanver, 1967). At least five samples were taken at each sampling site and each sample was cut into specimens with a length of 22,5 mm.

Bulk susceptibility (K) was measured by means of a bridge method (Fuller, 1967). The A.C. bridge methods make use of the change of inductance of air-cored coils brought about by the introduction of the rock specimen. The fractional change of inductance ($\Delta L/L$) is linearly proportional to the susceptibility of the specimen and the volume ratio of the sample to the air space (p).

The anisotropy of magnetic susceptibility (Girdler, 1961; Fuller, 1963) was measured with a Digico spinner magnetometer (Noltimier, 1967). Spinning the sample in a d.c. field produces a time-varying signal of frequency twice

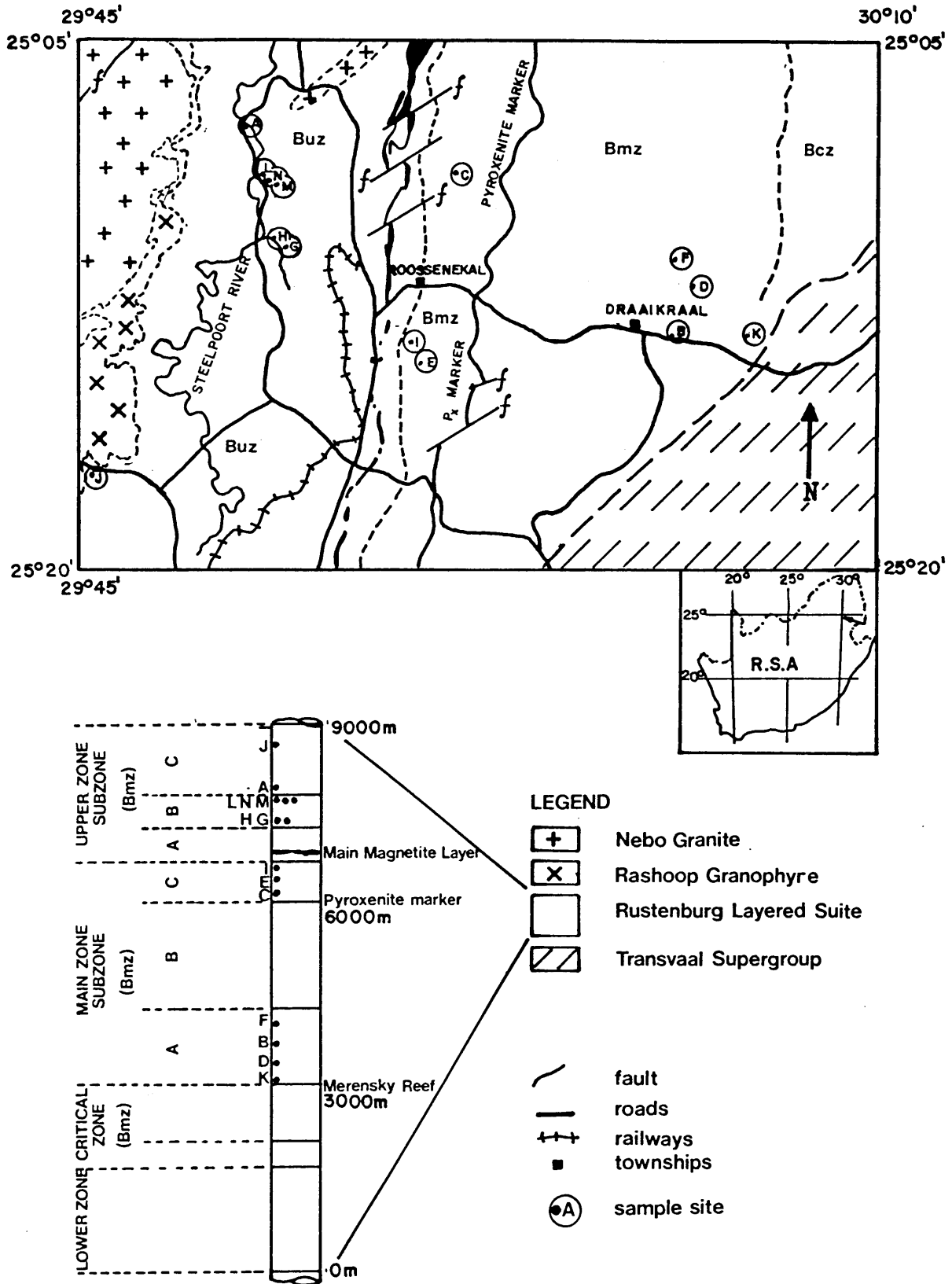


Fig. 3.3 Geological map of the Draaikraal-Roossenekal area showing the location of the sampling sites and their stratigraphical positions.

the spinning frequency, and in magnitude proportional to the applied field and to the anisotropy in the plane at right angles to the spinning axis. When the sample is spun about the z-axis the anisotropy is measured in the x,y plane. It is not usually considered necessary to invert the specimen about each axis if the field applied to the specimen is uniform over the volume swept out by it, so only three spins about x, y and z are required.

The remanent magnetizations of specimens were measured using a Digico fluxgate spinner magnetometer. Continuous thermal demagnetization was done with a slightly modified form of this instrument namely the Digico two axes high temperature rig. Alternating field (AF) demagnetization of specimens was done with an apparatus built at the Geological Survey of South Africa, following a description by McElhinny (1964). The operation of these instruments is described by Hattingh (1983).

The first step in the laboratory procedures was to measure the NRM of each specimen. Bulk susceptibility and anisotropy measurements were then carried out on each specimen. Stepwise AF demagnetization of at least two pilot specimens from each site was done and the remanent magnetization determined after each step. To find the optimum alternating demagnetization field to optimise the grouping of stable remanent magnetization directions, the Briden stability index (SI) (Briden, 1972) was calculated for each demagnetization step. For some specimens this stability index was unreliable and therefore an alternative method described by Zijdeveld (1967) was used. Bulk AF cleaning was then carried out on two specimens from each core sample at an AF value indicated by the Zijdeveld diagram as being the optimum for a given site. At least one specimen per site was retained for thermal demagnetization. The specimens were demagnetized thermally in steps of approximately 100°C, and as the Curie point was approached, this was reduced to intervals of approximately 20°C and 10°C. At each step the remanent magnetization was measured.

3.2.1.2 Treatment and presentation of data

The directions of remanent magnetization of specimens were first averaged to give a sample mean. Sample means were then, in turn, combined to yield site mean directions. The overall formation mean direction may be established either as the direction of the vector resultant of the site mean directions or by the direction of the vector resultant of all the specimens. In igneous units with a wide variety of rock types, such as the Rustenburg Layered Suite, the within-site precision k_w (Fisher, 1953) varies according to the rock type sampled. Thus when k_w is variable from site to site, there is no satisfactory way known in which all the vector directions can be taken into account in estimating the overall formation mean. The group overall mean direction was thus calculated from the site mean directions.

A description of the standard procedures followed during a statistical analysis of the direction of remanent magnetization is given by McElhinny (1973, p79).

The NRM directions with the radius of the cone of 95% confidence (Irving, 1964) and k the estimate of the precision for each site, where the in-site grouping of magnetization directions is significant at the 95% confidence limit (Watson, 1965) are given in Table 3.2 and the directions are presented in Fig. 3.4.

The susceptibility of rocks varies according to the amount, form and composition of the magnetic minerals which they contain (Nagata, 1953). The wide scatter of the intensities of magnetization (induced and remanent) (Fig. 3.5) of samples from one geological formation and the fact that only positive values occur, cause the Gaussian distribution to be a poor fit to such data. Therefore the procedure of calculating an arithmetic mean intensity of magnetization for a geological formation is not meaningful. The logarithmic normal distribution provides a much better fit (Runcorn, 1967) to the susceptibility and intensity of magnetization data. Histograms in which the intensity and susceptibility are plotted on a logarithmic abscissa scale and normal curves fitted to the data are shown in Fig. 3.9, 3.14, 3.21 and 3.23.

The magnetic anisotropy of a sample is defined by the orientations of the maximum, intermediate and minimum susceptibilities, plotted as points on a stereographic (equal angle) net, and by the shape of the susceptibility ellipsoid. Following Kligfield et al. (1977) the axial ratios X_{max}/X_{int} and X_{int}/X_{min} are plotted on a Flinn diagram (Flinn, 1962) on which any ellipsoid will be represented as a point. The line with slope equal to one divides the plot into two fields: above that line shapes are prolate and below they are oblate. If rocks have an intrinsic anisotropy, the thermo-remanent magnetization (TRM) may be deflected away from the direction of the applied field towards the direction of easy magnetization. Therefore anisotropy may be a factor contributing to the scatter in the directions of NRM. The degree of anisotropy (A_n) is expressed as the ratio of maximum to minimum susceptibility,

$$A_n = \frac{X_{max}}{X_{min}} .$$

The maximum deflection angle θ_{max} through which the TRM is deflected if the applied field lies in the plane containing the maximum and minimum susceptibility directions is given by

$$\theta_{max} = \tan^{-1} \frac{(A_n - 1)}{2\sqrt{A_n}}$$

(McElhinny, 1973).

The mean and 95% confidence interval for A_n values from each site are shown in Fig. 3.8.

The secondary magnetizations removed during AF demagnetization are caused primarily by lightning discharges to the ground and chemical weathering. The weathering of igneous rocks is mainly restricted to the surface layer and cracks, and the current from lightning strikes decays exponentially with

depth so that its magnetic effects are restricted mainly to the top 20 metres (Graham, 1961). Only the top few centimetres of a rock are sampled and therefore to interpret the effect of the rock mass, the data after AF demagnetization is used. The Zijdeveld diagram (Zijdeveld, 1967) gives a combination of a few orthogonal projections of the curve which the end-point of the resultant vector of magnetization describes in space during progressive demagnetization. The projection combination allows a quick survey of the magnetizations present and their directions and size-ratios (Dunlop, 1979). Fig. 3.13 gives an example of the stereographic projection, intensity decay curve and two Zijdeveld plots (of which the second plot is a magnification of the first) for a sample submitted to stepwise AF demagnetization. After the Zijdeveld plots were studied, an optimum demagnetization field for bulk cleaning was chosen for each site.

The results from the bulk AF demagnetization of sites are given in Table 3.3 and the magnetization directions are plotted in Fig. 3.6. Histograms in which the intensity of magnetization is plotted on a logarithmic abscissa scale and normal curves fitted to the data are shown in Fig. 3.9, 3.14, 3.21 and 3.23. Königsberger ratios calculated before and after bulk cleaning are plotted in Fig. 3.7.

Thermal demagnetization was performed to compare end-point directions with AF demagnetization as well as gaining information on the composition of the magnetic minerals carrying the remanence.

3.2.1.3 Interpretation and discussion of data

Two sites, F and K, had random NRM directions at sample level according to the criterion of Watson (1956) at the 95% confidence limit (Table 3.2). The NRM directions of the remaining sites are scattered (Fig. 3.4) and have low k values. This is due to the presence of secondary magnetizations with random

TABLE 3.2

SUMMARY OF MAGNETIC MEASUREMENTS ON ROCK SAMPLES

Site	No of samples	Susceptibility ($\times 10^{-3}$ SI)			NRM intensity ($\times 10^{-3}$ Am ⁻¹)			NRM direction			
		(95% conf. interval)		K	(95% conf. interval)		J	Dec	Inc	α_{95}	k
		Kmax	Kmin		Jmax	Jmin					
A	4	1,14	0,92	1,03	7	2	5	62,6°	-70,2°	14,4°	29
B	5	2,97	1,28	2,13	1515	574	1044	243,9°	0°	51,3°	3
C	5	1,03	0,97	1,00	461	415	438	203,3°	-46,1°	2,8°	772
D	4	1,23	1,15	1,19	1731	662	1196	355,5°	16,9°	50,3°	4
E	4	1,38	1,29	1,34	1868	1524	1696	207,8°	-45,2°	48,4°	5
F	5	0,42	0,39	0,41	212	141	177	-	-	-	-
G	5	156,00	134,00	145,00	3299	2130	2715	201,6°	61,6°	20,9°	14
H	6	60,30	23,90	42,10	880	430	655	143,8°	-71,9°	27,2°	7
I	5	4,67	4,34	4,50	12862	10972	11917	300,3°	57,1°	17,8°	19
J	5	2,52	1,61	2,06	139	117	128	174,6°	2,2°	14,5°	29
K	5	0,48	0,45	0,47	579	359	469	-	-	-	-
L	5	147,00	140,00	143,00	2172	1915	2044	174,4°	-77,2°	12,9°	36
M	5	67,50	57,60	62,60	999	539	769	312,2°	-77,2°	26,7°	9
N	5	109,00	96,00	102,00	1934	1451	1693	137,8°	-48,5°	19,7°	16

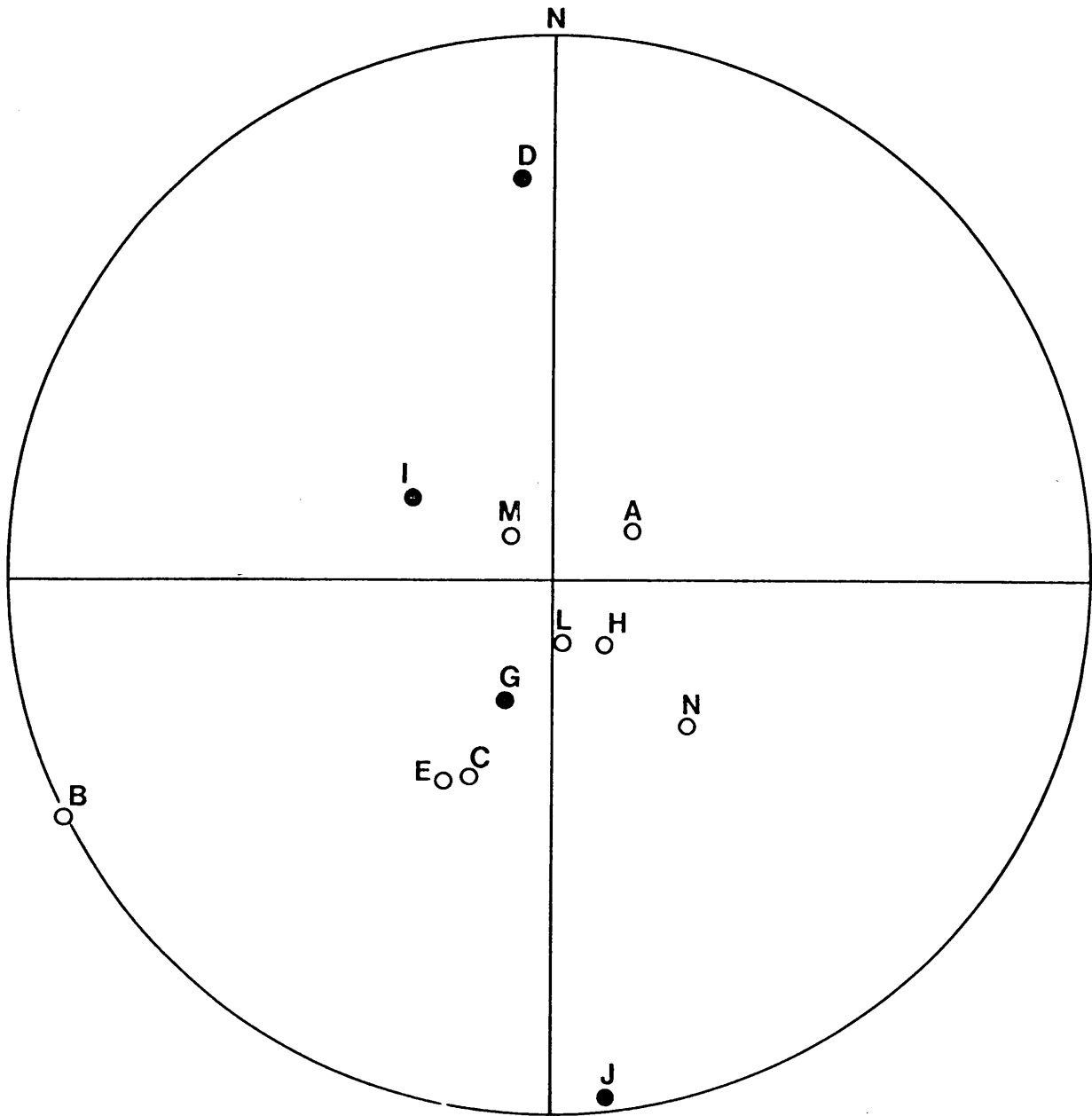


Fig. 3.4 Stereographic projection (equal angle) of NRM directions.
● = lower hemisphere, ○ = upper hemisphere.

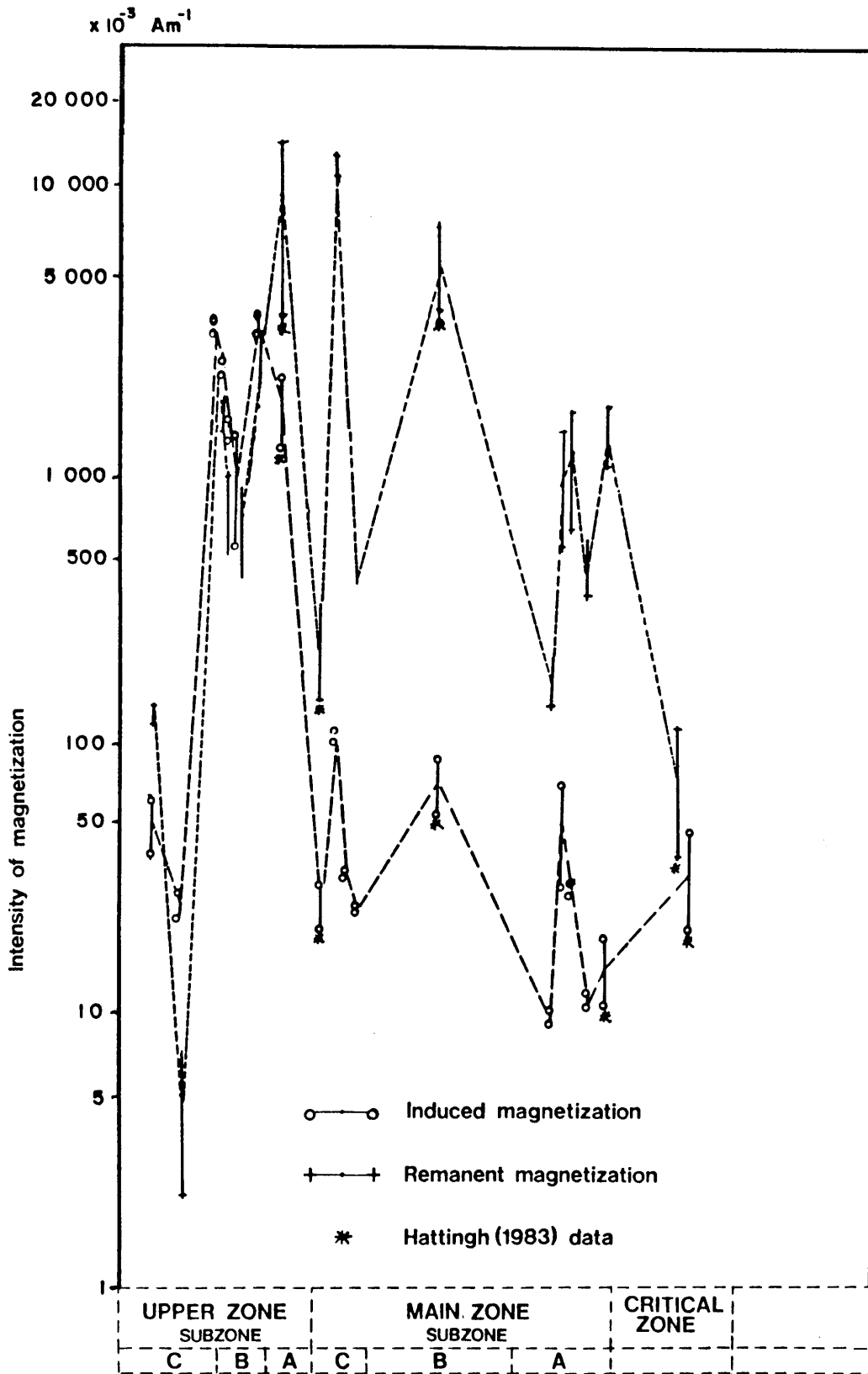


Fig. 3.5 Intensities of magnetization along the lithostratigraphic column of the Rustenburg Layered Suite. The average intensity and 95% confidence interval of both the induced and remanent magnetizations are indicated for each site.

orientations. The induced intensity of magnetization for the sites situated in the magnetite gabbro ranges from .6 to 4 Am^{-1} , and the NRM intensity of magnetization for these sites is of the same order of magnitude (Fig. 3.5). The induced intensity of the remaining sites falls in the range 10^{-2} to 10^{-1} Am^{-1} , while the NRM intensity varies between 2×10^{-3} and 15 Am^{-1} . It is thus evident that remanent magnetization is an important factor and often a dominant one.

Sites A and M yielded consistent NRM directions but on AF demagnetization these became unstable and the sites were rejected. Sites F and K, which had inconsistent NRM directions at sample level, group significantly after AF demagnetization of the specimens. Site H, which was intended as a baked contact test, had to be rejected due to insufficient sampling. From Table 3.3 it is evident that bulk AF demagnetization improved the grouping of the majority of the magnetization directions from the different sites.

The magnetization directions of all the specimens subjected to stepwise thermal demagnetization at progressively higher temperatures, changed after each successive demagnetization step. The patterns generally followed great circles, the movement being towards the individual site mean magnetization direction calculated after bulk AF cleaning. For a few samples the remaining intensities of magnetization at high temperatures were too low to be measured accurately and the changes in direction became random. From the shape of the intensity response curves it appears that the final Curie point of the specimens is in excess of 500°C and that they have thermally distributed blocking temperatures which indicate that magnetite is not the only source of magnetization. A detailed description of the mineralogy of the opaque minerals and their Curie points is given by Hattingh (1983).

TABLE 3.3 MAGNETIZATION DIRECTIONS OF SITES AFTER ALTERNATING FIELD DEMAGNETIZATION

Site	Alternating field (mT)	Dec	Inc	α_{95}	k
B	20	15,5°	56,2°	18,6°	25
C	15	201,8°	-45,0°	4,7°	269
D	40	18,8°	56,7°	12,1°	59
E	20	24,2°	36,0°	7,1°	167
F	25	40,7°	77,6°	14,3°	30
G	15	219,6°	-62,8°	6,0°	161
I	20	12,4°	71,6°	15,7°	25
J	10	177,5°	15,3°	6,0°	164
K	50	228,0°	60,3°	13,0°	36
L	10	151,2°	-38,6°	19,0°	17
N	10	172,4°	-37,4°	13,7°	33

Fig. 3.7 shows the Königsberger ratio (Q_1) calculated for each site using the data listed in Table 3.2 and the Königsberger ratio (Q_2) calculated from the average logarithmic data after AF demagnetization. For individual sites Q_1 ranges from .08 to 120 but it is less than 1 in only 4 sites. The majority of the sites show a significant decrease in Königsberger ratios after AF demagnetization, which indicates that secondary magnetizations are dominant factors in calculating Q_1 .

The anisotropy (A_n) for all the sites ranges from 5 to 52%. The variation of the orientation of the principal axes of the susceptibility ellipsoids of individual specimens and the shapes of these ellipsoids within each site define anisotropy types (Kligfield et al., 1977). Three basic spatial patterns can be recognised in the individual site data.

1. The Xmin axes of individual specimens are clustered and the Xmax and Xint axes are dispersed about a great circle or widely scattered.
2. The Xmax, Xint and Xmin axes of individual specimens are all grouped about their respective site means.

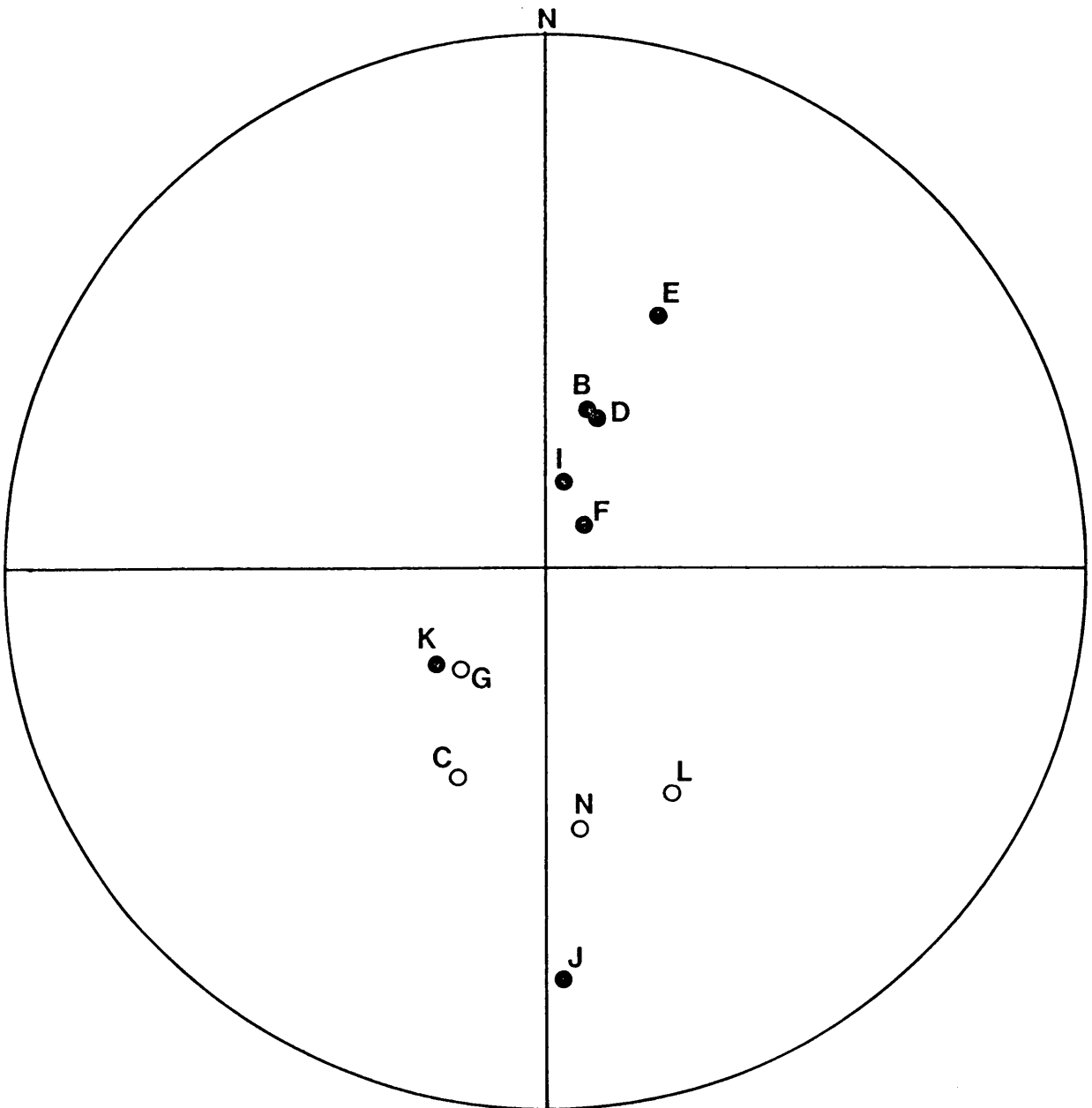
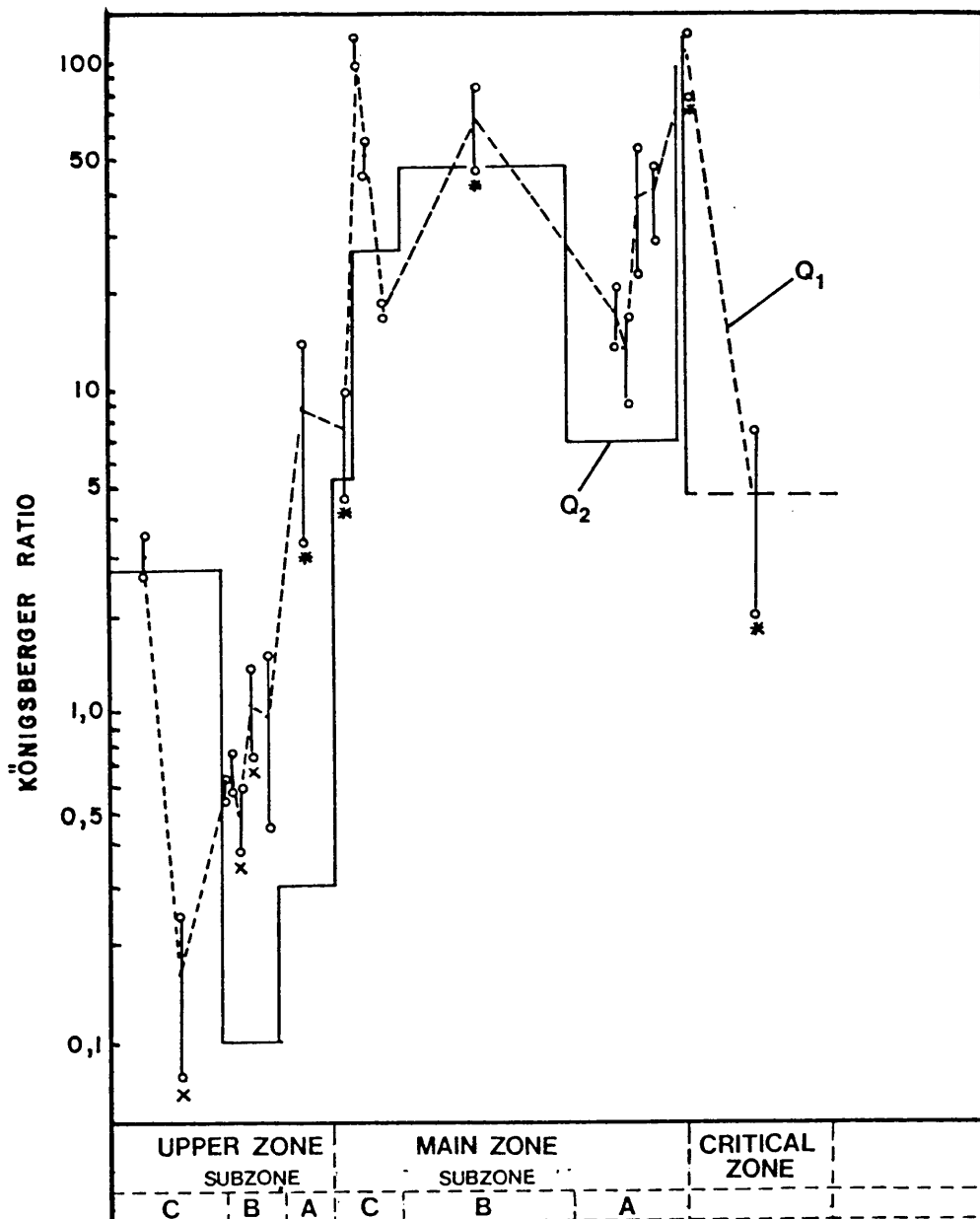


Fig. 3.6 Stereographic projection of magnetization directions of sites after bulk alternating field demagnetization. Plotting convention as in Fig. 3.4.



* Hattingh (1983) data

Fig. 3.7 Königsberger ratios of sites calculated before (Q_1) and after (Q_2) bulk alternating field demagnetization. The average ratio (Q_1) and 95% confidence interval ($\circ-\circ$) are indicated for each site. The bar chart indicates the mean ratio (Q_2) for each subzone. x = site excluded from zonal data.

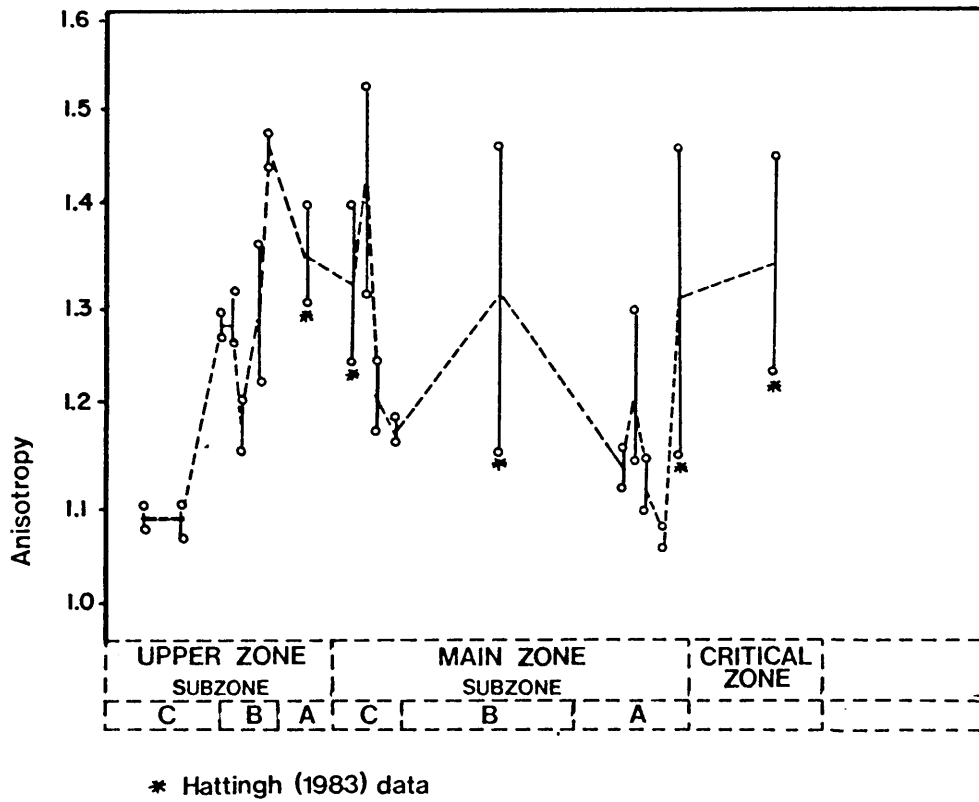


Fig. 3.8 Anisotropy data along the lithostratigraphic column of the Rustenburg Layered Suite. The average anisotropy and 95% confidence interval are indicated for each site.

3. X_{max} axes are clustered and X_{min} and X_{int} axes are dispersed about a great circle or widely scattered.

The basic combinations of ellipsoid shapes are: (a) all prolate, (b) some prolate and some oblate, or (c) all oblate. For most of the site data it is seen that the minimum susceptibilities are close to the vertical and the maximum and intermediate susceptibilities are all close to the horizontal plane but are widely scattered within it. This scatter of directions of principal susceptibility is related to the differences between their magnitudes. If X_{min} is considerably different from both X_{max} and X_{int} , the X_{min} axes will be closely grouped; but for X_{max} and X_{int} with nearly equal magnitudes their directions will be widely scattered in the horizontal plane. The study of the anisotropy of each site has shown that the scatter in directions of NRM from a few sites is caused by differences in magnetic anisotropy and therefore differences in magnetic fabric of the magnetic minerals.

Zonal interpretation from the Draaikraal-Roosenekal area

Main Zone Subzone A

Four sampling sites are situated in this zone, which is known as the Winnaarshoek Norite - Anorthosite (Fig. 3.3). Rock types sampled from sites K, D and F consist of norite while site B was sampled on the contact between the norite and the main mottled anorthosite layer. The NRM's of samples are characterised by high intensity of magnetization (Fig. 3.5) with inconsistent and unstable magnetization directions at sample and site levels. Fig. 3.9(a) shows the sample and site mean directions after alternating field demagnetization. The magnetization direction of site K differs considerably from the other sites. Fig. 3.10, 3.11 and 3.12 show that the shapes of the susceptibility ellipsoids for all the sites fall in both the flattening and constriction fields. From the orientation of the principal axes of the

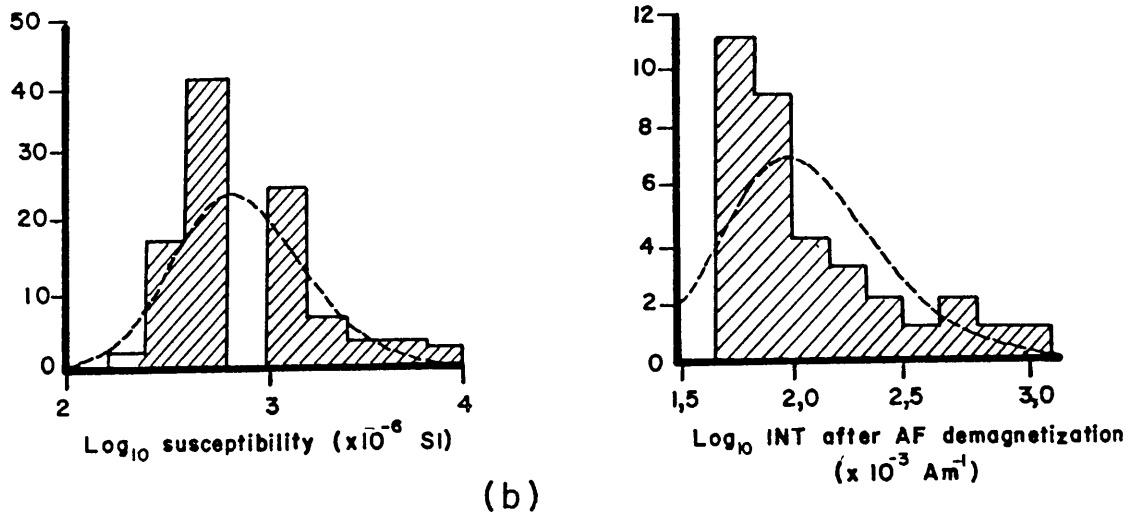
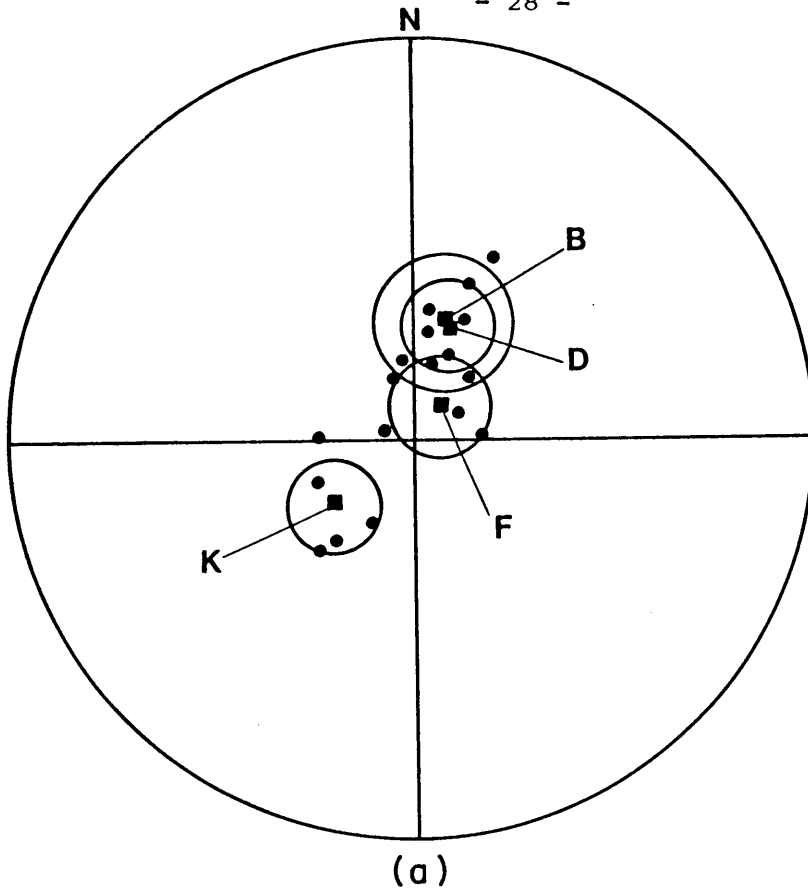


Fig. 3.9 (a) Sample (●) and site (■) mean directions with the circle of 95% confidence (plotting convention as in Fig. 3.4), and (b) histograms of the logarithmic susceptibility and intensity of magnetization after bulk AF demagnetization of sites B, D, F and K situated in subzone A of the main zone.

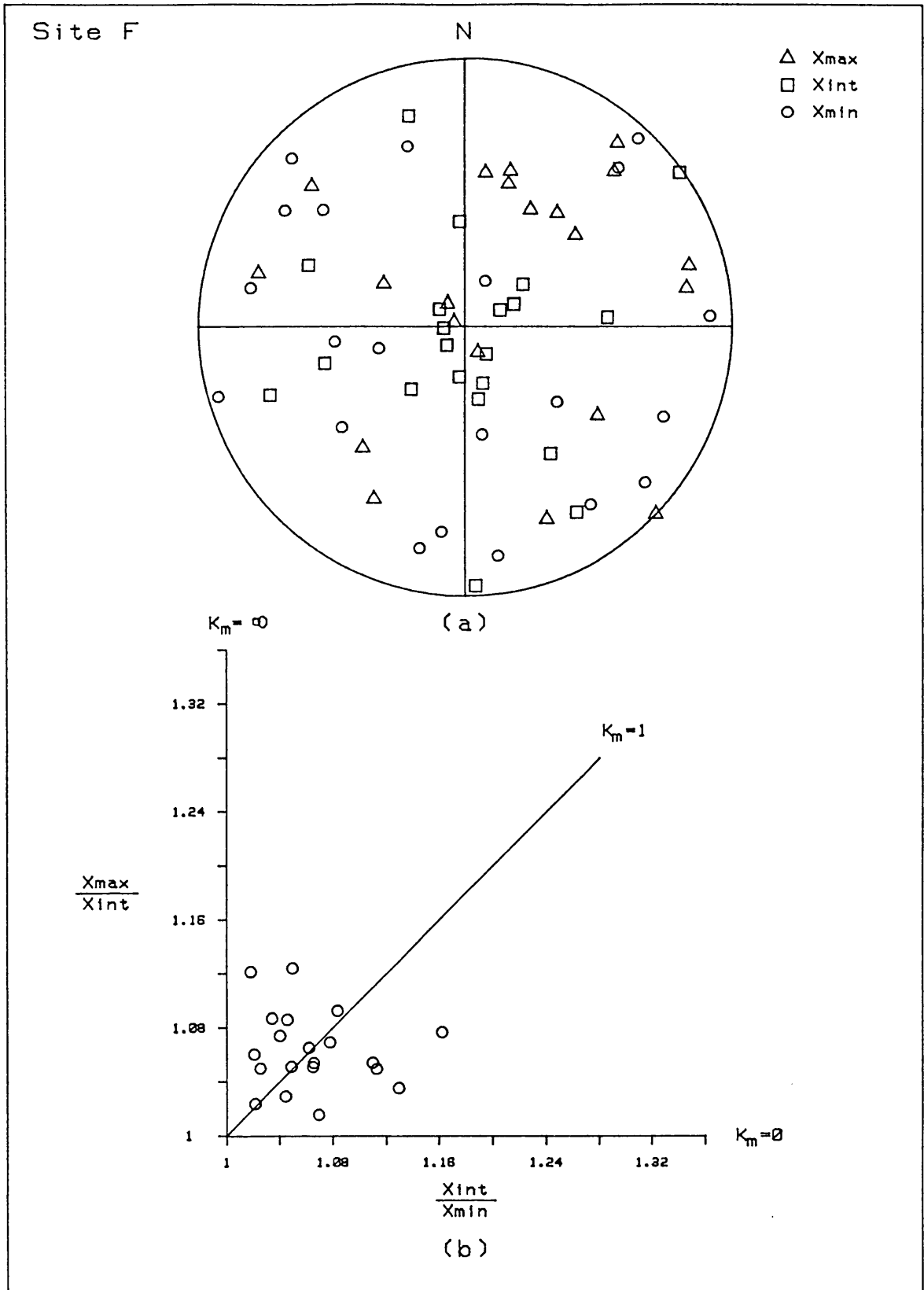


Fig. 3.10 Magnetic anisotropy data for site F. (a) Orientation of maximum (triangles), intermediate (squares) and minimum (circles) axes of susceptibility plotted on the upper hemisphere of an equal-angle net. (b) Shapes of susceptibility ellipsoids plotted on a Flinn diagram.

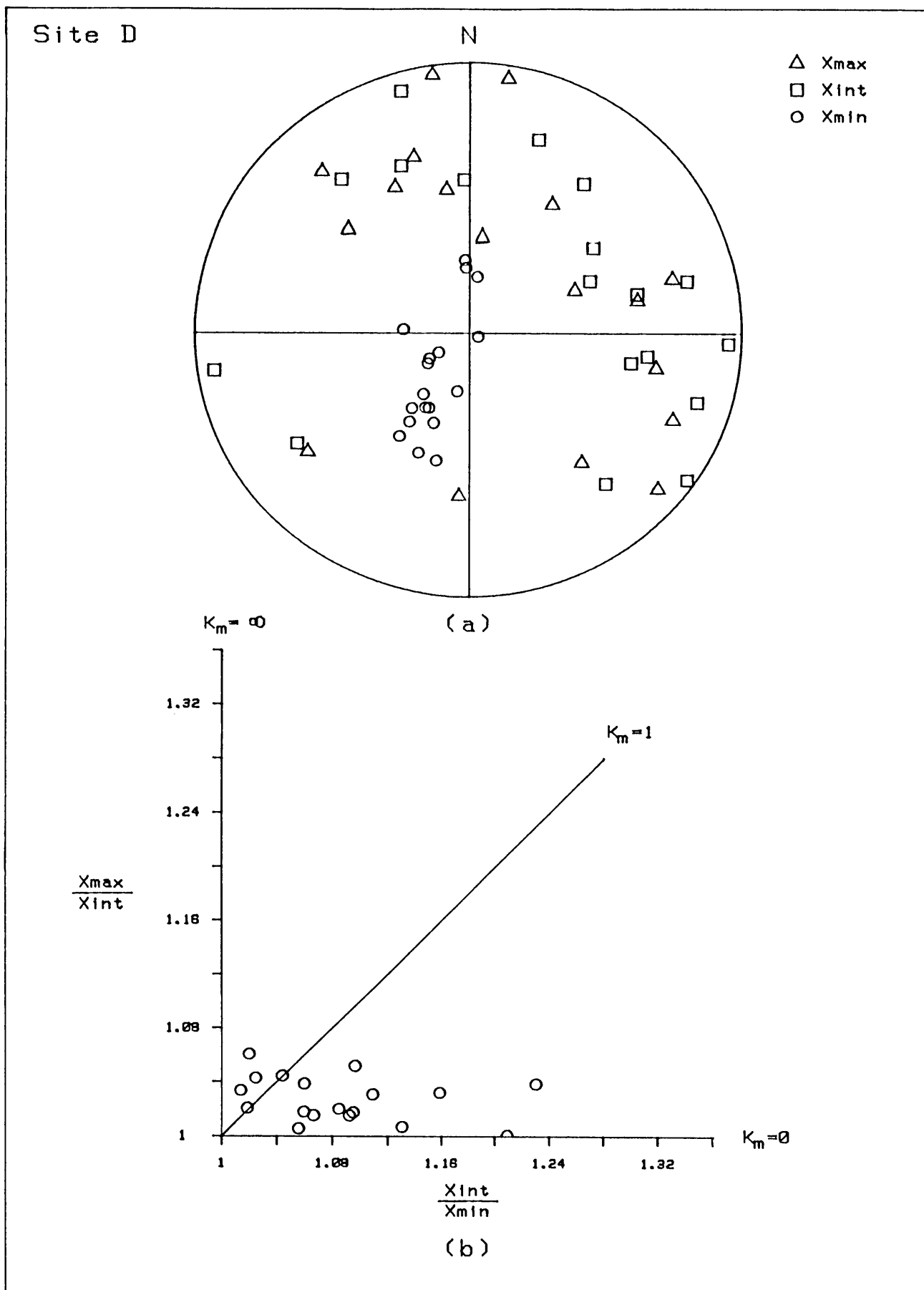


Fig. 3.11 Magnetic anisotropy data for site D. Plotting conventions as in Fig. 3.10.

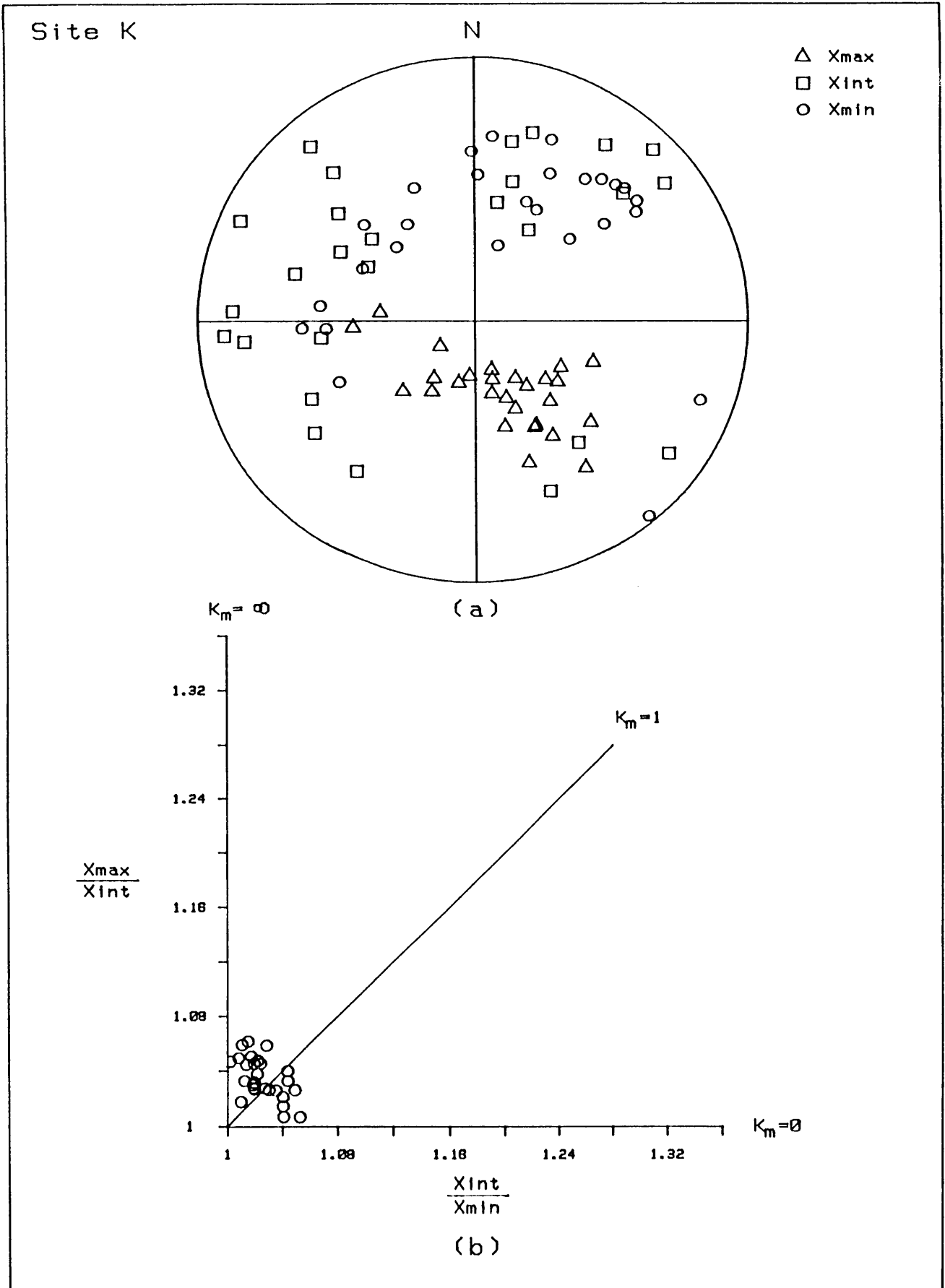


Fig. 3.12 Magnetic anisotropy data for site K. Plotting conventions as in Fig. 3.10.

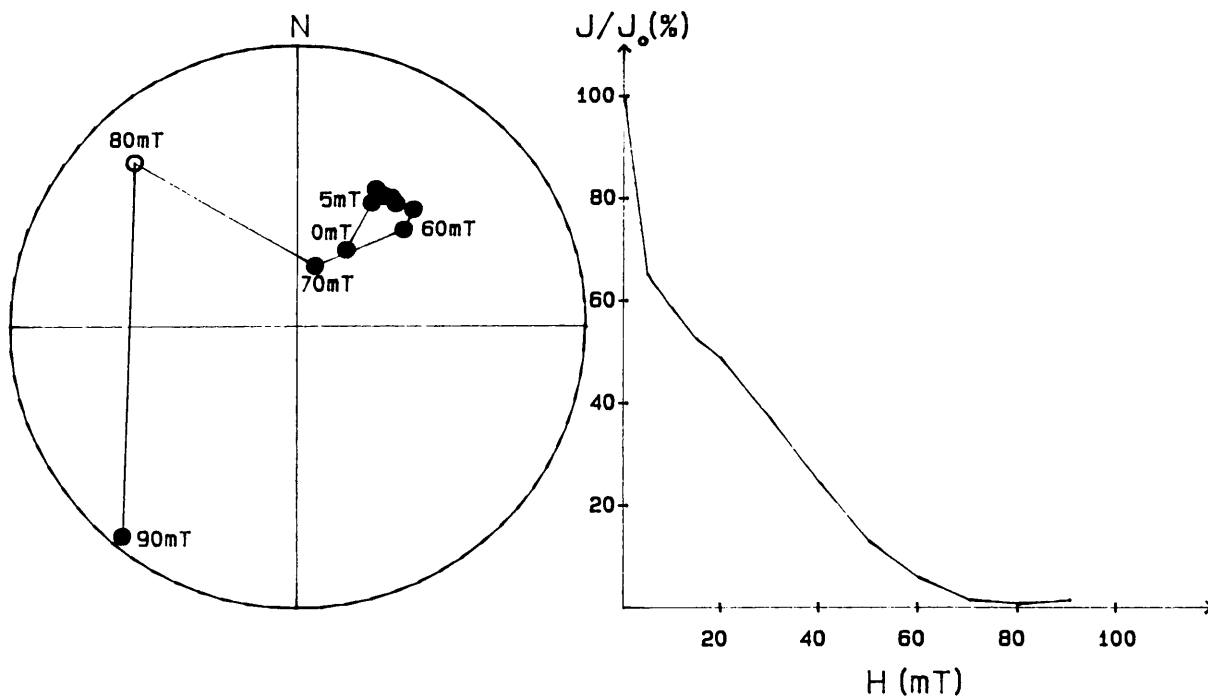
susceptibility ellipsoids of individual samples it is evident that sites F (Fig. 3.10) and B have random orientations, site D has a type 1 spatial pattern (Fig. 3.11) which shows that the plane of maximum - intermediate susceptibility lies in the igneous layering, and site K has a type 3 spatial pattern (Fig. 3.12). The possibility exists that site K is sampled in a dyke if one assumes that the anisotropic magnetic minerals orientate themselves with their X_{max} axes nearly vertical.

The histograms of the logarithmic susceptibility and intensity of magnetization after bulk AF cleaning are plotted in Fig. 3.9(b). The mean susceptibility of this unit is very low (726×10^{-6} SI) and the mean intensity of remanent magnetization is $121 \times 10^{-3} \text{ Am}^{-1}$ which gives a value of 7 for the Königsberger ratio (Q_2). Because the angle between the earth's field and the mean remanent magnetization directions is large and the Q_2 value is large, the total resultant magnetization directions will be considerably different to that of the inducing field.

Main Zone Subzone C

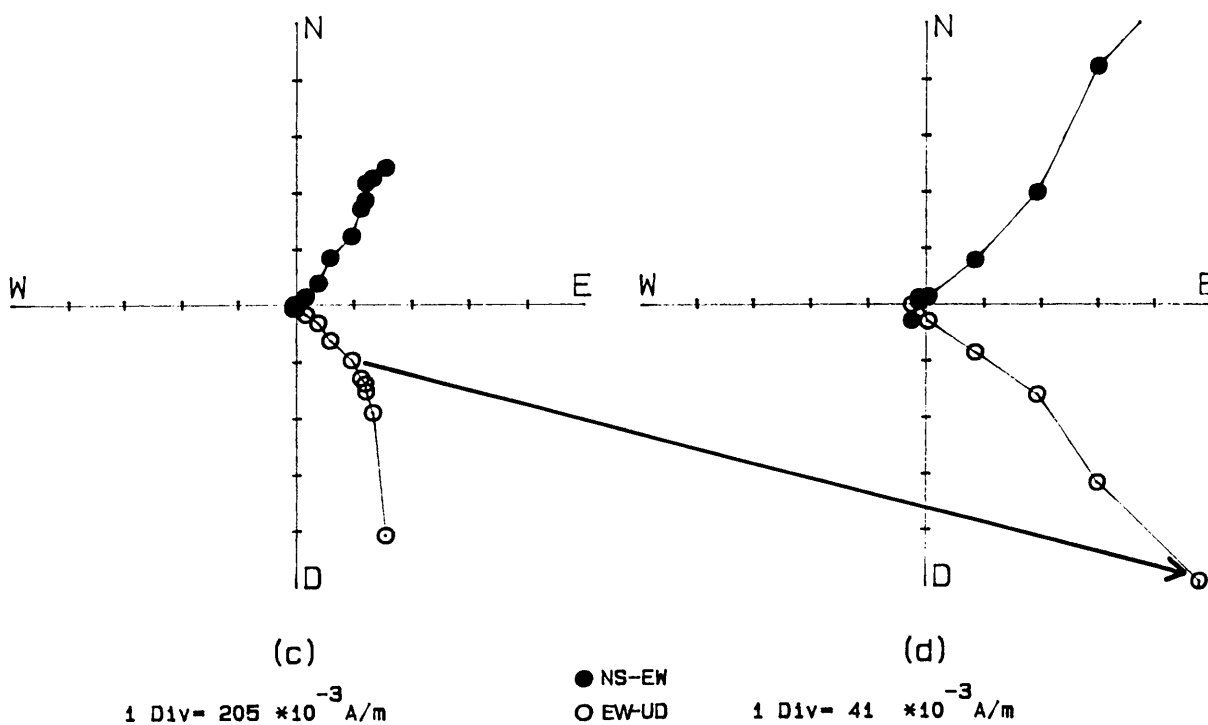
Sites I, E and C are situated in the Mapoch Gabbro-Norite. The NRM intensity of these sites ranges between $415 \times 10^{-3} \text{ Am}^{-1}$ and $12\,862 \times 10^{-3} \text{ Am}^{-1}$. Site I is situated on the contact between gabbro-norite and anorthosite containing abundant magnetite needles which could be the cause of the high NRM intensity. The normalised demagnetization intensity decay curves for all three sites show the presence of a low coercivity, secondary component and a moderate to high coercivity, primary component (Fig. 3.13(b)). Fig. 3.14 shows that Site I and E are reversely magnetized (positive inclinations) while site C has normal polarity.

Sites E and C show type 1 spatial patterns on the susceptibility plot in Fig. 3.15(a) with the X_{min} axes approximately vertical. The shapes of the ellipsoids are oblate (Fig. 3.15(b)). From both the susceptibility plot and the Flinn diagram of Site I (Fig. 3.16) it is evident that the gabbro-norite contains inclusions of anorthosite, which have different anisotropies. The



(a)

(b)

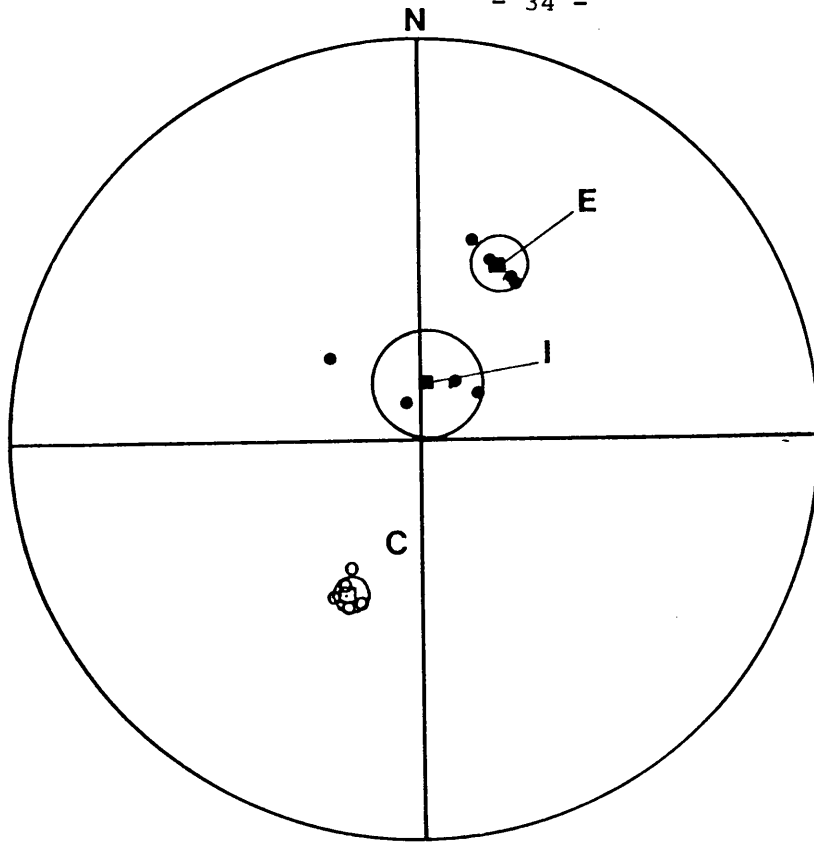


(c)

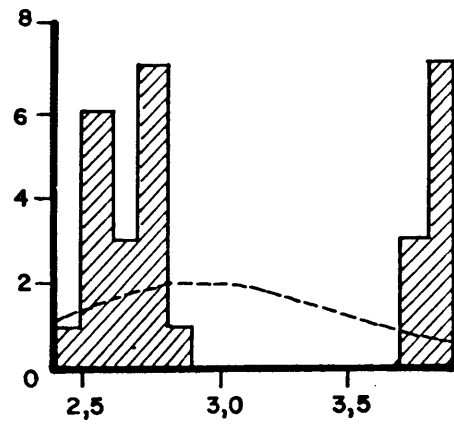
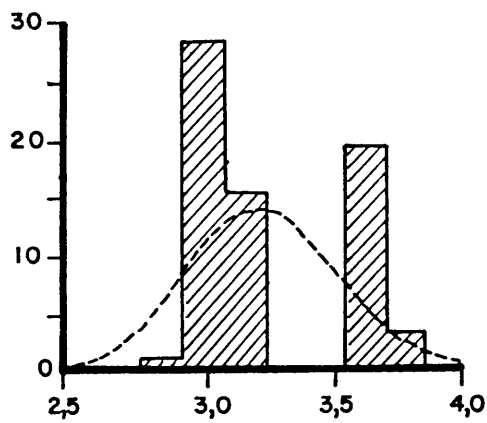
(d)

Fig. 3.13

(a) Stereographic projections (plotting convention as in Fig. 3.4), (b) intensity decay curve and (c+d) Zijderveld plots for specimen E3b submitted to AF demagnetization.



(a)



Log₁₀ susceptibility (x 10⁶ SI)

Log₁₀ INT after AF demagnetization
(x 10⁻³ Am⁻¹)

(b)

Fig. 3.14 (a) Sample and site mean directions with the circle of 95% confidence (plotting convention as in Fig. 3.4), and (b) histograms of the logarithmic susceptibility and intensity of magnetization after bulk AF demagnetization of sites C, E and I situated in subzone C of the main zone.

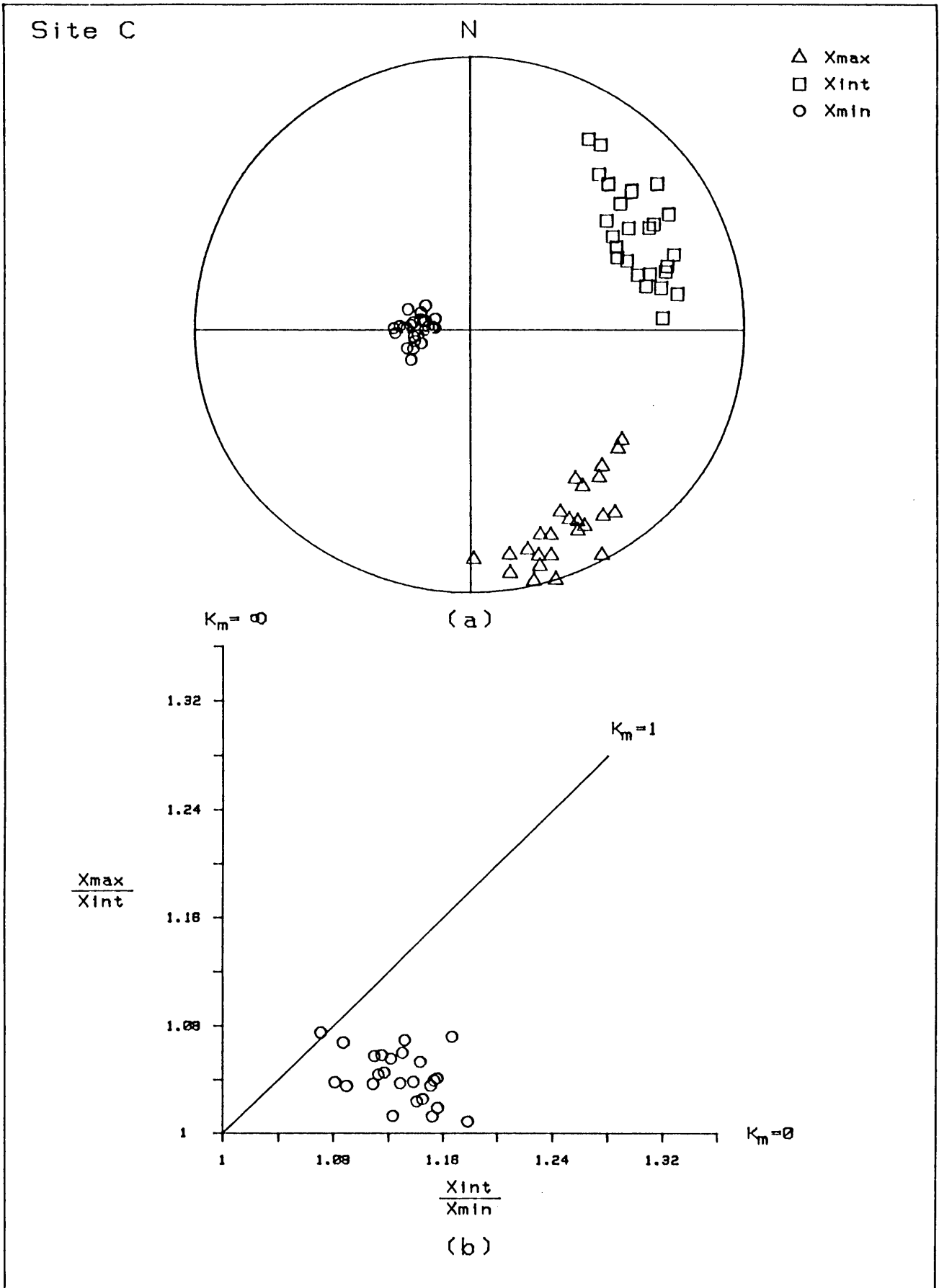


Fig. 3.15 Magnetic anisotropy data for site C. Plotting conventions as in Fig. 3.10.

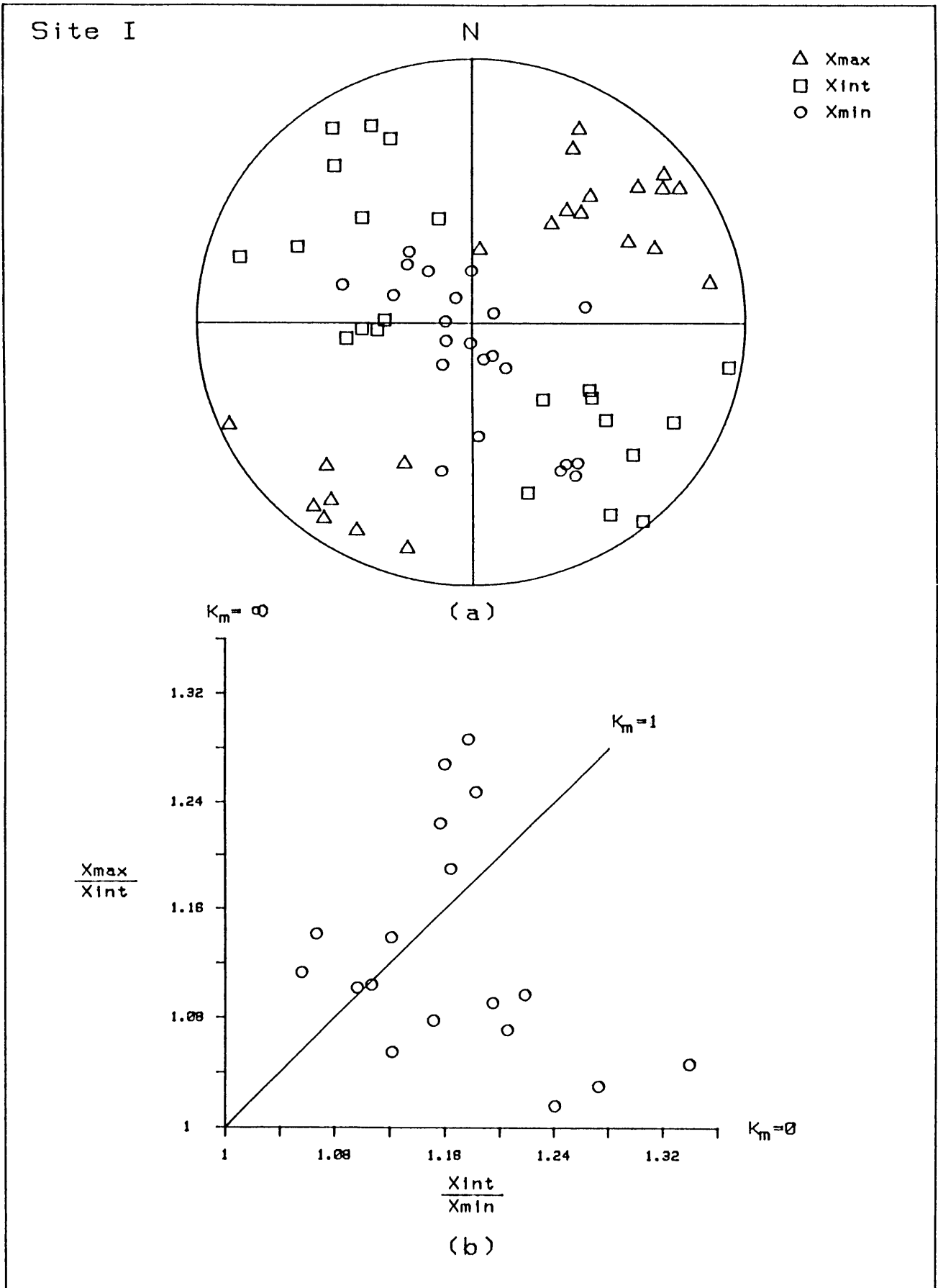


Fig. 3.16 Magnetic anisotropy data for site I. Plotting conventions as in Fig. 3.10.

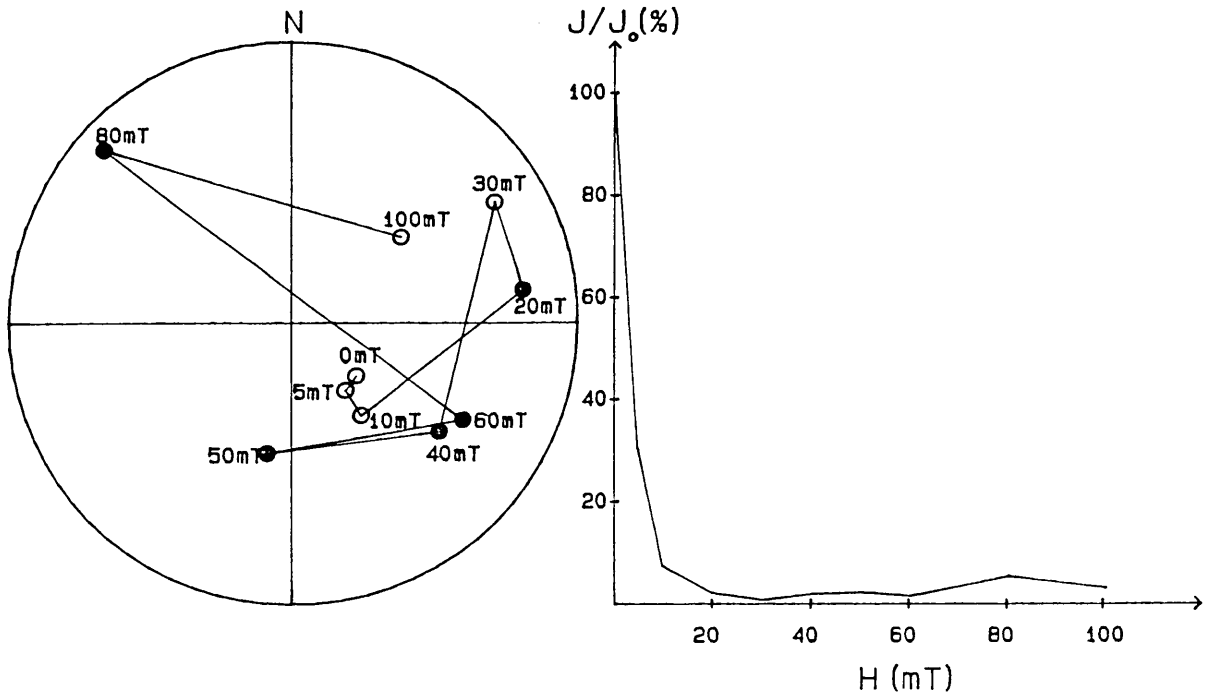
histogram plots of the intensity of magnetization of site E, C and I are given in Fig. 3.14(b). The mean value $1172 \times 10^{-3} \text{ Am}^{-1}$ given by the lognormal distribution curve is not representative as the high intensity samples from site I affects the calculations. The mean susceptibility for this unit is $1.786 \times 10^{-6} \text{ SI}$ and the Königsberger ratio (Q_2) is 28. From the high Q_2 value and the anisotropy data it is evident that the main carrier of the remanent magnetization are magnetite lamellae in the pyroxene and plagioclase crystals (Hattingh, 1983) which have a high degree of shape anisotropy, with the X_{max} and X_{int} axes approximately horizontal. The direction of magnetization of sites I and E fall in the group formed by sites B, D and F from subzone A of the main zone while site C can be grouped with group BMZ4AF (Hattingh, 1983), representing four sites situated in subzone C of the main zone.

Upper Zone Subzone B

Five sites are situated in streambeds in the Ironstone Magnetite Gabbro from which only three could be used after AF demagnetization. This zone is characterised by high values for both the NRM and induced intensities of magnetization (Fig. 3.5). The intensity response curves to stepwise AF demagnetization of specimens from sites G, L, M and N all have a very characteristic shape, indicating that approximately 80% of the NRM intensity is destroyed after 10 mT (Fig. 3.17(b)). This patterns indicates very "soft" and sometimes unstable magnetizations.

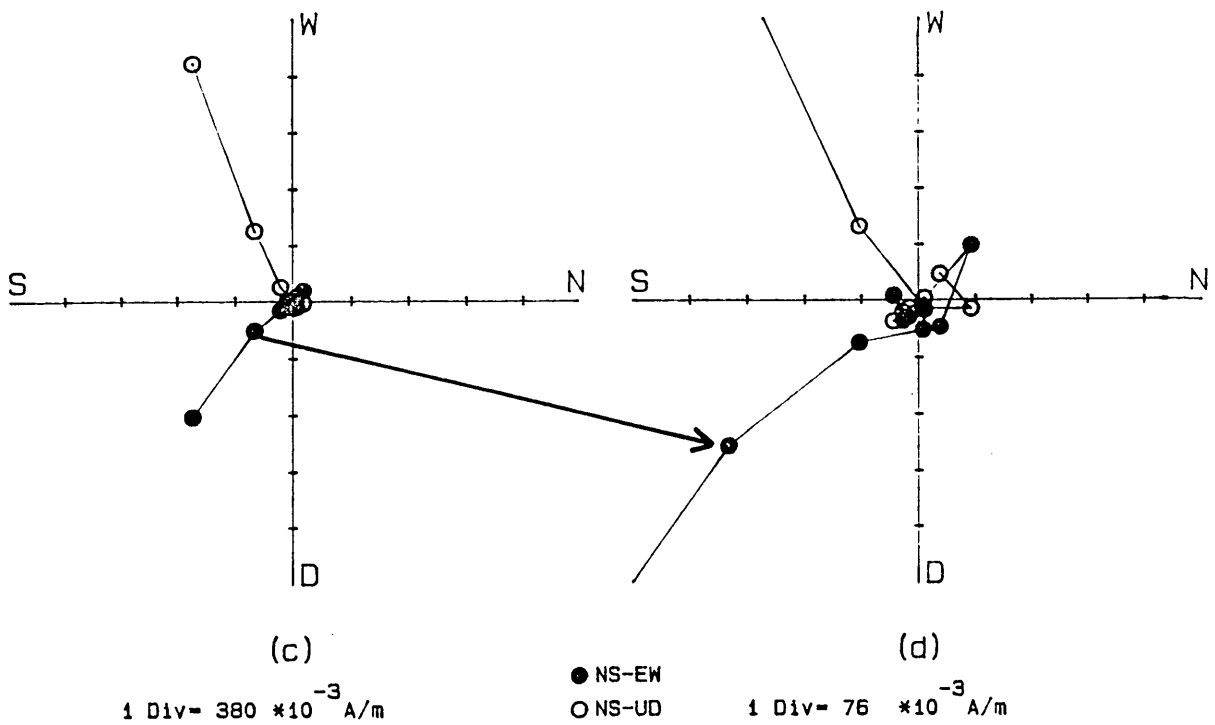
Site H is situated on the contact between a dyke and the magnetite gabbro. These data couldn't be used as a baked contact test as insufficient samples were taken. The anisotropy data from this site clearly indicate the difference in orientation of the X_{max} axes of samples taken in the magnetite gabbro to that of samples taken in the dyke (Fig. 3.18).

During stepwise AF demagnetization of specimen M6c, rotational remanent magnetization (RRM) (Hillhouse, 1977) was observed (Fig. 3.19). Thermal demagnetization of specimen M2c proved that a stable magnetization was present (Fig. 3.20), but as only one specimen was submitted to thermal demagnetization, site M was rejected from further analyses.



(a)

(b)



(c)

(d)

Fig. 3.17 (a) Stereographic projections (plotting convention as in Fig. 3.4), (b) intensity decay curve and (c+d) Zijderveld plots for specimen N1b submitted to AF demagnetization.

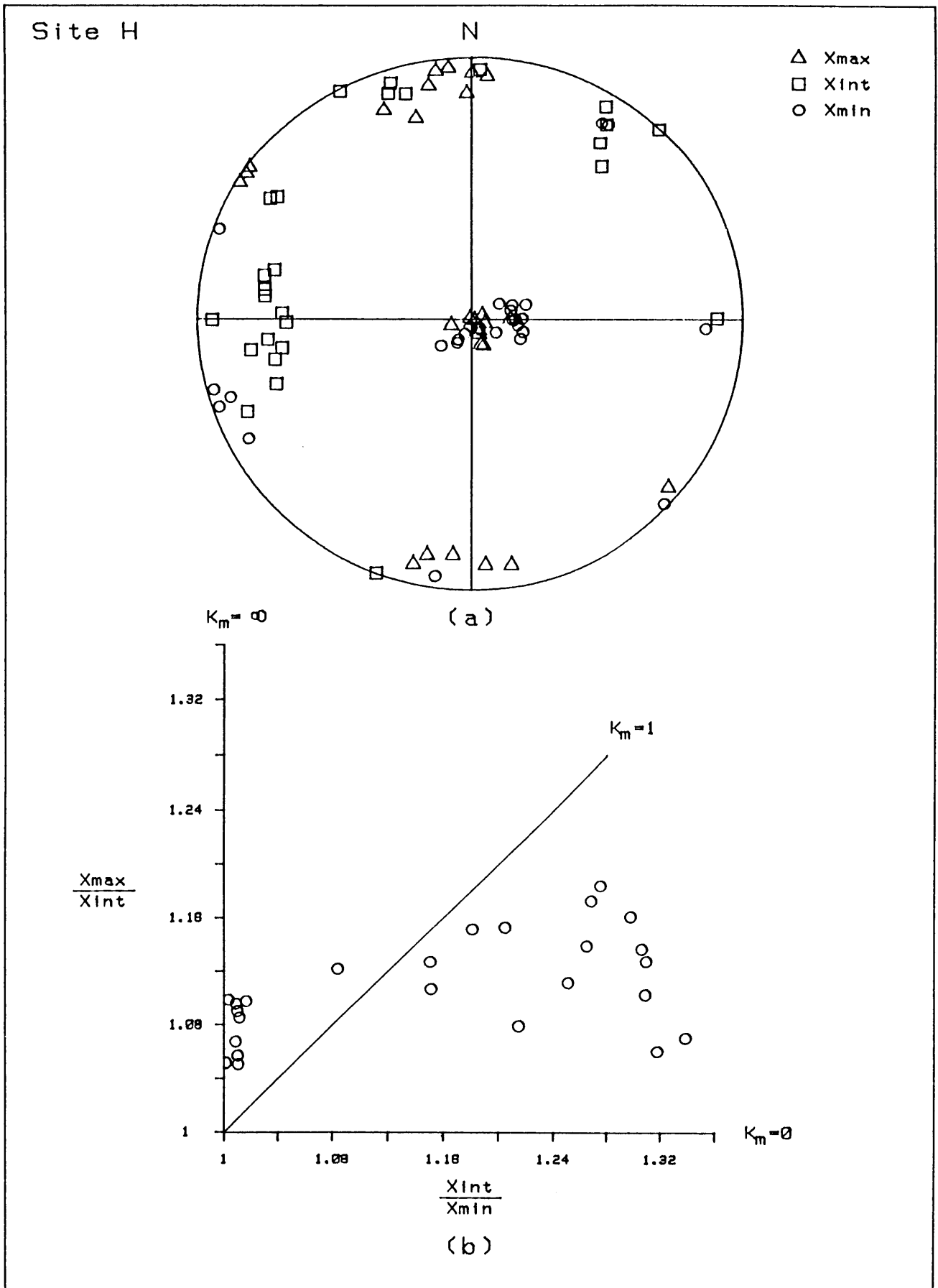


Fig. 3.18 Magnetic anisotropy data for site H. Plotting conventions as in Fig. 3.10.

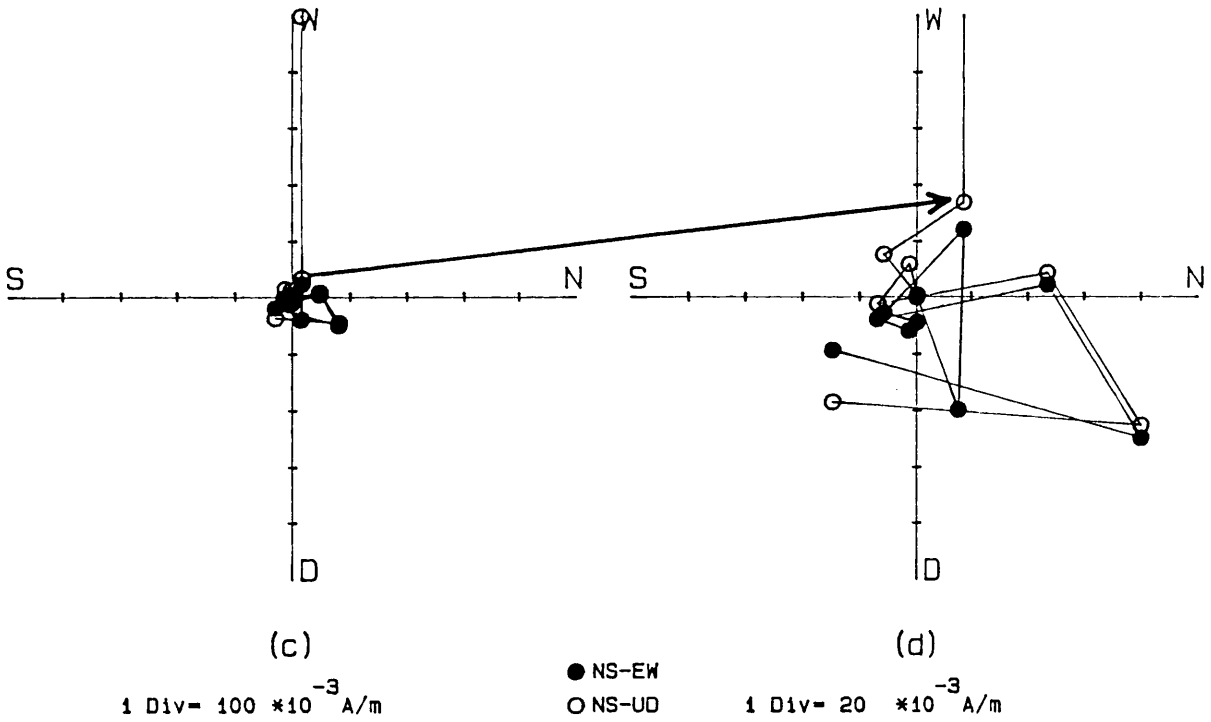
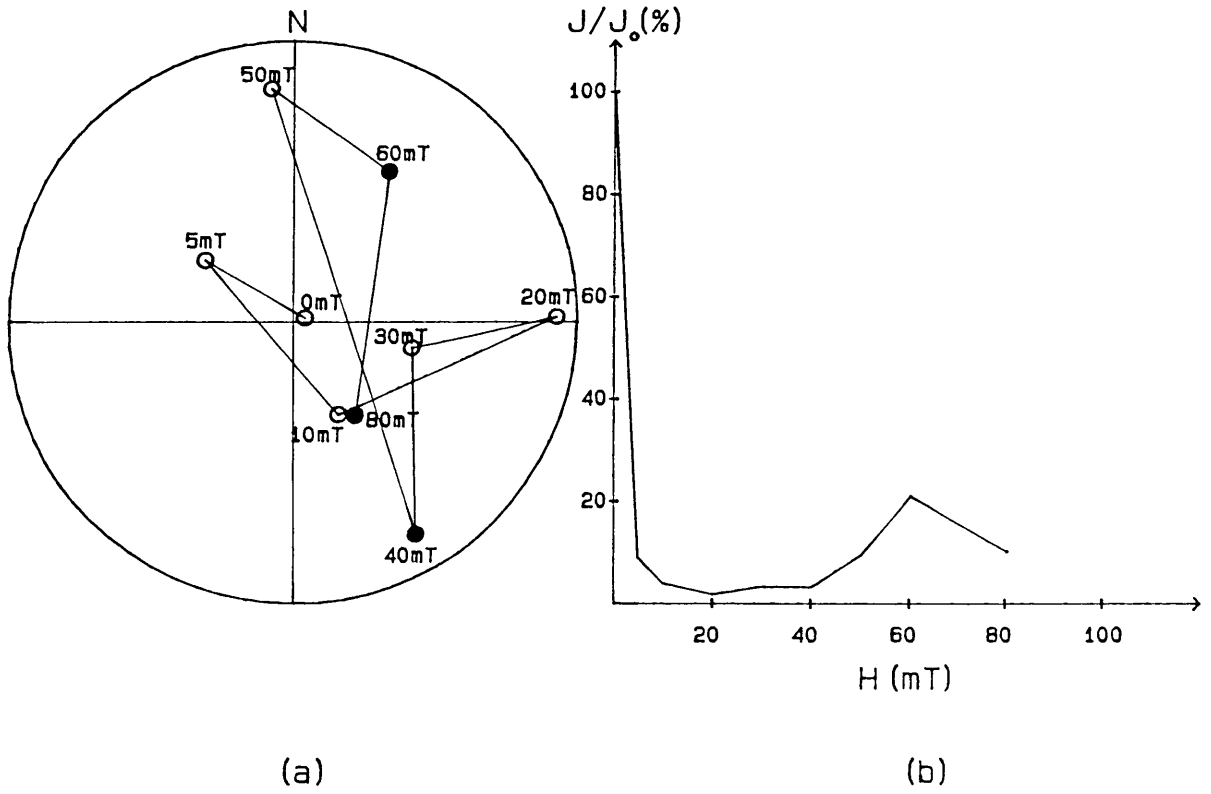


Fig. 3.19 (a) Stereographic projections (plotting convention as in Fig. 3.4), (b) intensity decay curve and (c+d) Zijderveld plots for specimen M6c submitted to AF demagnetization.

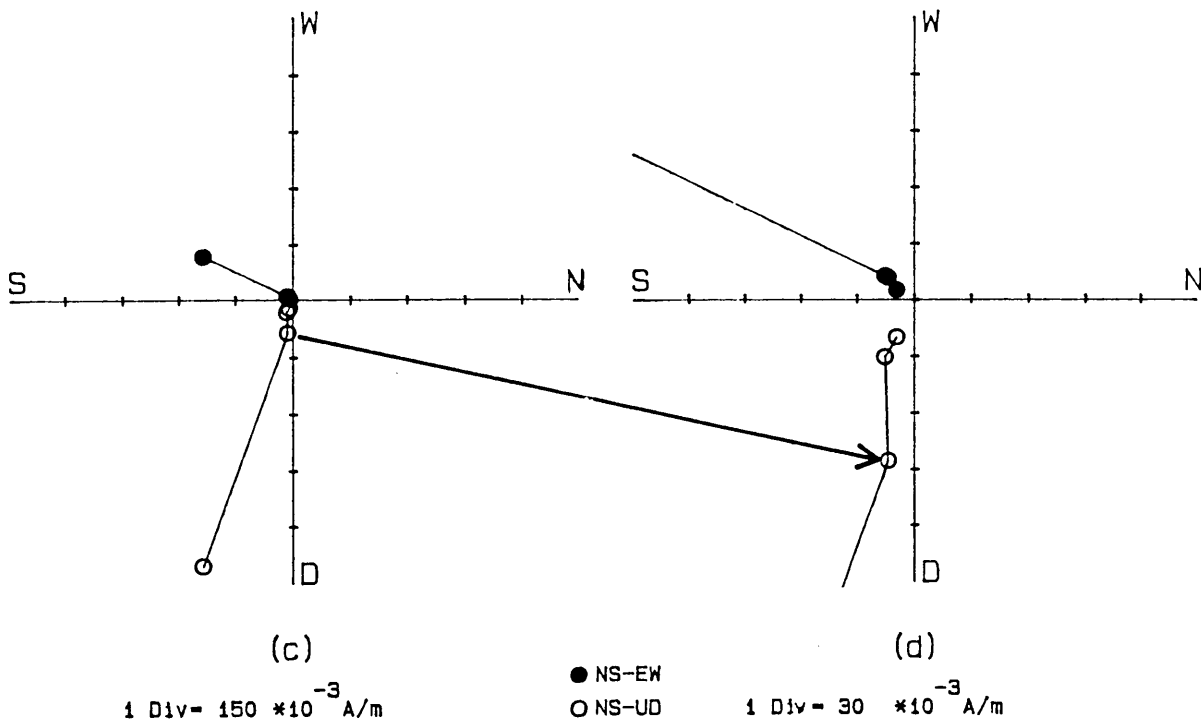
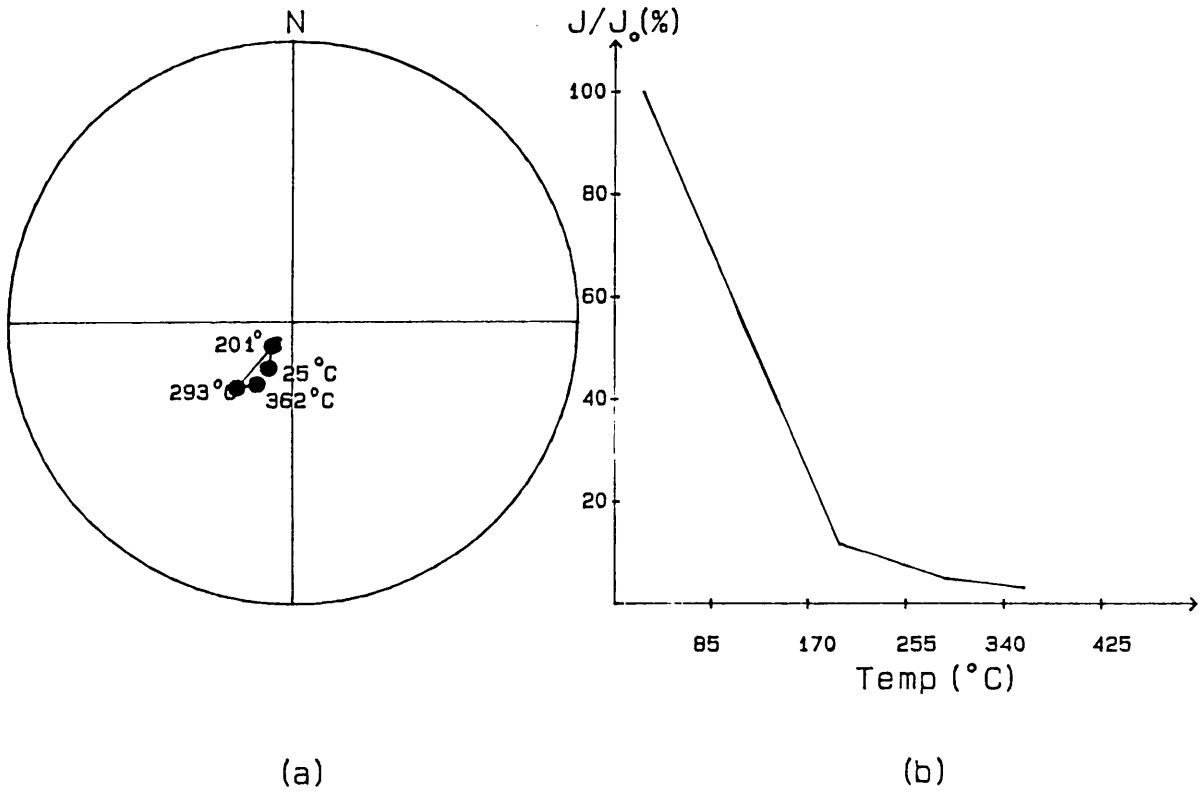


Fig. 3.20 (a) Stereographic projections (plotting convention as in Fig. 3.4), (b) intensity decay curve and (c+d) Zijderveld plots for specimen M2c submitted to thermal demagnetization.

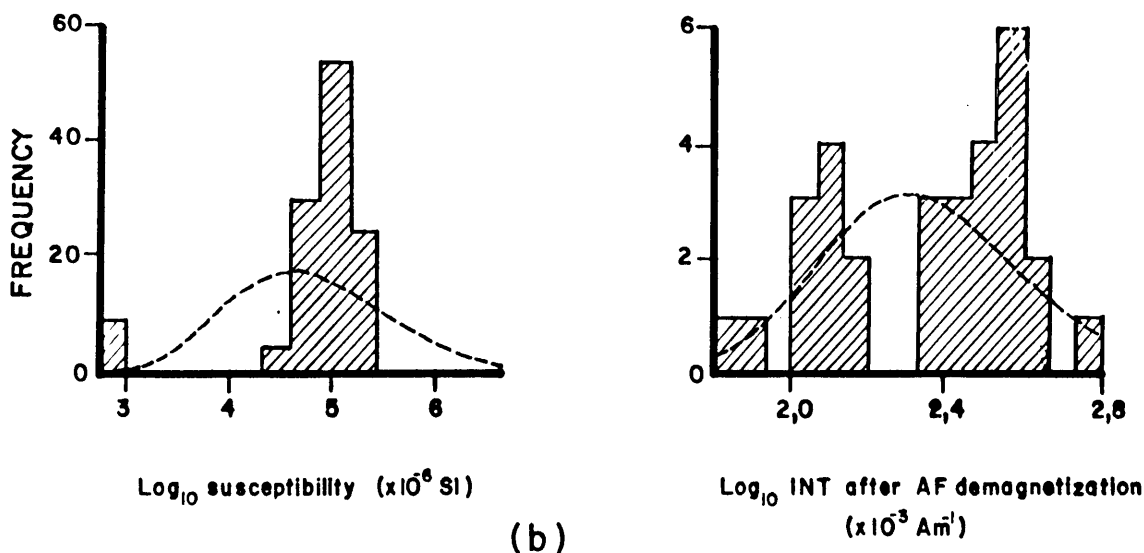
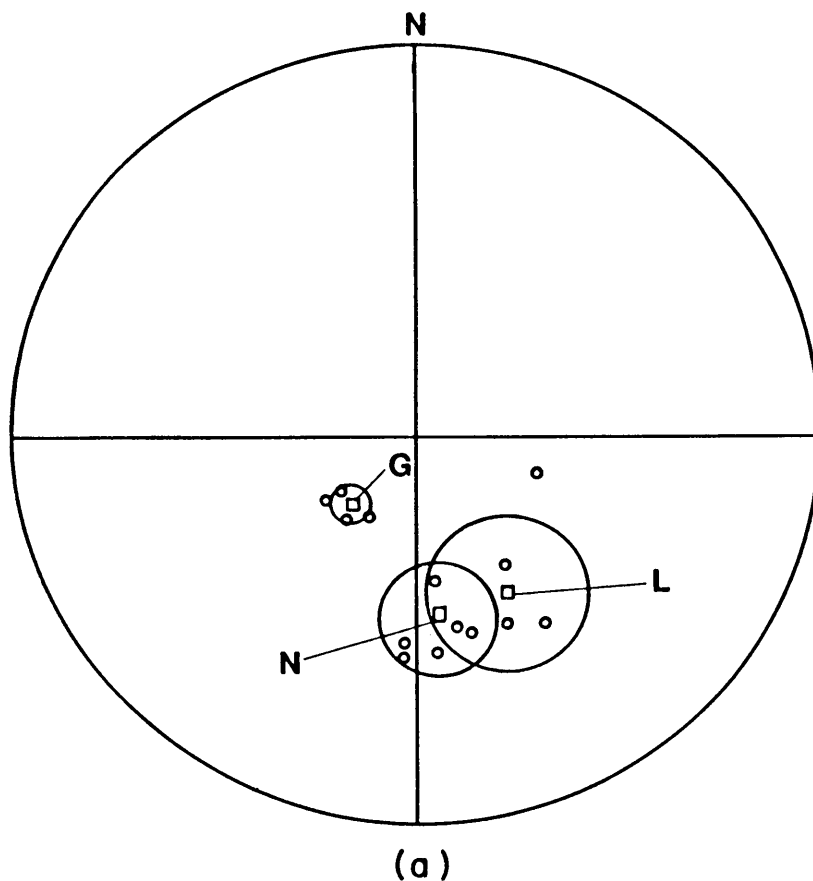


Fig. 3.21 (a) Sample and site mean directions with the circle of 95% confidence (plotting convention as in Fig. 3.4), and (b) histograms of the logarithmic susceptibility and intensity of magnetization after bulk AF demagnetization of sites G, L and N situated in subzone B of the upper zone.

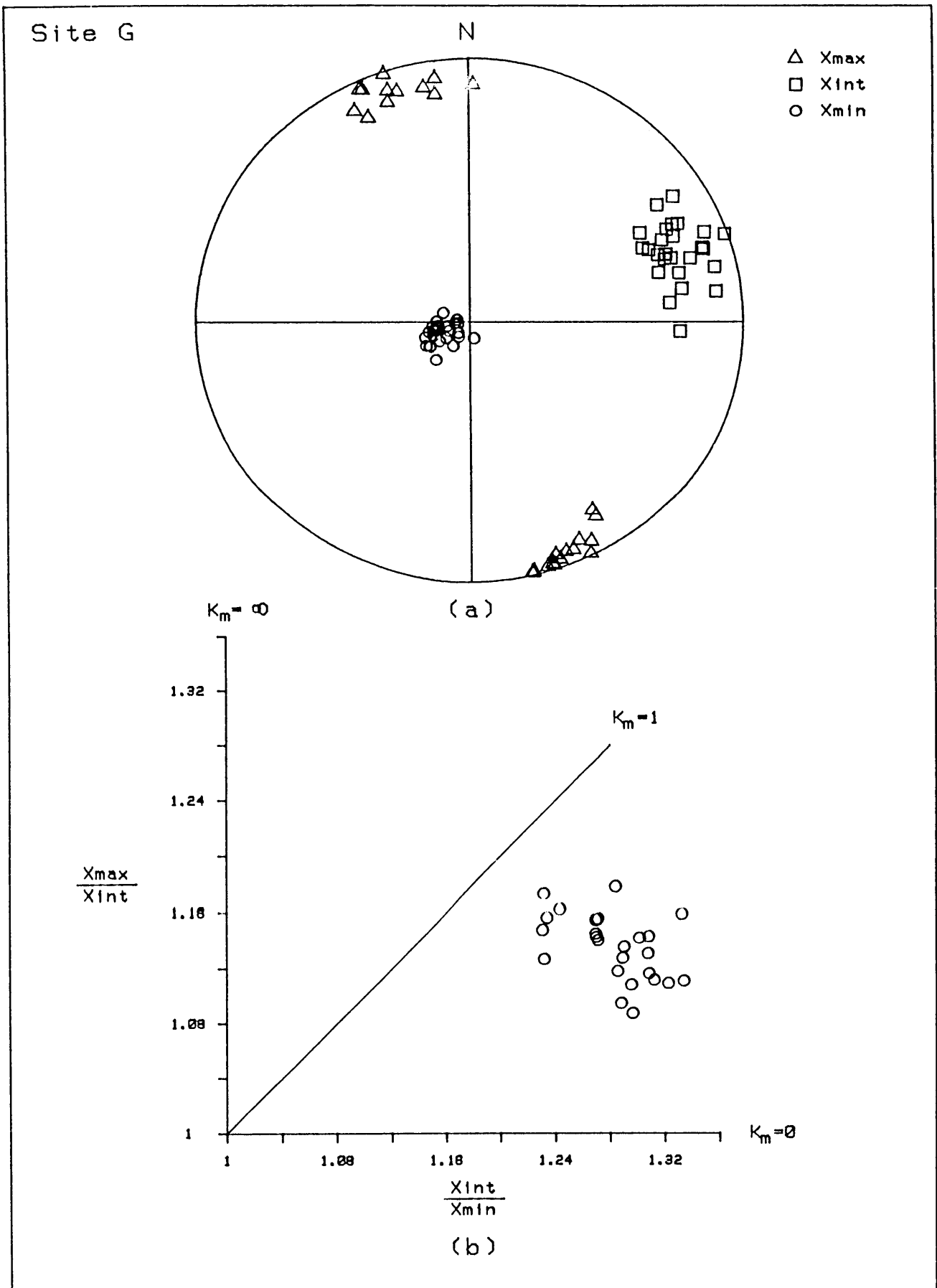


Fig. 3.22 Magnetic anisotropy data for site G. Plotting conventions as in Fig. 3.10.

The magnetization directions of sites G, N and L are normal and plotted in Fig. 3.21(a).

All the sites (excluding site M) show type 1 spatial patterns on the susceptibility plots and plot in the flattening field (0 Km⁻¹) on the Flinn diagrams (Fig. 3.22). The Xmin axes are approximately vertical poles to the plane of high susceptibility which lies within the igneous layering.

The mean susceptibility of all the samples from this zone is $68\ 077 \times 10^{-6}$ SI and the mean intensity of magnetization after AF demagnetization is $222 \times 10^{-3} \text{ Am}^{-1}$ (Fig. 3.21(b)). Even though the Königsberger ratio (Q_2) is 0,1, the angle between the earth's field and the remanent magnetization directions of the sites is large, and therefore the total resultant magnetization direction for subzone B of the upper zone will be slightly deflected from the direction of the earth's field.

Upper Zone Subzone C

Due to the absence of suitable sampling sites in the upper zone only two sites were sampled in this subzone viz in the Luipershoek Olivine Diorite. Site A had a very low NRM intensity ($<5 \times 10^{-3} \text{ Am}^{-1}$) and had to be rejected from further analyses. Bulk AF demagnetization improved the grouping of the magnetization of site J but as RRM was observed on the data, the intensity of magnetization is not reliable. Site J is reversely magnetized, with an intensity of magnetization of $90 \times 10^{-3} \text{ Am}^{-1}$, susceptibility of $1\ 400 \times 10^{-6}$ SI and a Königsberger ratio of 3 (Fig. 3.23).

Both sites have ellipsoid shapes which fall in the constriction field (1 Km⁻¹) on the Flinn diagram (Fig. 3.24(b)). The stereographic projections of the susceptibility axes show a type 3 spatial pattern with the Xmax axes nearly vertical (Fig. 3.24(a)).

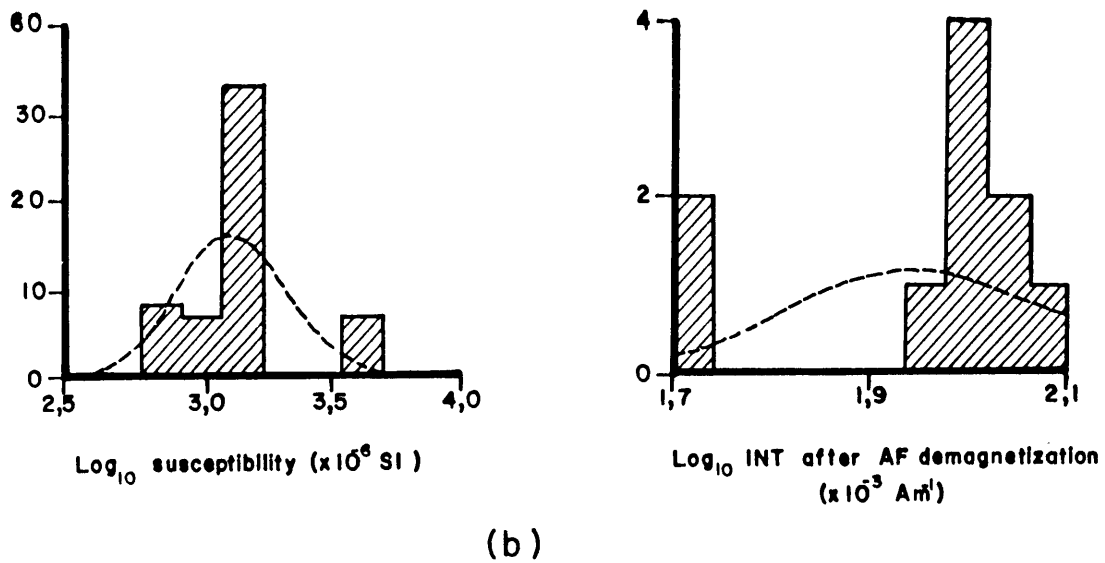
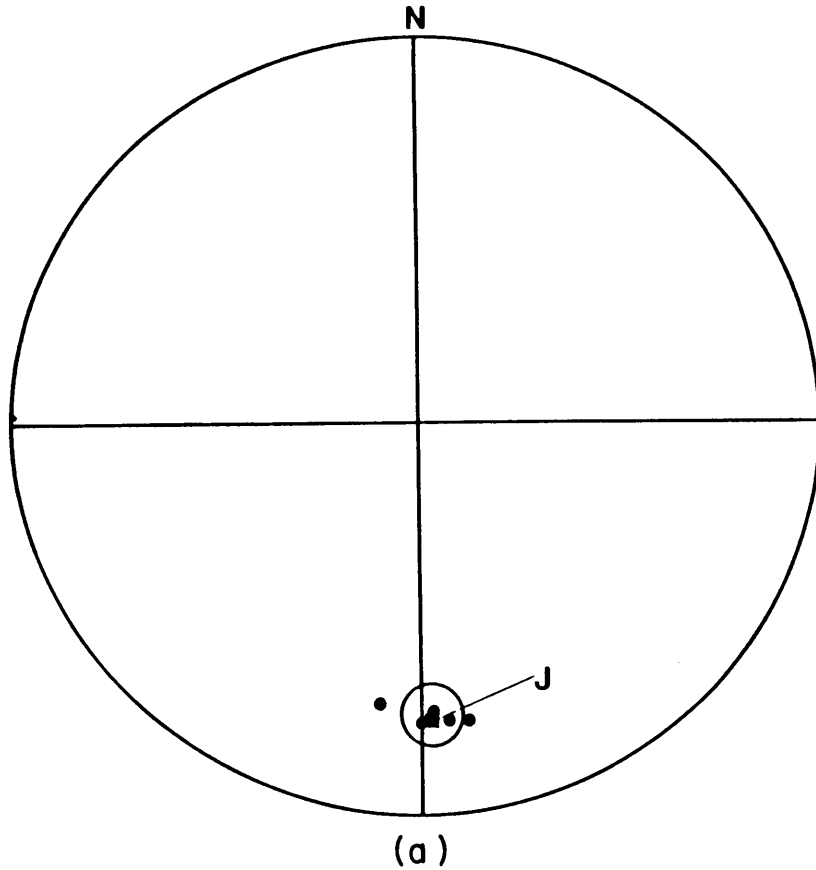


Fig. 3.23 (a) Sample and site mean directions with the circle of 95% confidence (plotting convention as in Fig. 3.4), and (b) histograms of the logarithmic susceptibility and intensity of magnetization after bulk AF demagnetization of sites J, situated in subzone C of the upper zone.

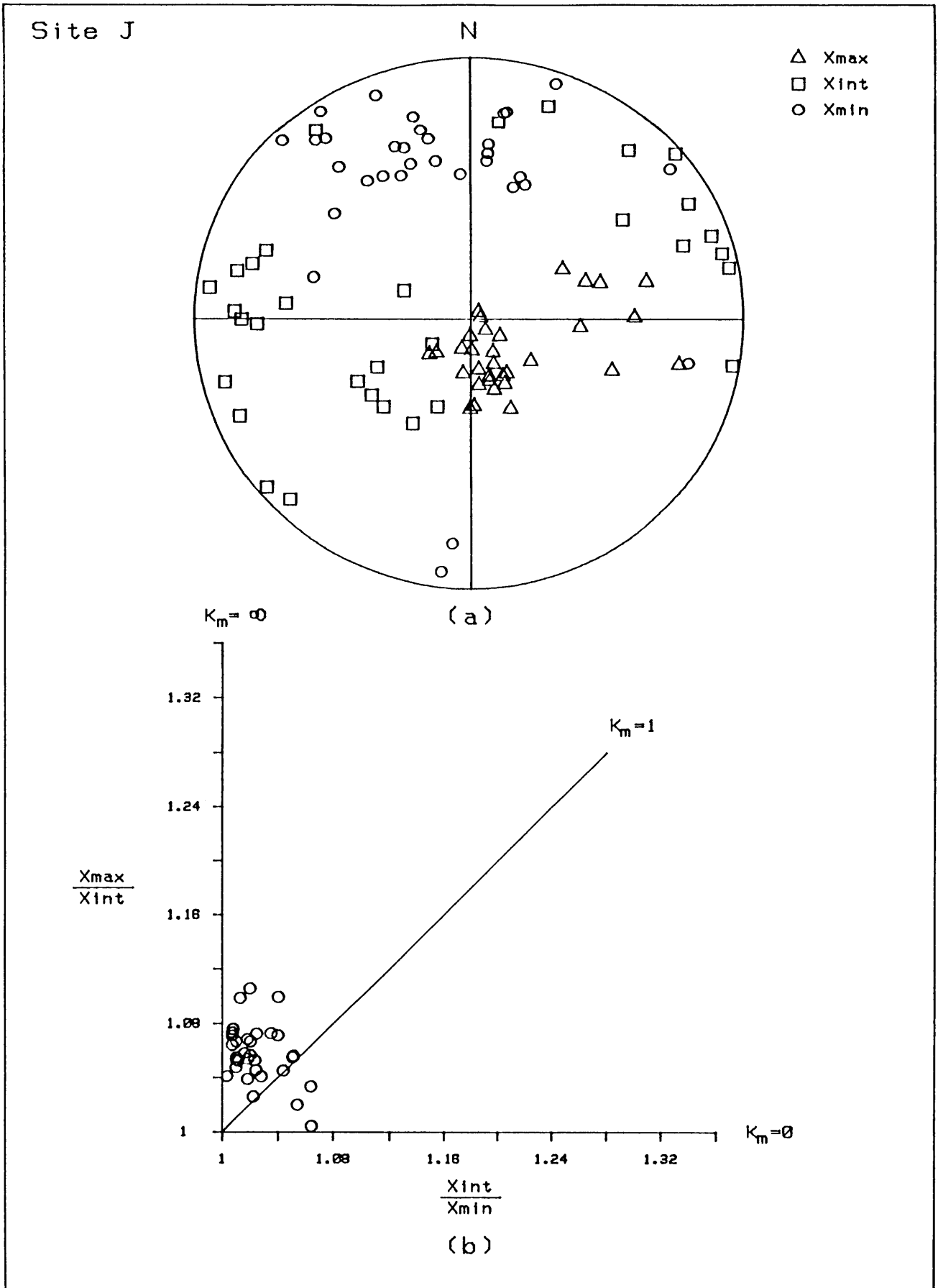


Fig. 3.24 Magnetic anisotropy data for site J. Plotting conventions as in Fig. 3.10.

Site J cannot be used in further calculations, as more sampling sites are needed in this subzone.

Polarity zones and intensity of magnetization

The data from this study and the data from Hattingh (1983) were used to calculate a mean direction of magnetization for the normal and reversed polarity zones, and the mean remanent and induced intensity of magnetization for each subzone (Table 3.4).

TABLE 3.4 SUMMARY OF INDUCED AND REMANENT INTENSITY OF
MAGNETIZATION FOR EACH SUBZONE OF THE RUSTENBURG LAYERED SUITE

Zone	Induced intensity ($\times 10^{-3} \text{ Am}^{-1}$)	Remanent intensity ($\times 10^{-3} \text{ Am}^{-1}$)
Upper Zone Subzone C	33	90
B	1627	222
A*	1184	310
Main Zone Subzone C*	25	135
C	43	1172
B*	47	2265
A*	14	1366
A	17	121

* Data from Hattingh (1983)

The magnetization directions of sites in the reversed polarity zone in the main zone are listed in Table 3.5 and plotted in Fig. 3.25.

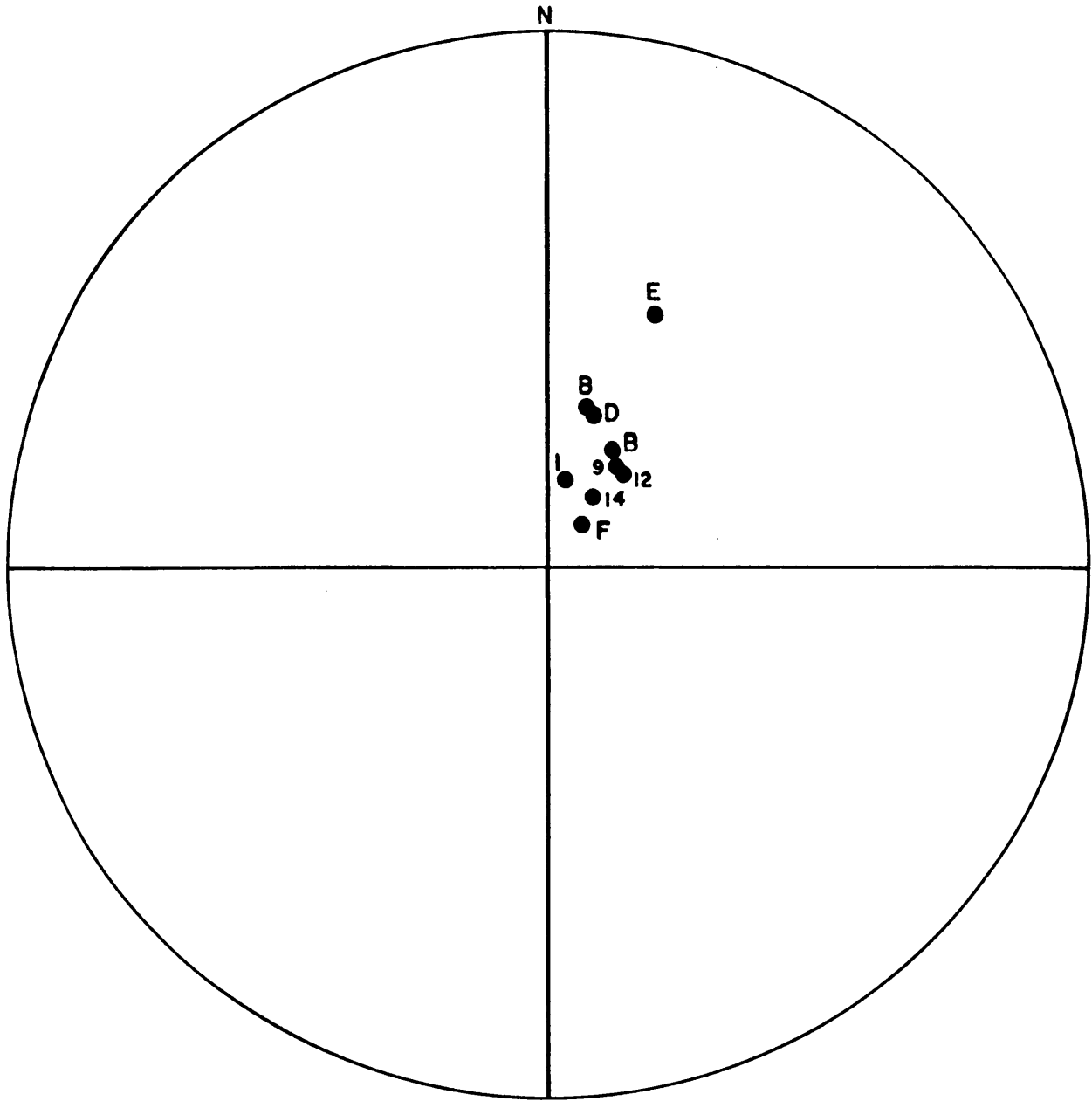


Fig. 3.25 Stereographic projection of magnetization directions of sites in the reversed polarity zone MPZB in the main zone of the Rustenburg Layered Suite. Plotting convention as in Fig. 3.4.

TABLE 3.5 MAGNETIZATION DIRECTIONS OF SITES IN THE
REVERSED POLARITY ZONE (MPZB)

Site	Declination	Inclination
B	15,5°	56,2°
D	18,8°	56,7°
E	24,2°	36,0°
F	40,7°	77,6°
I	39,1°	67,8°
9*	35,7°	64,4°
12*	38,4°	64,2°
13*	37,8°	64,2°

* Data from Hattingh (1983)

The following group statistics were calculated from Table 3.5: N=8;
D=29,6°; I=62,4°; $\alpha_{95} = 8,1°$; k = 41

The magnetization directions of sites in the normal polarity zone MPZC/1
(Subzone C of the main zone) are listed in Table 3.6 and plotted in
Fig. 3.26.

TABLE 3.6 MAGNETIZATION DIRECTIONS OF SITES IN THE NORMAL
POLARITY ZONE MPZC/1 (SUBZONE C OF THE MAIN ZONE)

Site	Declination	Inclination
C	201,8°	-45,0°
19*	198,6°	-62,9°
22*	211,5°	-77,5°
33*	202,7°	-14,7°

* Data from Hattingh (1983)

The data listed in Table 3.6 formed a group with the following statistics:
N = 4; D = 202,4°; I = -50,4°; $\alpha_{95} = 32,1°$; k = 9

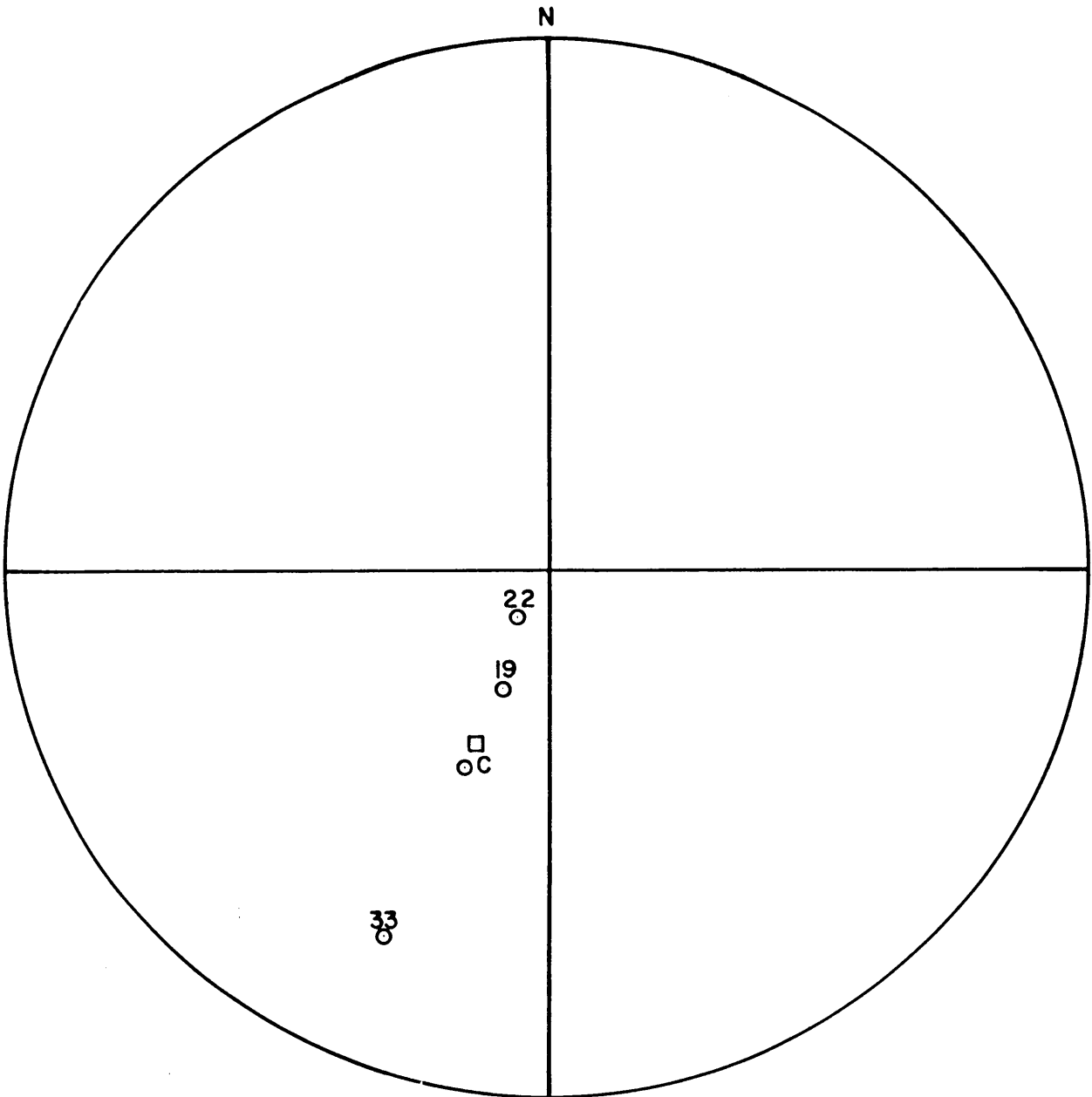


Fig. 3.26 Stereographic projection of magnetization directions of sites in the normal polarity zone MPZC/1 (subzone C of the main zone) of the Rustenburg Layered Suite. Plotting convention as in Fig. 3.4.

The magnetization directions of sites situated in subzone A and B of the upper zone were grouped to form the normal polarity zone MPZC/2 (Table 3.7 and Fig. 3.27) , with the following group statistics:

$$N = 7; D = 186,3^{\circ}; I = -59,8; \alpha_{95} = 15,8^{\circ}; k = 16$$

TABLE 3.7 MAGNETIZATION DIRECTIONS OF SITES IN THE NORMAL POLARITY ZONE MPZC/2 (UPPER ZONE)

Site	Declination	Inclination
G	219,7°	-62,8°
L	151,2°	-38,6°
N	172,4°	-37,4°
15*	231,1°	-71,0°
16*	194,8°	-52,4°
17*	180,5°	-75,1°
18*	198,3°	-62,9°

* Data from Hattingh (1983)

The total resultant intensity J , declination D , and inclination I completely define the magnetization of each subzone. The horizontal and vertical components of J are denoted by H and Z . The horizontal component can be resolved into two components X (northwards) and Y (eastwards). The various components are related by the equations:

$$H = J \cos I, Z = J \sin I, \tan I = Z/H$$

$$X = H \cos D, Y = H \sin D, \tan D = Y/X$$

$$J^2 = H^2 + Z^2 = X^2 + Y^2 + Z^2$$

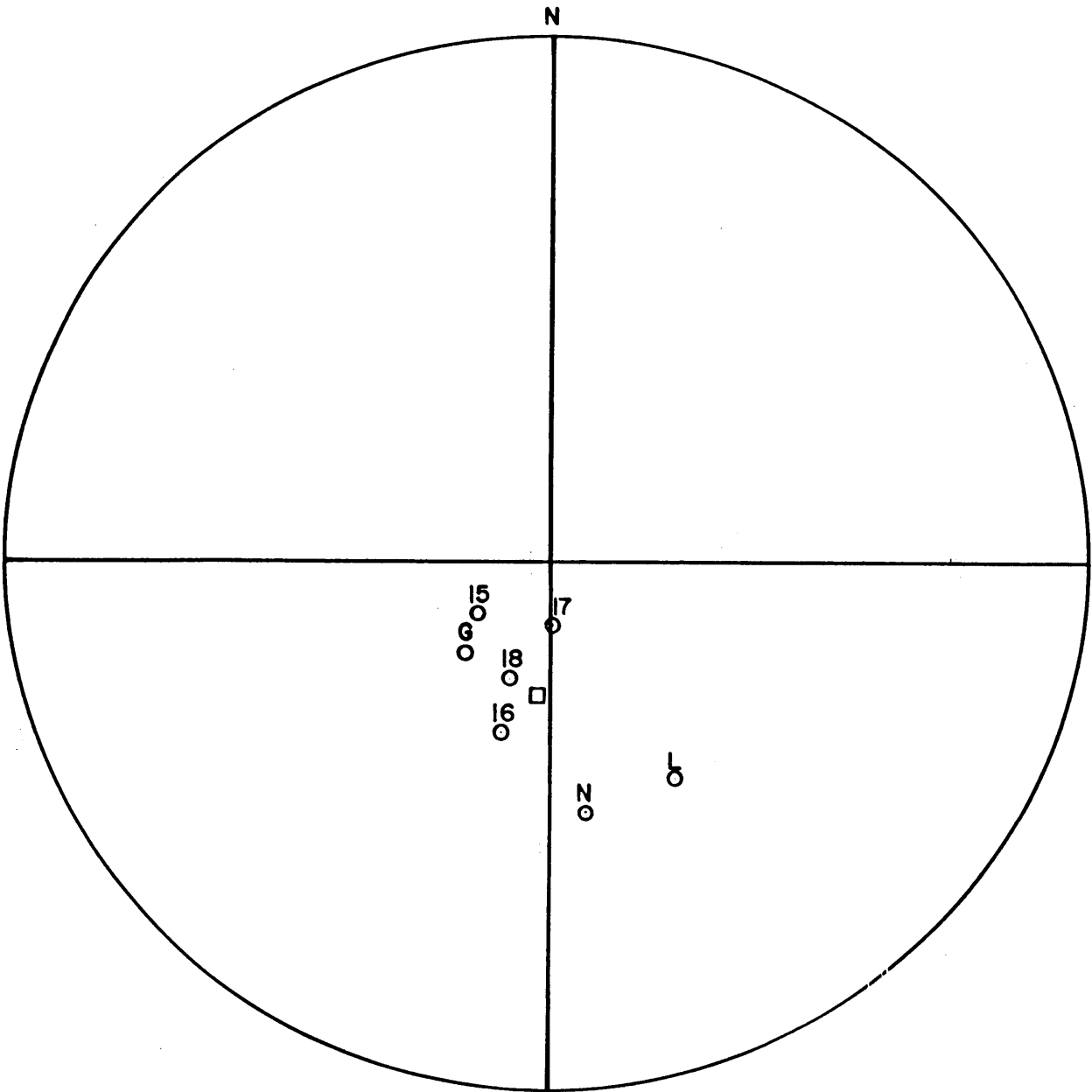


Fig. 3.27 Stereographic projection of magnetization directions of sites in the normal polarity zone MPZC/2 (upper zone) of the the Rustenburg Layered Suite. Plotting convention as in Fig. 3.4.

An example of the method of calculating the resultant magnetization vector follows:

Example 1 Magnetization vector for subzone B of the upper zone

Remanent vector:

$$D = 186^\circ \quad I = -60^\circ \quad J = 222 \times 10^{-3} \text{ Am}^{-1}$$
$$H_R = 111 \times 10^{-3} \quad X_R = -110 \times 10^{-3} \quad Y_R = -12 \times 10^{-3} \quad Z_R = -192 \times 10^{-3}$$

Induced vector:

$$D = 344^\circ \quad I = -60^\circ \quad J = 1627 \times 10^{-3} \text{ Am}^{-1}$$
$$H_I = 814 \times 10^{-3} \quad X_I = 782 \times 10^{-3} \quad Y_I = -224 \times 10^{-3} \quad Z_I = -1409 \times 10^{-3}$$

Resultant vector:

$$X = X_R + X_I = 672 \times 10^{-3}$$
$$Y = Y_R + Y_I = -236 \times 10^{-3}$$
$$Z = Z_R + Z_I = -1601 \times 10^{-3}$$
$$D = 341^\circ \quad I = -66^\circ \quad J = 1752 \times 10^{-3} \text{ Am}^{-1}$$

Because of the large ranges of susceptibility and remanent intensity of magnetization one should actually calculate resultant vectors within these ranges. If the remanent vector in Example 1 had the same intensity as the induced vector, the following resultant vector would be calculated:

$$D = 265^\circ; \quad I = -84^\circ; \quad J = 2835 \times 10^{-3} \text{ Am}^{-1}$$

which is significantly different to that calculated in Example 1.

For the interpretation of magnetic anomalies, the best approach is to use the direction of magnetization for a certain zone and vary the susceptibility and remanent intensity within the ranges calculated from the logarithmic statistics.

Conclusions

1. The remanent intensity of magnetization of the subzones situated in the main zone is greater than the induced intensity of magnetization.
2. Most of the sites sampled have high susceptibility within the plane of layering.
3. The maximum susceptibilities are found in the upper zone.
4. The maximum remanent intensities of magnetization are found in the black magnetite gabbro of subzone B of the main zone.

4. QUALITATIVE INTERPRETATION

4.1 Total Field Aeromagnetic Map

The colour coded aeromagnetic map of the eastern Transvaal (in folder) was compiled from the following aeromagnetic surveys:

11/71	Potgietersrust
12/71	Pretoria
15/73	Nylstroom
21/74	Witbank
25/78	Barberton-Pilgrim's Rest

Figure 4.1 and Table 4.1 present the location, date, terrain clearance and flight-line directions of the above-mentioned surveys. The flight-line spacing for all the surveys is approximately 1 000 metres. The "warm" colours (red, purple) on the colour coded aeromagnetic map correspond to positive anomalies, while the "cold" colours (blue, black) correspond to negative anomalies. Note that the colour intervals are not constant.

The map displays a few anomaly groups. Firstly there is a north-trending, broad positive anomaly bounded by a negative on its eastern side and made distinctive by numerous minor superimposed positive peaks. The anomaly is coincident with the outcrop pattern of the upper zone of the Rustenburg Layered Suite and is caused by magnetic units within this zone. In the southern sector of the map this broad anomaly is fringed by a remanent anomaly which coincides with the outcrop of the black magnetite gabbro from the main zone of the Rustenburg Layered Suite.

The second anomaly group comprises a number of north-northeast trending high frequency anomalies, certain of which can be traced individually for 100 km or more. Some of the high frequency anomaly patterns are expected to

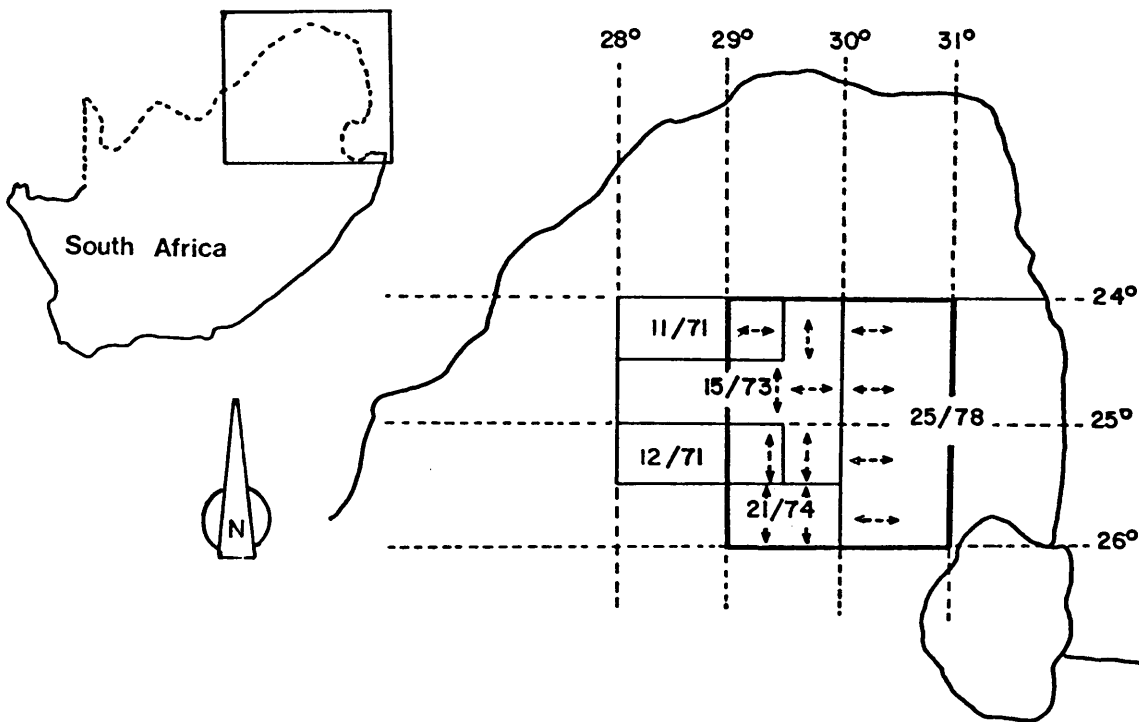


Fig. 4.1 Locality map of the aeromagnetic surveys used in the compilation of the colour coded aeromagnetic map of the eastern Transvaal.

TABLE 4.1 FLIGHT SPECIFICATIONS FOR THE AEROMAGNETIC SURVEYS OF THE AREA BETWEEN 29°-31° LONGITUDE AND 24°-26° LATITUDE

SURVEY	DATE	DATUM	HEIGHT
11/71 POTGIETERSRUS	DES 1971-APRIL 1972	26 000 nT	150 m
12/71 PRETORIA	DES 1971-APRIL 1972	28 000 nT	150 ± 50 m
15/73 NYLSTROOM	JUN, JUL 1974	25 000 nT	150 ± 15 m
21/74 WITBANK	FEBR 1975	25 000 nT	150 ± 15 m
25/78 BARBERTON/ PILGRIM'S REST	FEBR-OCT 1979	25 000 nT	100 ± 15 m

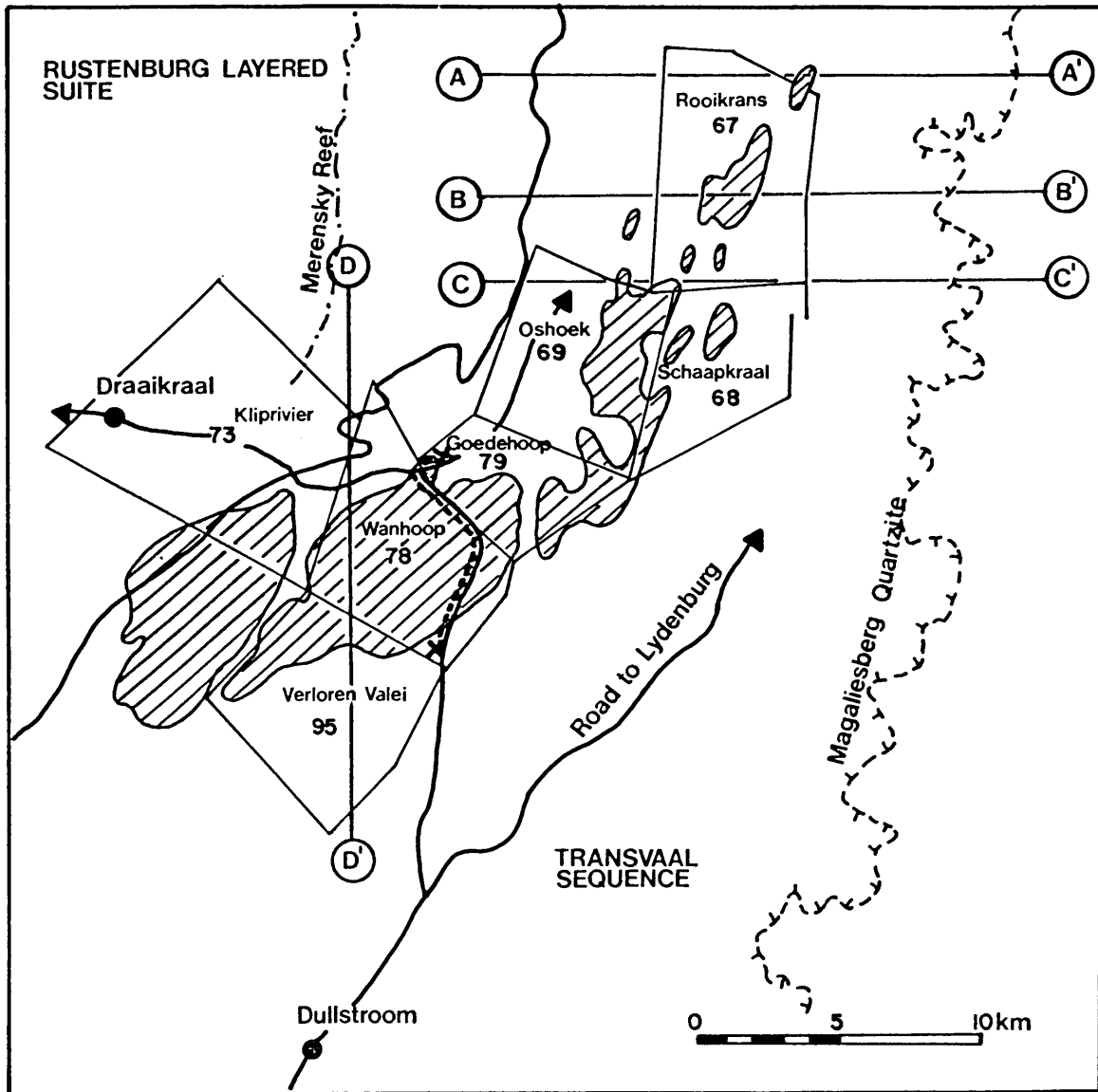
be caused by near vertical inductively magnetized dykes, while a few probably arise from remanently magnetized dykes.

The third distinctive group is formed by iron-rich rocks from the Transvaal Supergroup. The Penge iron-formation of the Chuniespoort Group has a distinctive magnetic pattern which follows the margin of the Transvaal Basin in the northern sector of the map. Iron-rich shales from the Timeball Hill Formation of the Pretoria Group are also preserved along the eastern escarpment in the topography and cause typical magnetic anomalies.

The anomalies described above can easily be correlated with geological units (Fig. 2.1), as the causative magnetic bodies outcrop. However, in the Dullstroom-Lydenburg and Nelspruit areas, the fourth group which consists of 2 magnetic anomalies, is found which cannot be explained by the known surface geology. The first is a negative magnetic anomaly in the Dullstroom-Draaikraal area that is approximately 30 km long and best developed on the farm Wanhoop 78 (Fig. 4.2). The second is due to a magnetic body west of Nelspruit that has a well defined, east-west trending, positive anomaly on the northern boundary and a negative anomaly on the southern boundary, which indicates that the body is magnetized by induction (Fig. 4.3). This anomaly will be referred to as the Mooiland anomaly, named after the farm Mooiland 294 which is situated in close proximity to the eastern margin of the interpreted magnetic body.

4.2 The Gravity Anomaly Maps

The 1:1 000 000 isostatic gravity anomaly map (Kleywegt, 1986) of the area between latitudes 24°S and 26°S and longitudes 29°E and 31°E (Map 3 in folder) shows positive and negative anomalies varying between +80 mgal and -60 mgal. As the isostatic corrections are calculated for a crustal density of 2670 kg/m³, rocks with a positive or negative density contrast with respect to the crustal rocks account for these anomalies.



LEGEND

- ✕ - - - - ✕ Ground magnetic profile
- ⊙ ——— ⊙ Aeromagnetic profile

Fig. 4.2 Location map of the Dullstroom-Lydenburg area showing the outline of the Wanhoop magnetic anomaly and the positions of the magnetic profiles.

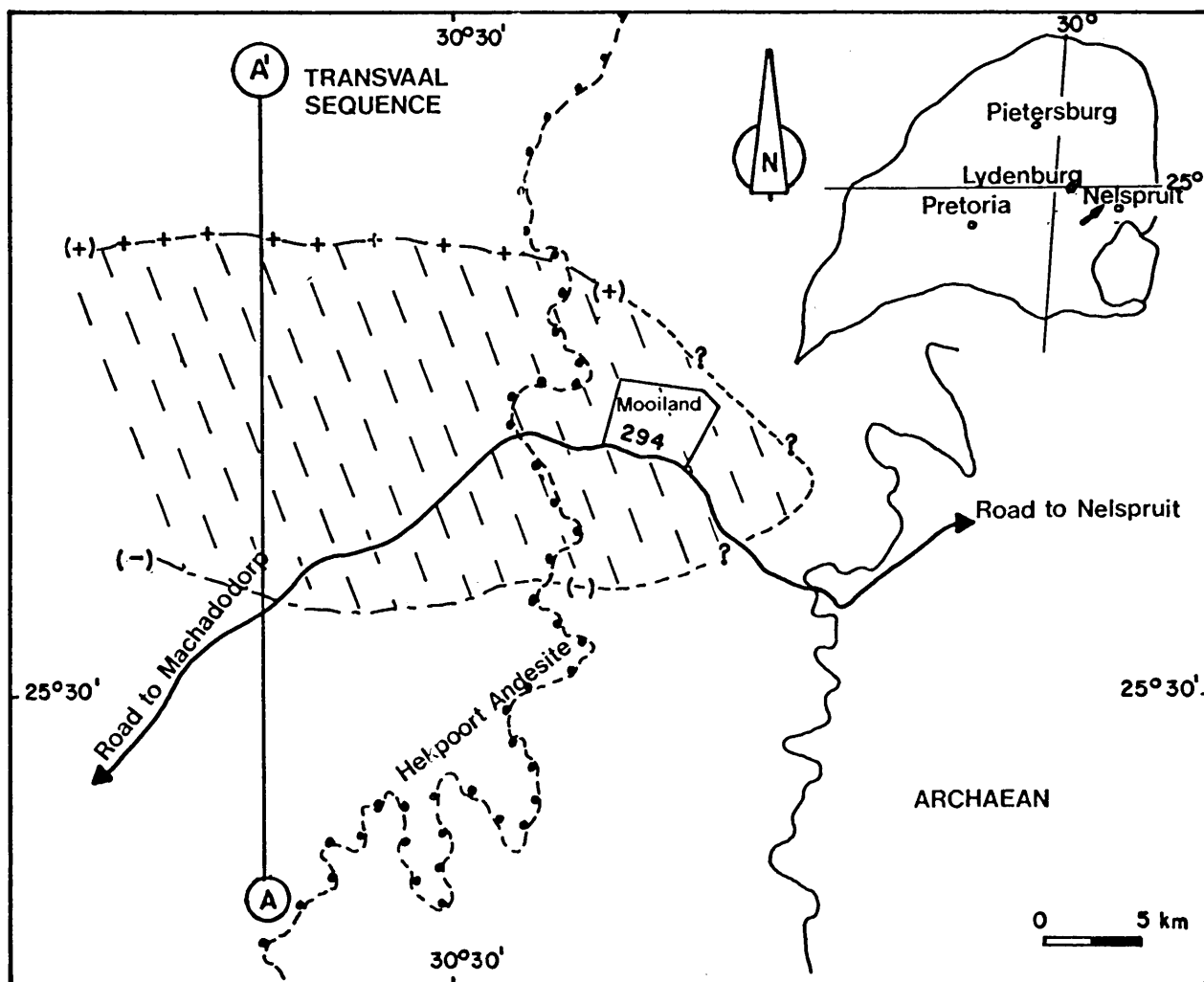


Fig. 4.3 Location map of the Mooiland magnetic anomaly showing the outline of the anomaly and the position of the magnetic profile.

The gravity highs dominating the central part of the area are mainly due to the presence of mafic rocks from the Rustenburg Layered Suite. In the north-eastern Transvaal, the negative anomalies are either due to the compensation of the former topography which has been eroded away as the escarpment retreated, or to the possible presence of sediments below the granites, which is presently considered irrational.

The gravity gradient along line AA' on Map 3 (in folder) has a constant fall-off from a maximum of +60 mgal on the acid-mafic contact of the Bushveld Complex, to -30 mgal on the eastern margin of the Rustenburg Layered Suite, from where-on the gradient decreases and flattens out to a minimum of -60 mgal. However, the gravity gradient on line BB' (Map 3), from the +60 mgal gravity high to the -50 mgal gravity low near Nelspruit, has a completely different behaviour to that of line AA'. This is due to an abnormally high gravity field over the Transvaal Sequence in the area marked by a rectangle with broken lines on Map 3.

The colour coded Bouguer gravity anomaly map of this area (Fig. 4.4) was compiled from data collected by the Geological Survey of South Africa (unpublished) and Hattingh (1980). The "warm" colours (red, purple) correspond to gravity highs, while the "cold" colours (blue, green) correspond to gravity lows. A study of this map was made to investigate the possibility of the causative bodies of the Wanhoop and Mooiland magnetic anomalies also giving rise to gravity anomalies.

In the northern part of Fig. 4.4 a normal transition of the gravity field from high values over the Rustenburg Layered Suite to lower values over the Transvaal Sequence is seen. However, to the south, the gravity field is abnormally high over the Wanhoop magnetic anomaly and the area south of it. This gravity high continues eastwards, cutting across the strike direction of the Transvaal Sequence where it correlates well with the position of the Mooiland magnetic anomaly. In the south-eastern corner, the Bouguer anomaly

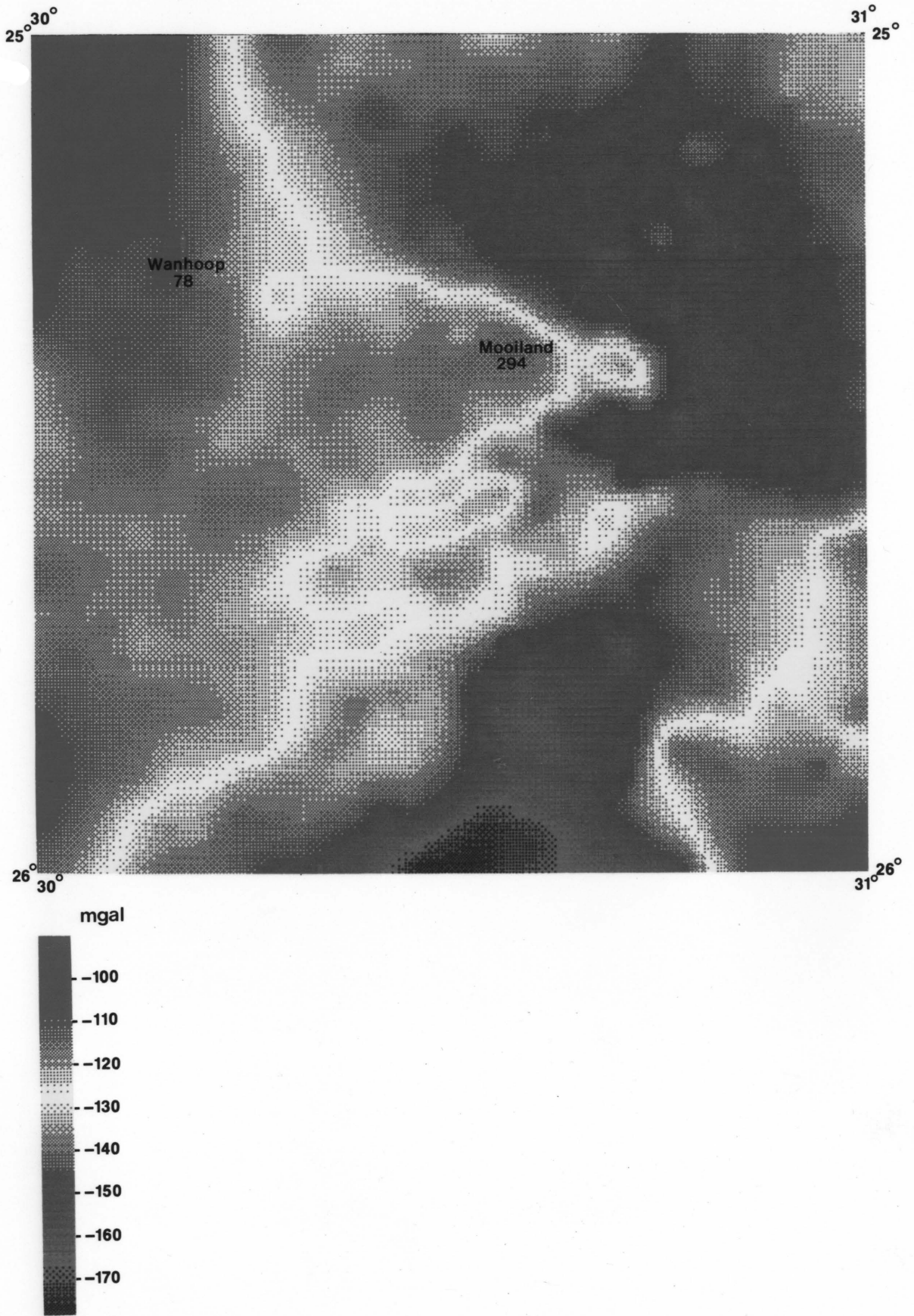


Fig. 4.4 Colour coded Bouguer gravity anomaly map of the area between latitudes 25°S and 26°S and longitudes 30°E and 31°E.

map mainly reflects the presence of high density mafic to ultramafic rocks of the Barberton greenstone belt. Gravity lows are observed over the young granite plutons to the west of the greenstone belt.

A number of insignificant gravity lows occur in areas with considerable topographic relief, which possibly originate from the fact that no terrain corrections were applied to the Bouguer anomaly values.

4.3 The Wanhoop Anomaly

The possibility that this magnetic anomaly was terrain induced was investigated by undertaking a detailed ground magnetic survey in the area. Although most of the roads were unsuitable for profiling perpendicular to the strike of the Wanhoop anomaly, a part of the long wavelength negative anomaly was intersected on a profile (Fig. 4.5 and 4.2), which confirmed the existence of the anomaly.

In Fig. 4.2 the aerial extent of the Wanhoop anomaly is shown. The maximum width of the anomaly is 6 km with an amplitude of approximately 300 nT. However, further eastwards the anomaly curves to trend north-eastwards parallel to the strike of the Pretoria Group indicating that the causative body is located amongst rocks of that succession and that its emplacement was controlled by their bedding planes. In the southwest where the anomaly is at its widest, it trends east-northeast at an oblique angle to the strike of the Pretoria Group - a clear indication that the causative body is unlikely to be part of that succession.

The regional gravity data from the Dullstroom-Lydenburg area (Fig. 4.6) was insufficient to outline the position of the Wanhoop magnetic anomaly. A detailed gravity investigation was therefore undertaken by the Geological Survey of South Africa along selected roads where the stations were spaced 400 to 1000 metres apart. The first order base station at Lydenburg (Hattingh, 1980) was used to create second order base stations at the localities shown in Fig. 4.7.

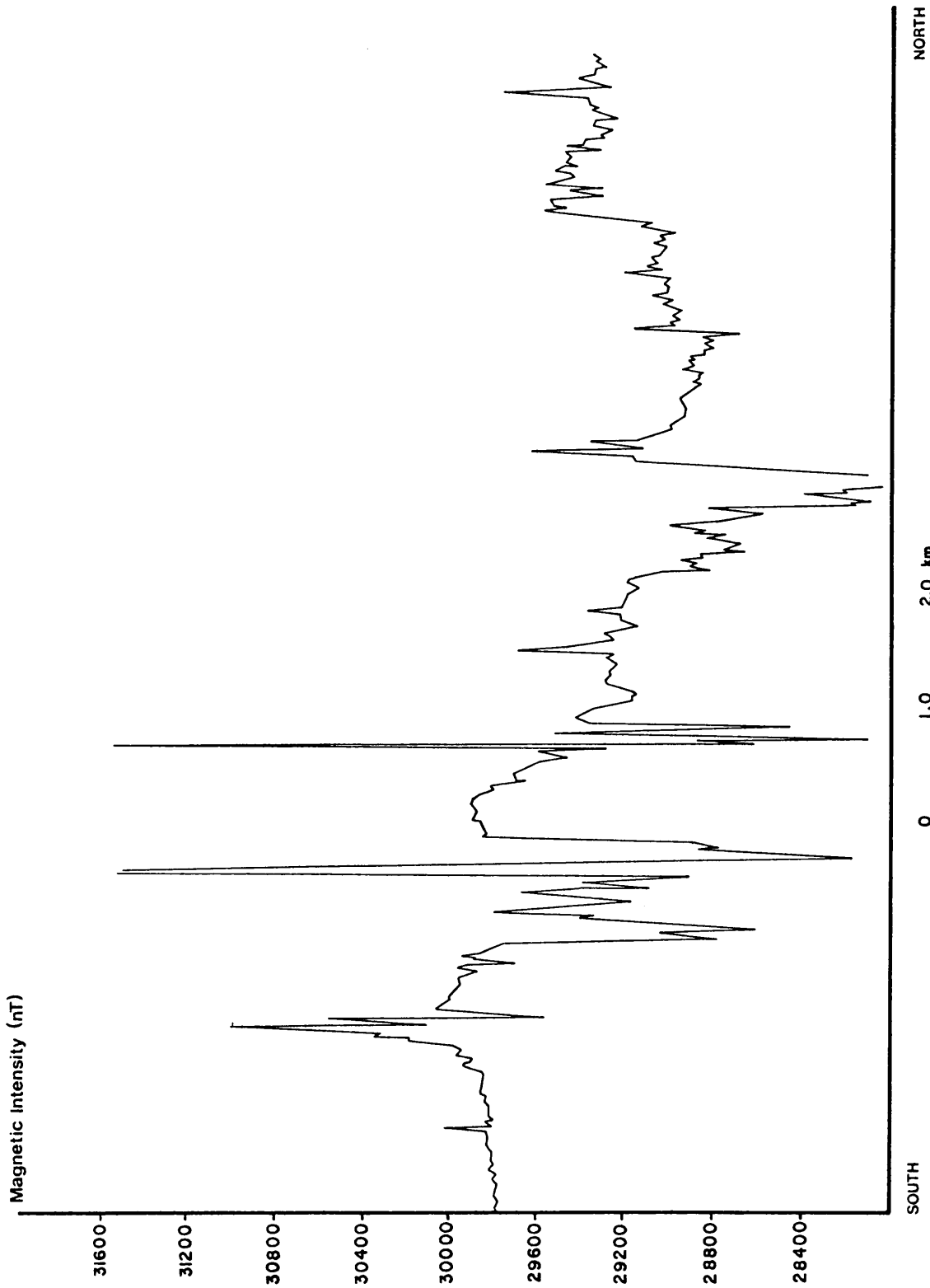


Fig. 4.5 Ground magnetic profile from the Wanhoop area. Position of profile is shown in Fig. 4.2.

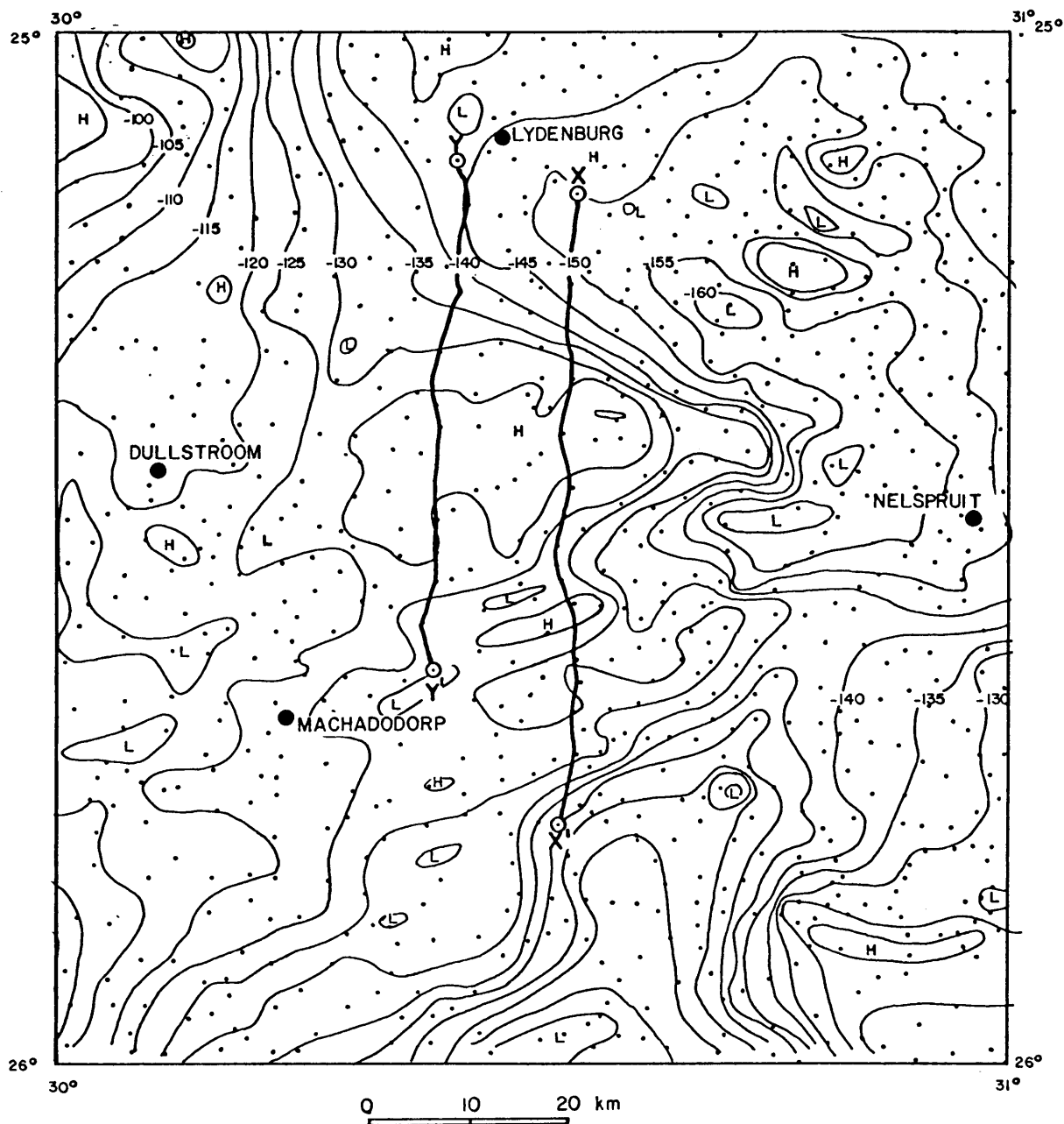
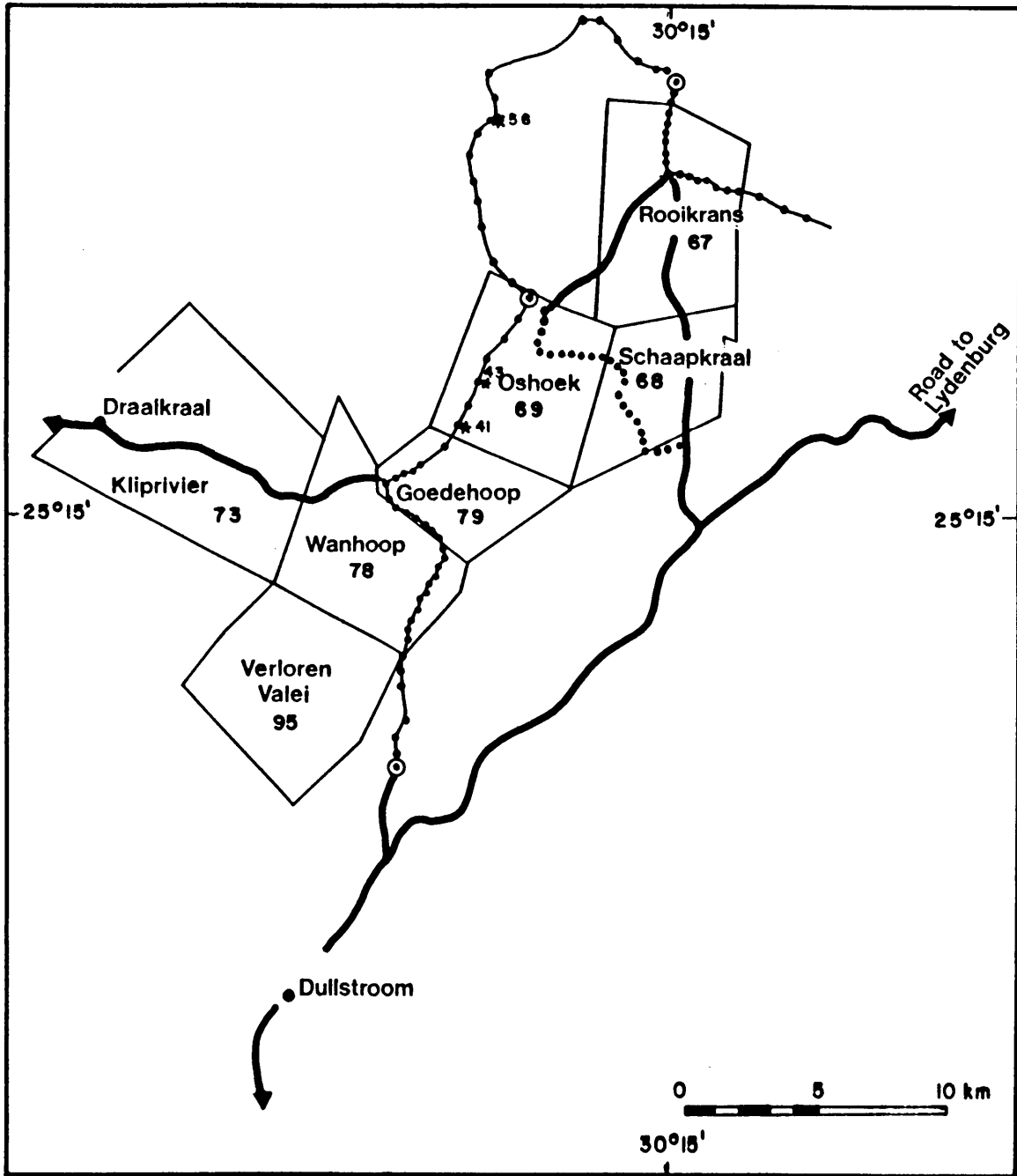


Fig. 4.6 Regional Bouguer anomaly map of the area showing the station locations and the positions of the gravity profiles.



- Gravity station
- ⊙ Second order base station
- * 56 Gravity station selected for two-dimensional terrain corrections

Fig. 4.7 Gravity station positions from the detailed gravity survey across the Wanhoop body.

The station co-ordinates were derived from the South African 1:50 000 map sheets. The positioning error on these maps is estimated to be about 20 metres. Micro-barometers were used to determine the elevations of the gravity stations, while the control points for the barometers were determined by theodolite. The maximum period between readings at these control points was one hour.

The Bouguer anomaly values were computed assuming a mean crustal density of 2670 kg/m^3 and using the International Gravity Standardisation Net 1971 (IGSN 1971) prepared by Morelli et al. (1974). The estimated accuracy of the data is 1,1 mgal.

Terrain effects due to the Steenkampsberg mountains were investigated by calculating two-dimensional terrain corrections for three selected gravity stations situated in areas of severe topographical relief (Fig. 4.7 and 4.8). Corrections of up to 3,6 mgal were obtained. As this value was higher than the estimated accuracy of the gravity data and a significant percentage of the gravity anomaly, three-dimensional terrain corrections had to be calculated. Rather than calculate corrections in the conventional way, e.g. as suggested by Hammer (1939), a quicker and more efficient computer-assisted method was used based on a paper by Kane (1962).

The basis of the three-dimensional terrain corrections program (Palmer, 1979) is a digital terrain model of the area surrounding the gravity observation points. This terrain model is constructed as a grid of elevation data points forming an "elevation grid" in such a way that it coincide with the gravity observation line, but extends a certain minimum distance beyond it. In his paper, Kane approximated the gravitational attraction (g) of a vertical prism to that of an annular ring of the same height.

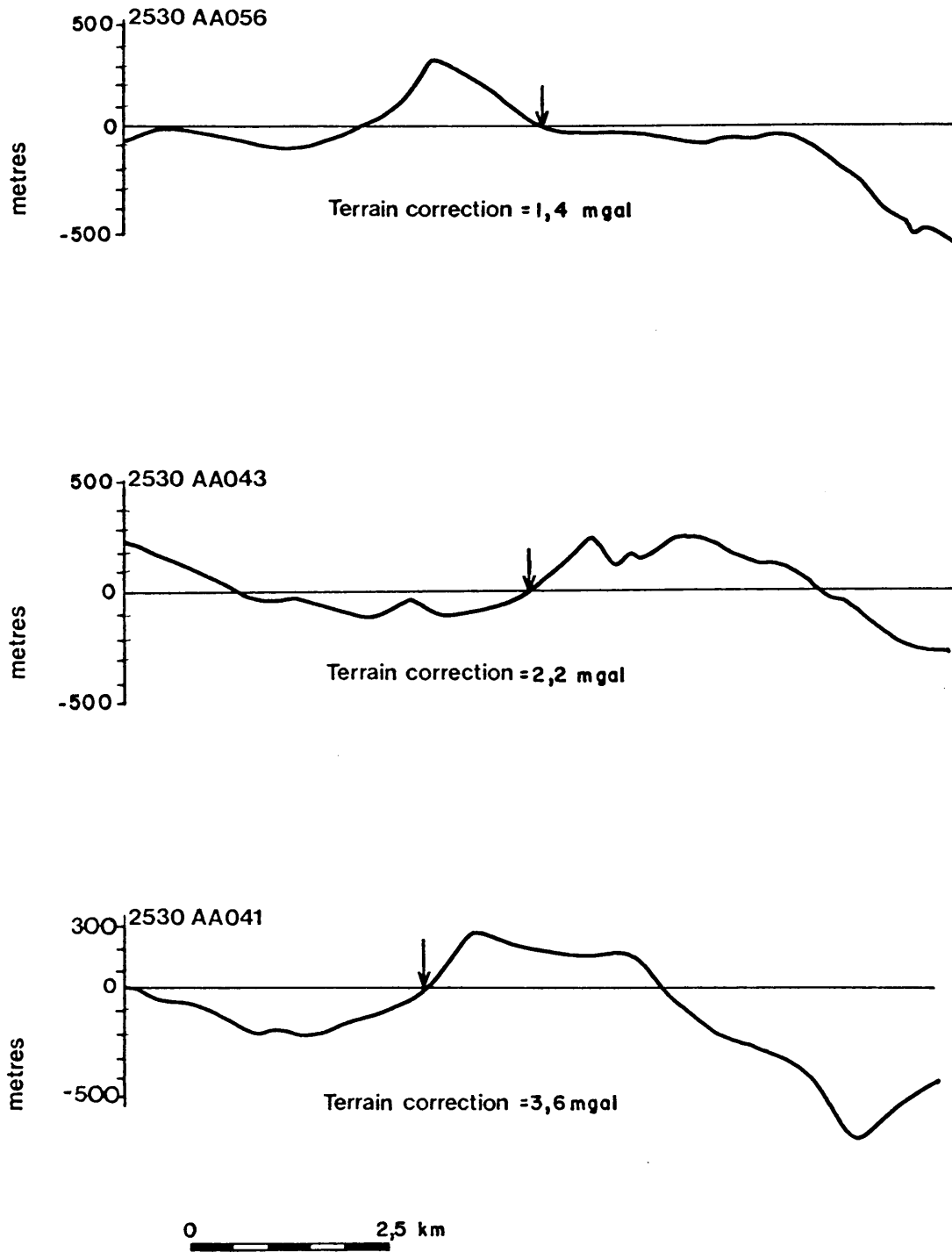


Fig. 4.8 Two-dimensional terrain corrections for three selected gravity stations situated in areas of severe topographical relief.

The gravitational attraction (g) is given by

$$g = \frac{GDA (1,26A + (R - 0,63A)^2 + H^2 - (R + 0,63A)^2 + H^2)}{1,26R}$$

where

G = Gravitational Constant

$$(6,6720 \pm 0,0041) \times 10^{-11} \text{ m}^3 \text{ s}^{-2} \text{ kg}^{-1}$$

D = Density

A = Length of horizontal side of prism

R = Distance from gravity station to elevation data point

H = Height difference between station and elevation point
under consideration

(Kane, 1962)

An "elevation grid" was established from the 1:50 000 topographic sheets of the Dullstroom-Lydenburg area by digitising the contours and calculating a grid with a 250 m interval. Elevation data points within a radius of 3 km from the gravity station were considered. As the stations from the gravity survey were unevenly spaced and the corrections calculated on a grid, the corrections at stations which did not coincide with the grid positions had to be interpolated by hand.

Fig. 4.9 shows the terrain-corrected Bouguer anomaly map superimposed on a simplified geological map of the area. From the position of the outline of the Wanhoop magnetic anomaly (Fig. 4.9) it is evident that the Wanhoop magnetic body is denser than the rocks from the Pretoria Group and its non-magnetic unit extends southward towards Dullstroom.

4.4 The Mooiland Anomaly

Even though the magnetic anomaly is situated in a terrain of severe topographical relief, there is no correlation between the anomaly shape and the topography. The aerial extent of the Mooiland magnetic anomaly is shown

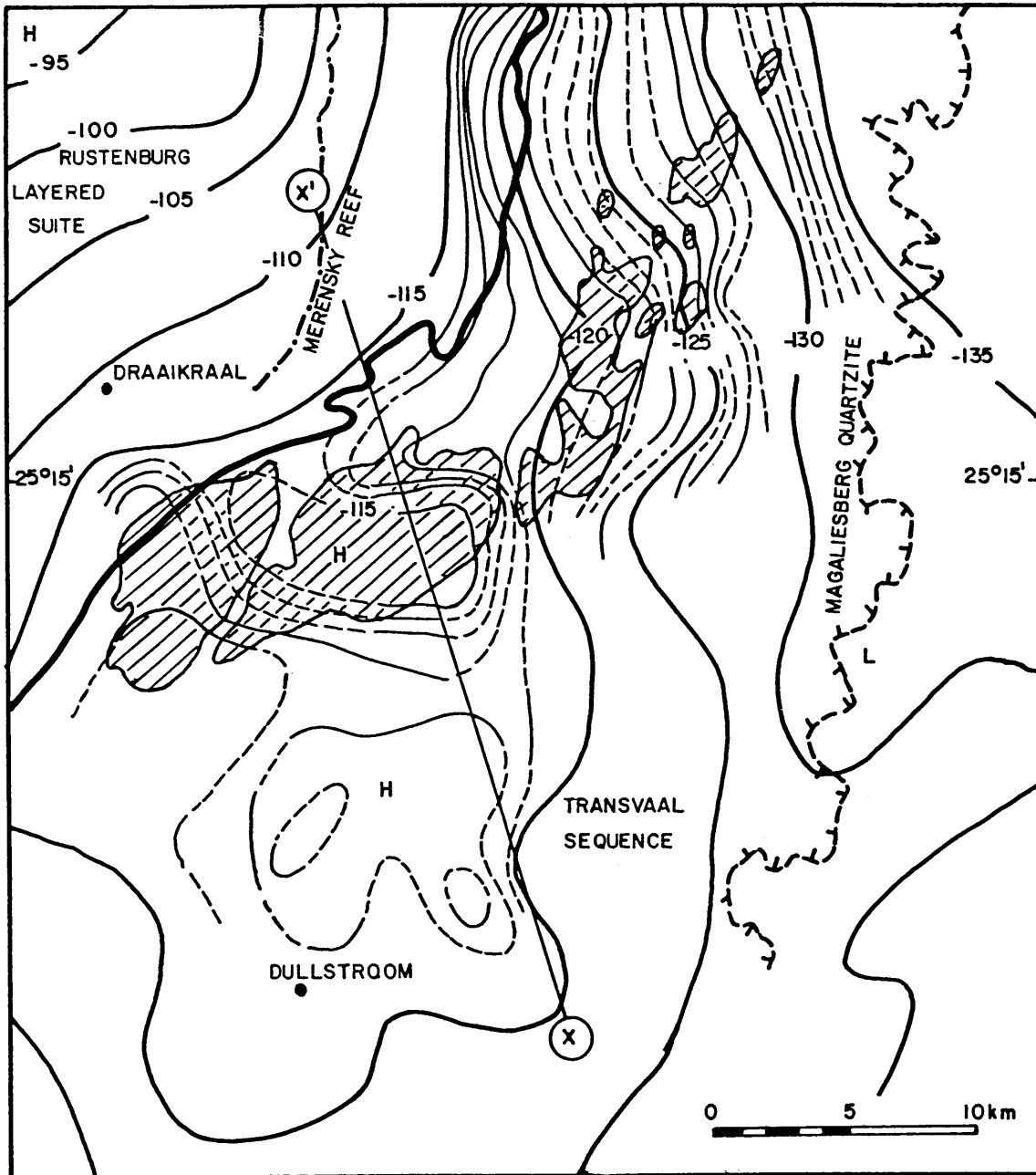


Fig. 4.9 Terrain corrected Bouguer anomaly map superimposed on a simplified geological map, showing the outline of the Wanhoop magnetic anomaly and the position of the gravity profile.

in Fig. 4.3. The magnetic body is approximately 17 km wide with an amplitude of 200 nT for both the positive and negative anomalies. Numerous north-northeast trending high frequency anomalies cut across the anomaly, obscuring the boundaries of the magnetic body, especially in the eastern part, in the vicinity of the farm Mooiland 294. As this anomaly cuts across the strike direction of the Transvaal Sequence it is very unlikely that the magnetic body is part of that succession.

The gravity high reaches a maximum over the Mooiland magnetic body, and is flanked by gravity lows on its northern and southern boundaries (Fig. 4.4 and 4.6). These two outstanding gravity lows are connected with the gravity lows at the base of the escarpment (Hattingh, 1980). The outline of the Mooiland magnetic body correlates with the northern part of the gravity anomaly (Fig. 4.3 and 4.6). North of the gravity high the gradients are fairly steep, while in the southern part the field stays constant for a considerable distance before it falls down rapidly to the peak of the gravity low.

Spurious anomalies and irregular anomaly shapes on Fig. 4.6 are probably due to terrain effects as the Bouguer anomaly values at these locations exhibit some degree of correlation with local topography.

5. QUANTITATIVE INTERPRETATION

5.1 The Wanhoop Anomaly

Two-dimensional interpretations of the magnetic anomaly were undertaken along four profiles in the area. The positions of these profiles, AA', BB', CC' and DD' are indicated in Fig. 4.2. Digital aeromagnetic data from the Barberton- Pilgrim's Rest survey were abstracted from magnetic tape and sections from flight-lines 2232, 2280 and 2310 and tie-line 9020 were selected.

The high frequency noise on these profiles (Fig. 5.1) is caused by multiple dyke intrusions and some of the long wavelength anomalies are due to the flight-lines running nearly parallel to the strike direction of the magnetic lineaments. Although these anomalies slightly obscure the position of the major negative anomaly, there is no doubt about its existence.

In Fig. 5.2 the log-energy spectrum of flight-line 2280 is given. The spectrum should reflect the effect of depth and depth extent of the sources present. The assumption is made that differences in slope are due to differences in depth between the near-surface and deepseated sources (Spector and Grant, 1976). However, if the near-surface sources are not depth limited, as in this area, they will contribute to the low frequency component of the spectrum as well as dominate the short wavelength end of the spectrum. As the deeper sources dominate the low frequency component of the spectrum, no distinct differences in slope are revealed by the spectrum, which make the design of a matched filter, to remove only the contribution of the shallow sources, very difficult and unreliable. It was therefore decided not to filter the aeromagnetic data.

When analysing the magnetic profiles, one is tempted to simulate the negative anomaly with the eastern edge of an inductively magnetized body. For

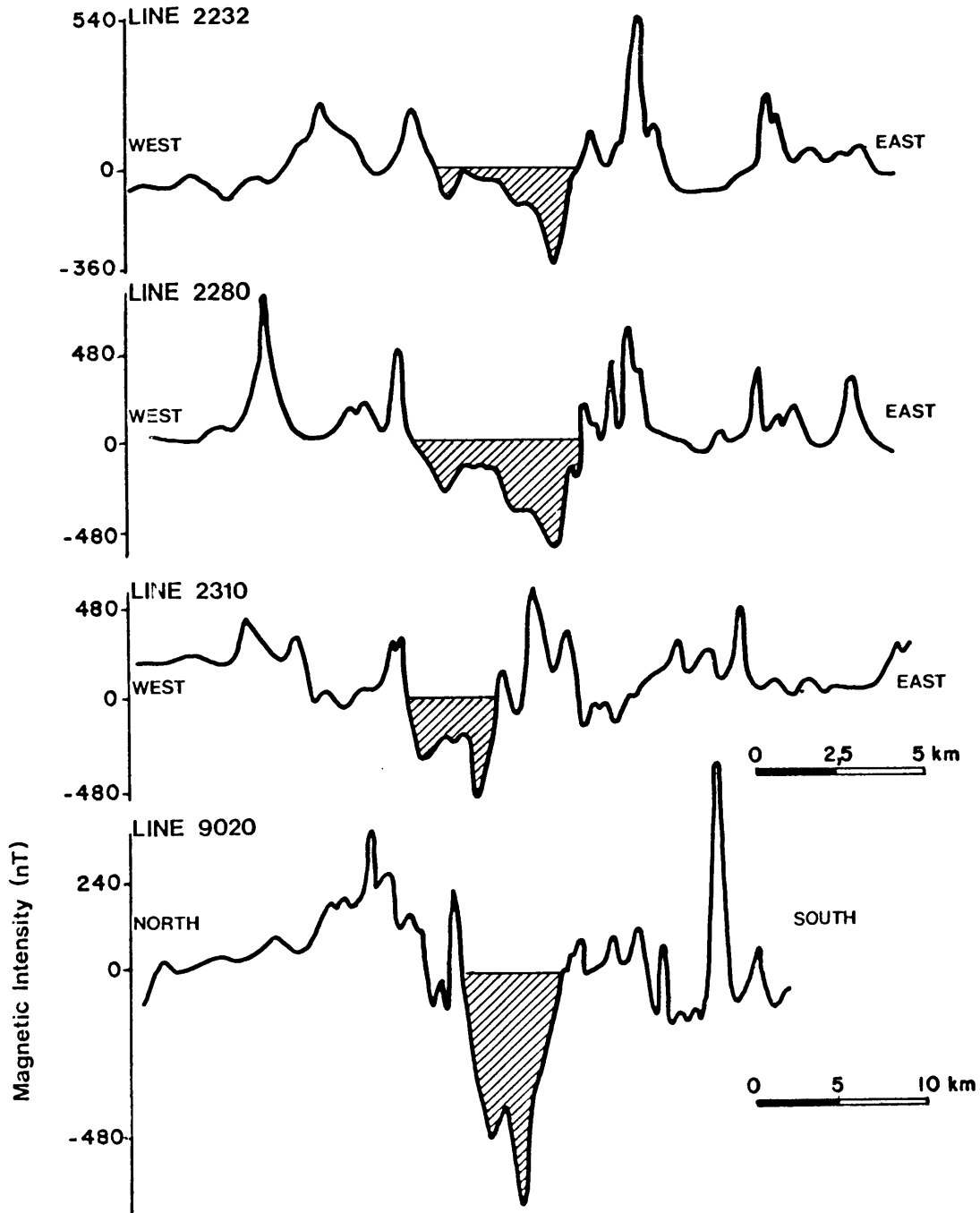


Fig. 5.1 Digital aeromagnetic data from the Barberton - Pilgrim's Rest survey. The shaded area on each flight-line indicates the position of the Wanhoop negative magnetic anomaly.

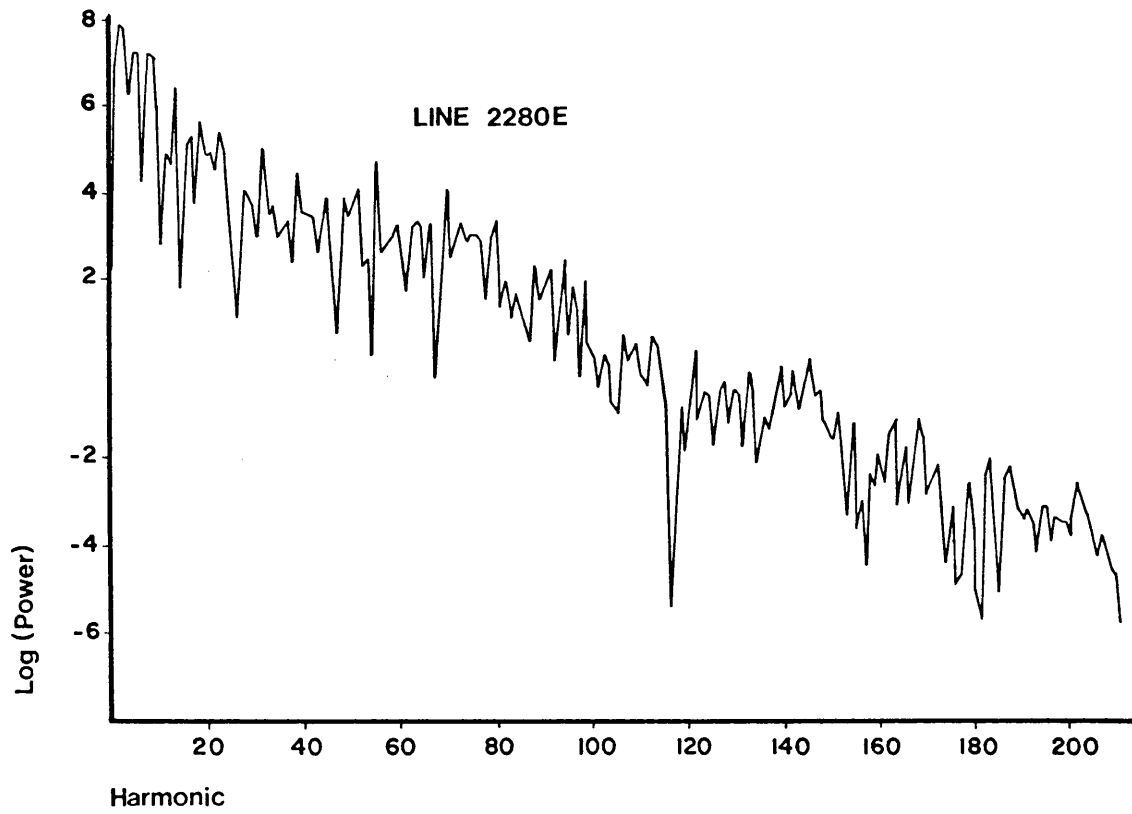


Fig. 5.2 Log-energy spectrum of flight-line 2280 from the Barberton - Pilgrim's Rest survey.

a dyke dipping westward by 20° , a positive anomaly, with the same amplitude as the negative anomaly, would be observed on the western edge of the body. No significant positive anomalies which could be related to the Wanhoop body are present on any of the four profiles, indicating that a significant remanent component is present.

Using the remanent direction of the reversed polarity zone (Table 3.5), models were deduced by computing the total magnetic field of various model shapes by the method of Talwani and Heirtzler (1964). This modelling method assumes a two-dimensional structure of the model perpendicular to the profile. The resultant model values were compared with the observed magnetic anomaly, the model and the intensity of magnetization adjusted, and the magnetic response of the theoretical model recomputed until they agreed with the observed field.

A reasonable fit was obtained by using an intensity of magnetization of $2000 \times 10^{-3} \text{ Am}^{-1}$ and a direction of magnetization $D=30^\circ$; $I=+58^\circ$ (Fig.5.3). The character of the bodies derived from the four profiles respectively are encouragingly similar. On all of the east-west profiles the body consists of a major westward dipping sheet-like unit of the order of 1 km in vertical extent, and approximately 500 m below surface at its shallowest edge. A second thinner sheet underlies the former one and extends approximately 7 km further east from the former main sheet, but terminates at much greater depth ($>1000 \text{ m}$).

It is evident from the fact that the Wanhoop magnetic anomaly could only be simulated by assuming a positive inclination ($+58^\circ$), that the causative body is remanently magnetized in a direction different to the present earth's field (inclination= -60°). In view of the nearness of the anomaly to the Rustenburg Layered Suite and the fact that the causative body has the same

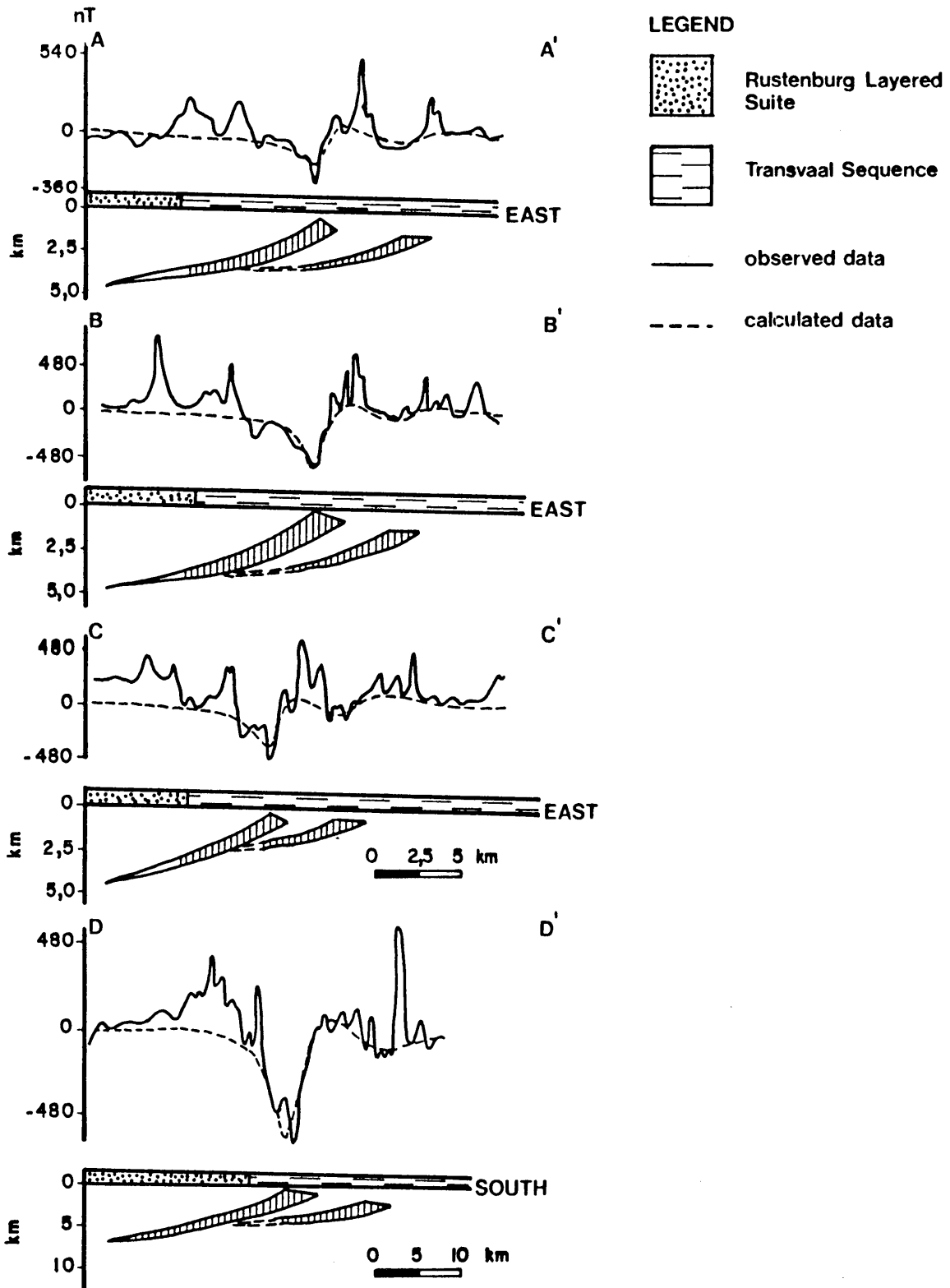


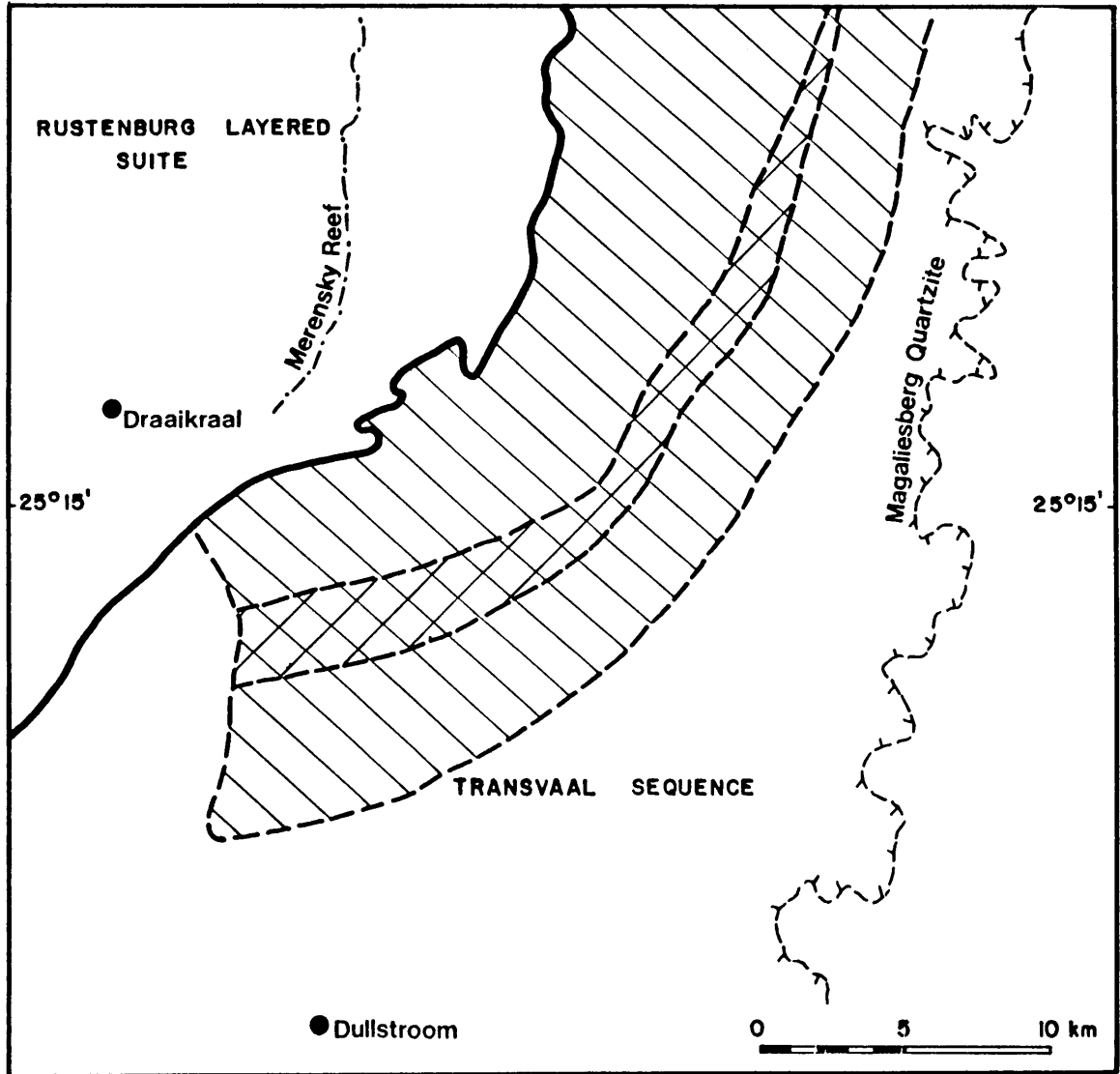
Fig. 5.3 Two-dimensional magnetic modelling of profiles AA', BB', CC', and DD' across the Wanhoop magnetic anomaly. The contact between the Rustenburg Layered Suite and the Transvaal Sequence is indicated on each profile.

dipping plate aspect to it as the Rustenburg Layered Suite as a whole (Du Plessis and Kleywegt, 1987) it is tempting to speculate on the possibility that the body relates to one of the known zones of the Rustenburg Layered Suite.

It follows that if the Wanhoop bodies are associated with the Rustenburg Layered Suite they most probably cooled to below the Curie point during the polarity interval when the major part of the main zone of the Rustenburg Layered Suite cooled down.

The shallowest part of the Wanhoop magnetic bodies are shown in Fig.5.4 and when this area is compared with the terrain corrected Bouguer anomaly map of the same area (Fig. 4.9) it becomes evident that the Wanhoop magnetic body causes a distinctive gravity anomaly. However, it is not the only dense unit present and the gravity high extends further south towards Dullstroom, indicating the presence of a non-magnetic, dense unit which occurs in the substratum that extends beyond the Wanhoop magnetic bodies. To illustrate this concept, a two-dimensional model was constructed in Fig 5.5 that simulates the gravity field observed on profile XX' in Fig.4.9 and depicts the greater aerial extent of the dense body.

From profile XX' in Fig 5.5 it is apparent that the regional gravity values increase northwards. This effect is due to the increasing volume of rocks of the Rustenburg Layered Suite. It proved to be very difficult and unreliable to remove this regional effect and it was therefore decided to subtract a base-level Bouguer value of -150 mgal from the data, which approximately represents the regional effect of the Archaean granites. Consequently the whole of the Transvaal succession formed part of the model that was fitted to the residual anomaly. The limitation of any gravity interpretation is the inherent non-uniqueness associated with the interpretation. A hypothetical solution for any gravity anomaly should be compatible with both the geology of the area and the results from other





-  Aerial extent of the Wanhoop magnetic bodies within the Pretoria Group
-  Position of the top of the major magnetic body

Fig. 5.4 Aerial extent of the Wanhoop magnetic bodies as determined from two-dimensional modelling.

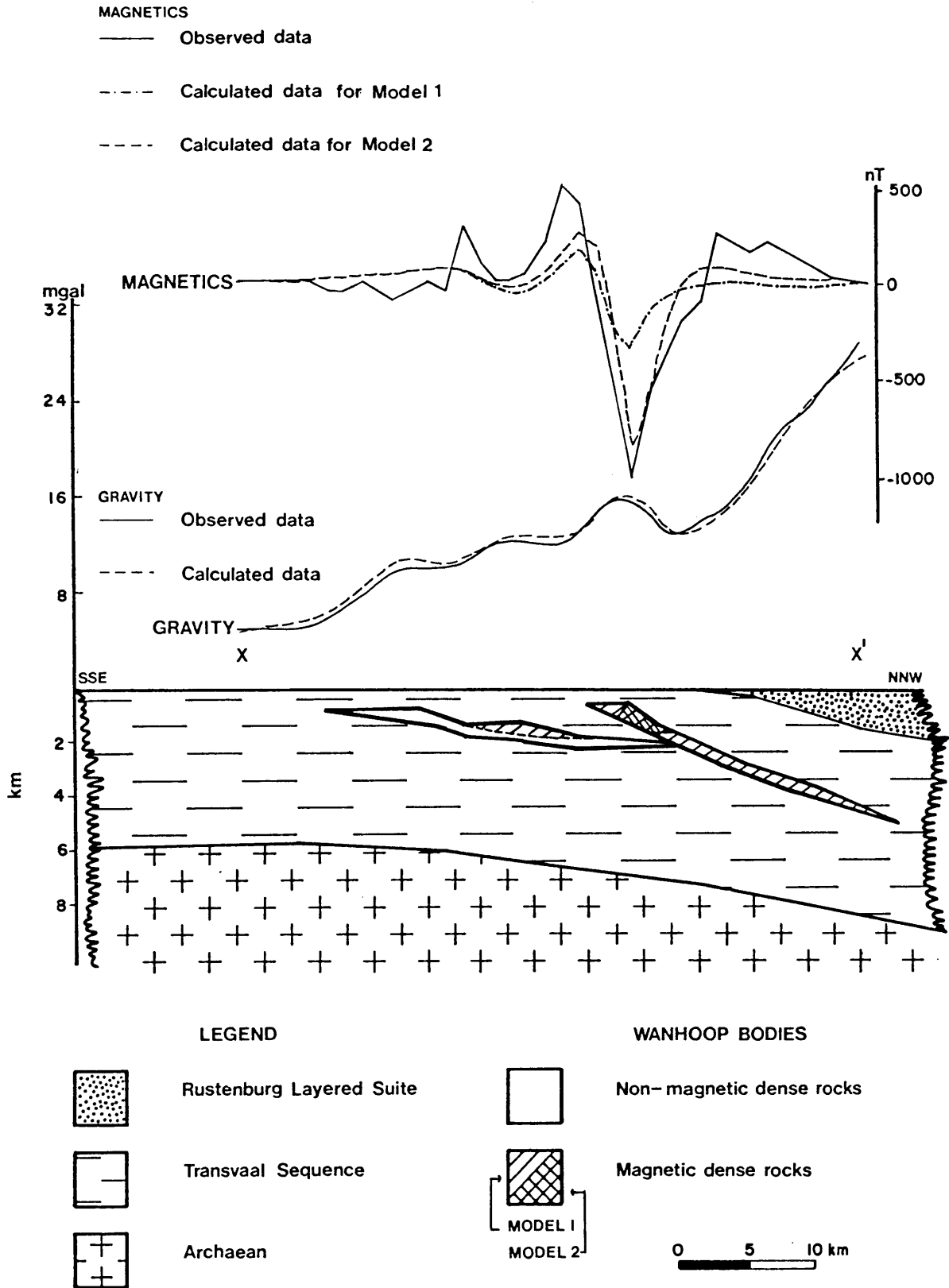


Fig. 5.5 Two-dimensional gravity and magnetic modelling of profile XX' across the Wanhoop bodies.

geophysical methods. Bearing this in mind, the shape of the magnetic dense rocks were inferred from those on profile DD' (Fig. 5.3) and a similar body shape was chosen for the non-magnetic dense rocks, which constrained the Wanhoop gravity model. A density contrast of 300 kg/m^3 in respect of the Transvaal Sequence (2780 kg/m^3) was used in the forward modelling process (Talwani et al., 1959). The two magnetic dense bodies in Fig 5.5 were given the same magnetization (Model 1) that was used to obtain the magnetic body models in Fig. 5.3, while the third body was considered non-magnetic. In Fig. 5.5 it is seen that the shape of the magnetic anomaly generated by this "gravity model" closely approximates the observed magnetic field. However, the maximum amplitude of the magnetic anomaly is approximately 1000 nT on this profile compared to the amplitude of 500 nT on profile DD' in Fig. 5.3. To simulate the magnetic anomaly, without changing the body shapes, the intensity of magnetization of the magnetic bodies in Figure 5.5 were increased and a part of the main magnetic unit was given an intensity of magnetization of $9000 \times 10^{-3} \text{ Am}^{-1}$ (Model 2). Note that this highly magnetic unit is absent on all the other profiles.

Because the initial model thicknesses as determined from the magnetic modelling were larger than those obtained from the gravity models the thickness of the magnetic models were reduced. To retain the magnetic amplitude of the models the intensity of magnetization had to be increased.

The calculated magnetic data from profile BB' (Fig.5.3) was used as observed data for the determination of models with different intensities of magnetization and body shapes. For each magnetic model which yielded a good fit to the observed magnetic data, the gravity field was then calculated using density contrasts which produced anomalies of less than 5 mgal (Fig.5.6).

It is concluded from the above-mentioned calculations that the depth to the major magnetic body of the Wanhoop anomaly varies between 200-500 metres

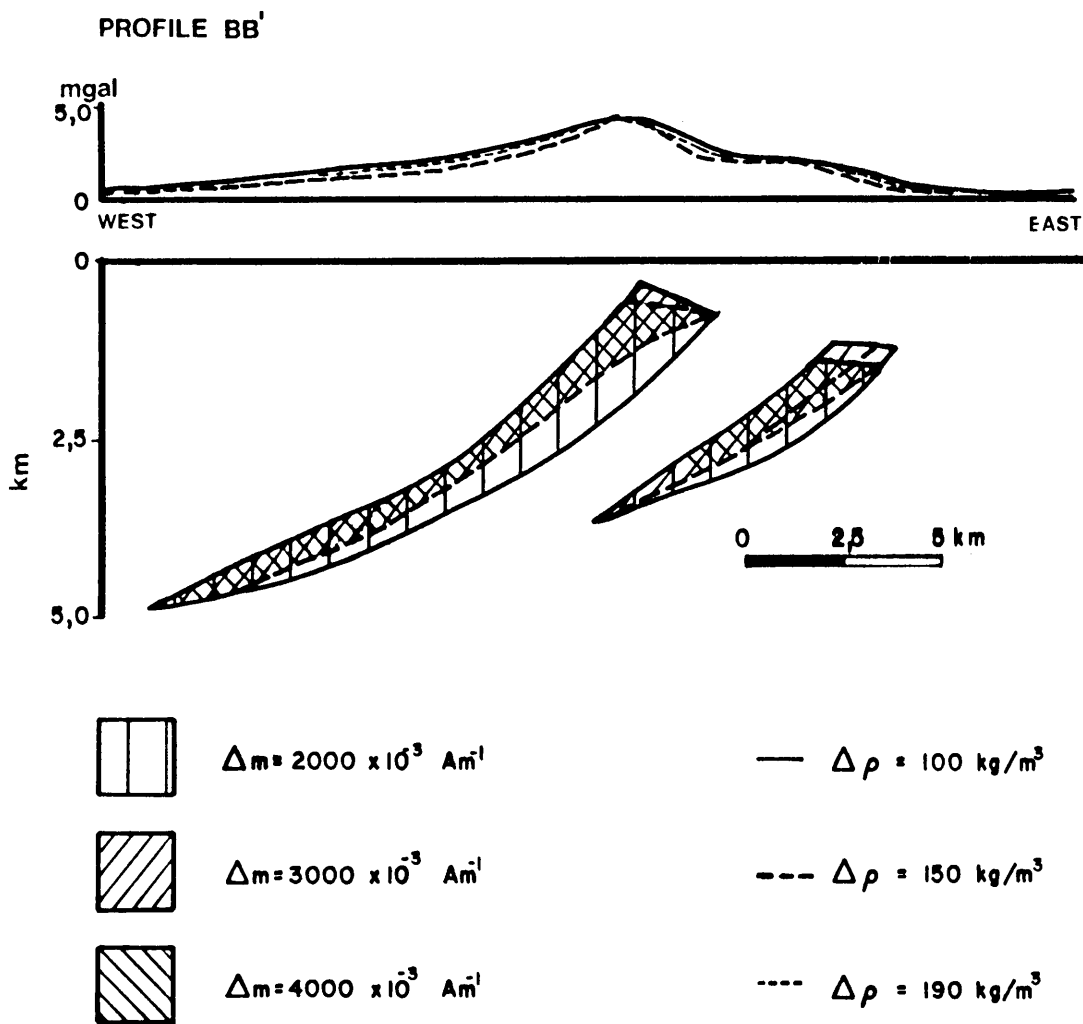


Fig. 5.6 Two-dimensional gravity modelling of profile BB' across the major Wanhoop body, using different intensities of magnetization and body shapes.

with a maximum thickness of approximately 1 000 metres. The depth to the non-magnetic body is approximately 1 000 metres and it has a maximum thickness of 500 metres.

5.2 The Mooiland Anomaly

Analogue aeromagnetic data from a section of tie-line 9051 (25/78 Barberton - Pilgrim's Rest Survey) was selected for two-dimensional magnetic modelling. The position of the tie-line is indicated by profile AA' in Fig. 4.3.

The smoothed magnetic anomaly along profile AA' (Fig. 5.7) was obtained by graphically removing the anomalies from sources other than the main magnetic body. The shape of the anomaly is typical of a sheet-like, inductively magnetized body with a positive anomaly on its northern boundary and a negative anomaly on the southern boundary. Two-dimensional modelling indicated that the Mooiland magnetic anomaly was caused by a sill-like body with a susceptibility of 0,25 SI units. The depth to the top of the body is 1400 metres and the thickness is approximately 500 metres. This high susceptibility is indicative of a high percentage magnetite present in the body, similar to that of the upper zone of the Rustenburg Layered Suite. Previous modelling of the upper zone by Molyneux and Klinkert (1978), proved that the susceptibility of this zone is 0,13-0,25 SI units.

The only other units with high susceptibilities are the Penge iron-formation and the magnetic shales of the Timeball Hill Formation. Modelling of the magnetic shales have shown that the susceptibility is 1,4 SI units, which is much higher than that calculated from the Mooiland magnetic anomaly.

To investigate the contribution of the magnetic body to the Bouguer anomaly map shown in Fig. 4.6, two north-south profiles were selected for two-dimensional gravity modelling.

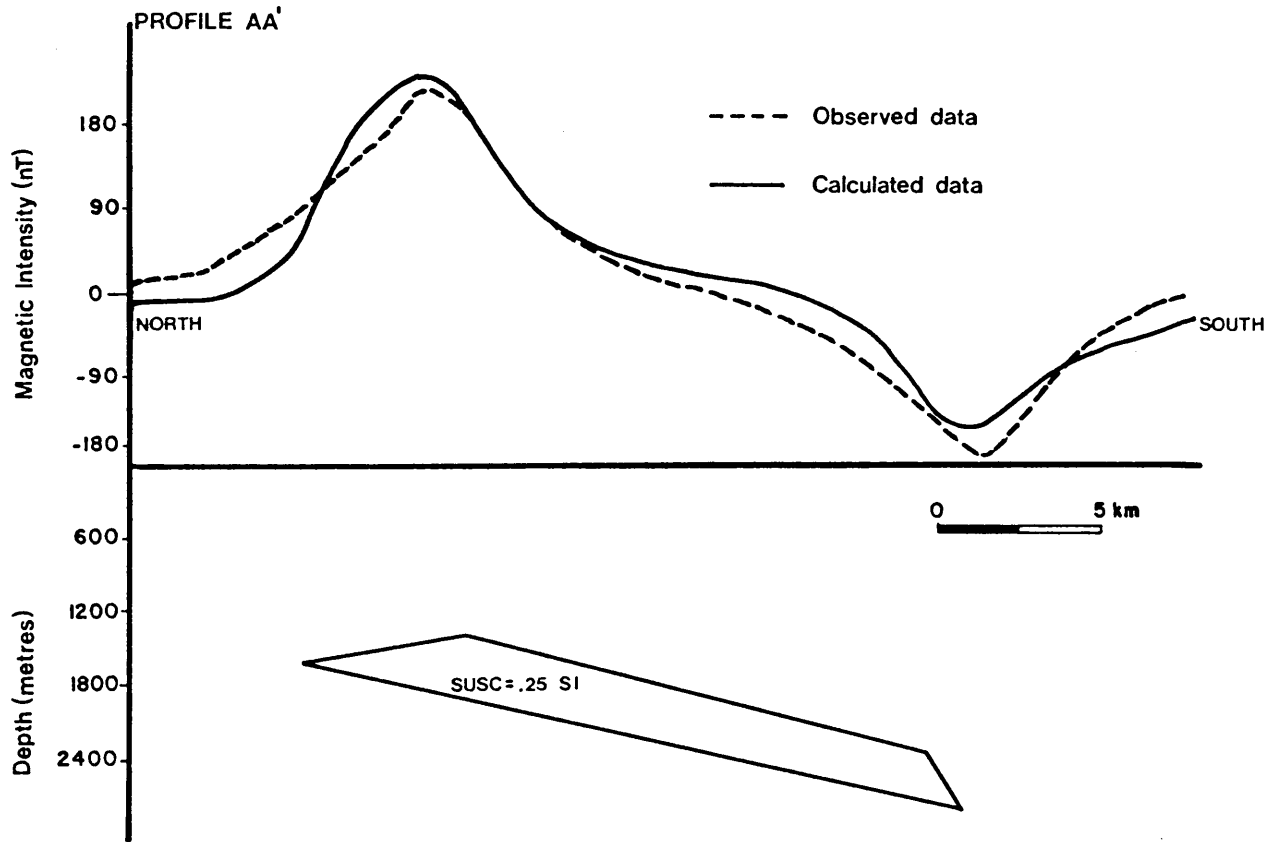


Fig. 5.7 Two-dimensional magnetic modelling of profile AA' across the Mooiland magnetic anomaly.

The conventional methods used in the reduction of gravity data do not lead to values that are effectively on the same horizontal plane and therefore, in regions of high topographic relief, as in the vicinity of the Mooiland gravity anomaly, failure to take into account local differences in vertical gradients can result in an appreciable error.

A method developed by Henderson and Cordell (1971) was used to reduce the gravity data observed at unevenly spaced stations, at various elevations, to a common level. In this method N data points on an uneven topography can be mathematically expressed as

$$g(x_i, z_i) = A_0/2 + \sum_{k=1}^m e^{2\pi k(z_i/\lambda)} \cdot (A_k \cos 2\pi k(x_i/\lambda) + B_k \sin 2\pi k(x_i/\lambda)) + \epsilon_{i,m}$$

and A_k, B_k = Fourier coefficients
 z_i = height of the i-th data point below or above a datum plane
 λ = fundamental wavelength of the complete data set
 x_i = position of the i-th data point
 $\epsilon_{i,m}$ = error term.

The Fourier coefficients are determined in a least-squares way whereafter the number of terms determining the Fourier representation is optimized. A new constant datum elevation height z_i is used in the expression to determine the anomaly at any plane of constant height above the anomalous body.

To counter high wavenumber oscillations, a smoothing function to correct for a type of Gibbs phenomenon in the neighbourhood of the end point of the profile was used. The series representation of this case is

$$g(x_i, z_i) = \alpha_i / 2 + \sum_{k=2}^{2m+1} \alpha_k e^{\pi(k-1)z_i/\lambda} \cdot \cos(\pi(k-1)x_i/\lambda) + \epsilon_{i,m}$$

where $i = 1, 2, \dots, N$ and $2m+1 \leq N$
 = Fourier coefficients

(Henderson and Cordell, 1971).

Fig. 5.8 depicts the Bouguer anomaly of the stations located on the topographical surface (profiles XX' and YY' from Fig. 4.6) and the true complete Bouguer anomaly on the reduction plane. Topographical relief of approximately 700 metres on profile XX' and 1000 metres on profile YY' is involved, resulting in maximum corrections of 0,5 mgal and 3 mgal respectively.

The regional effect of the Archaean granites were subtracted from the Bouguer gravity data to produce the residual anomalies shown in Fig. 5.9.(a) & (b). The residual Bouguer anomaly values along profile XX' reveal a major gravity high (34 mgal) over the inferred Mooiland magnetic anomaly. From there on southwards, the gravity field remains fairly constant (20 mgal) for approximately 20 km before it falls down rapidly to the regional field values over the Archaean granites. As mentioned before, a hypothetical solution for any gravity anomaly should be compatible with both the geology of the area and the results from other geophysical methods, and therefore any two-dimensional gravity model constructed from this data was restricted by the presence of the Mooiland magnetic body and rocks from the Godwan Formation and Barberton Sequence intersected by boreholes to the south.

The first two-dimensional model was constructed comprising rocks of the Transvaal Sequence, Godwan Formation and the Mooiland magnetic body. The positions of the magnetic anomaly and the boreholes are indicated in Fig. 5.8(b). To simulate the observed gravity field, "palaeovalleys" were

LEGEND

- ○ Station anomaly
- - - X Anomaly on reduction plane

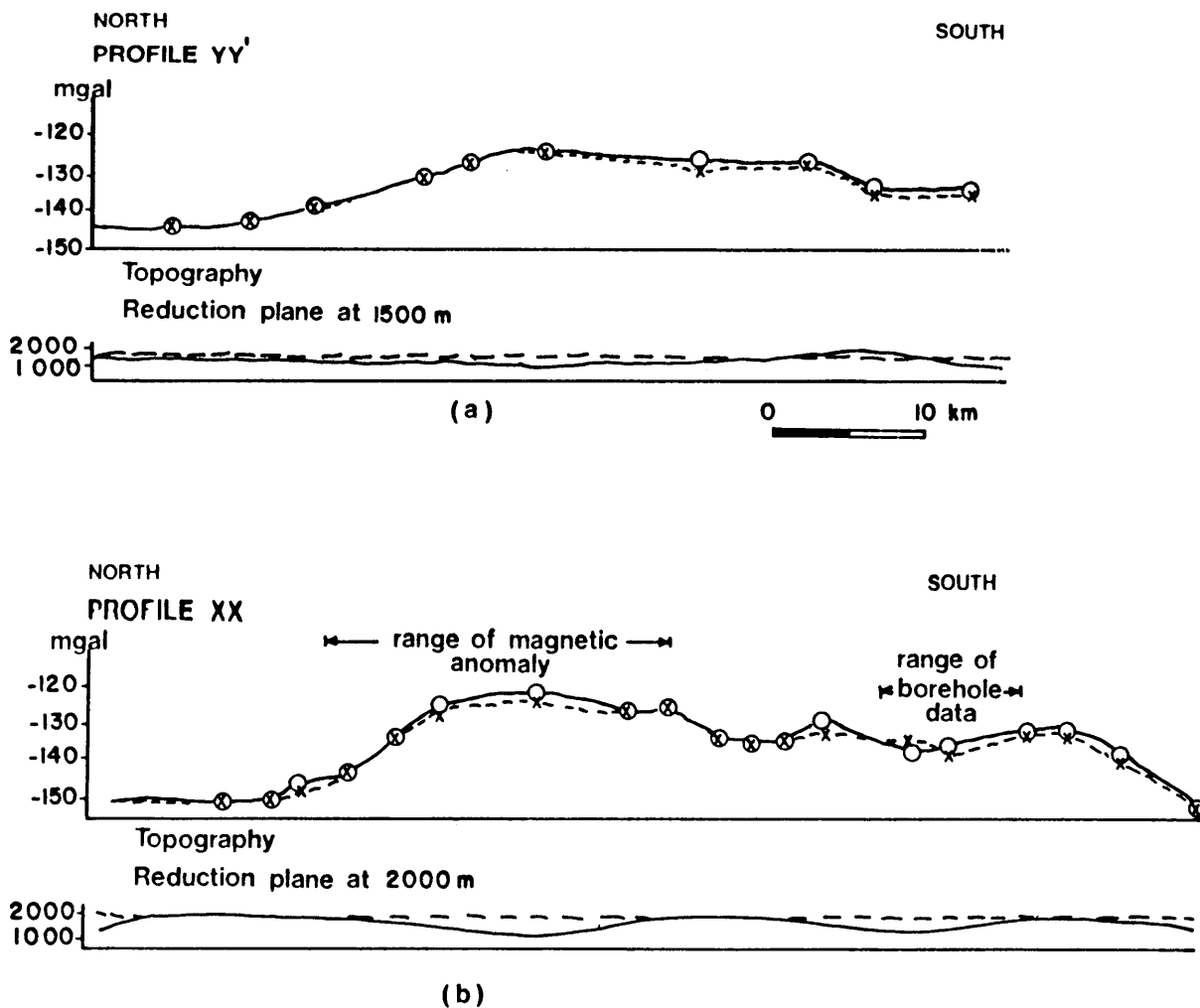


Fig. 5.8 Station complete Bouguer anomaly and true complete Bouguer anomaly (on the reference plane) along profiles (a) YY' and (b) XX' on the two-dimensional topographical surface in the Mooiland area.

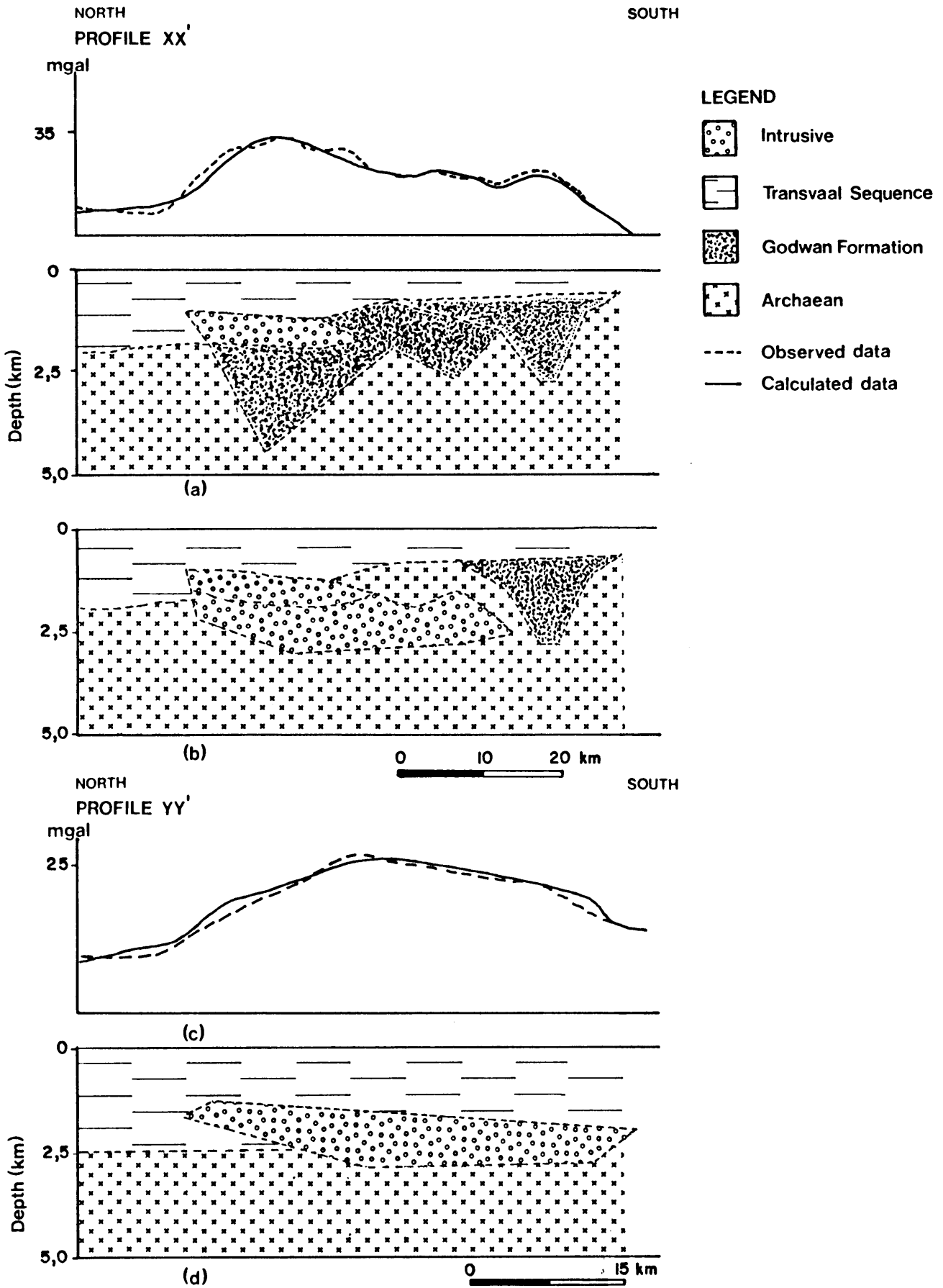


Fig. 5.9 Two-dimensional modelling of the residual gravity anomalies along profiles (a + b) XX' and (c) YY' across the Mooiland gravity anomaly.

created in the Archaean granites and filled with rocks from the Godwan Formation with a density contrast of 260 kg/m^3 . The Mooiland magnetic body and the Transvaal Sequence were modelled using density contrasts of 410 kg/m^3 and 110 kg/m^3 respectively. Borehole data revealed the presence of rocks from the Barberton Sequence at the base of the Godwan Formation, but at these depths (2500 m) the contribution to the gravity anomaly will be insignificant. Due to lack of borehole data in the central and northern part of the profile, the geological acceptability of the model depicted in Fig. 5.9(a) is uncertain.

Another two-dimensional model was constructed along profile XX' comprising rocks of the Transvaal Sequence, Godwan Formation, and a sill-like body of which the uppermost unit was defined by the Mooiland magnetic body (Fig. 5.9(b)). A good fit was obtained by using the density contrasts from the previous model and a density contrast of 410 kg/m^3 for the non-magnetic southward extension of the sill-like body. According to the interpreted model, the Mooiland gravity body has a maximum vertical thickness of 2000 metres centred over the major gravity high and the Godwan Formation has a vertical extent of 2000 metres, which correspond to the thickness calculated from borehole data.

The previous model revealed the presence of rocks from the Godwan Formation, centred over the gravity high, with a vertical extent of the order of 2500 metres. Boreholes to the west ($\pm 7 \text{ km}$) of those intersected by profile XX', intersected rocks from the Barberton Sequence at the base of the Transvaal Sequence. The absence of the Godwan Formation in this area is not reflected in the Bouguer anomaly map which proves that the gravity high is not caused by this formation but is rather due to the presence of dense rocks within the Archaean granites as revealed by the latter gravity model (Fig. 5.9(b)). Profile YY' (Fig. 5.9(c)) was modelled to confirm the body shapes determined from the second model of profile XX'.

It is concluded from the above-mentioned modelling results that the Mooiland body consists of a 500 metres thick upper magnetic unit at a depth of approximately 1400 metres, and a non-magnetic unit which extends to the south where it lies intrusive into the Archaean granites. The maximum thickness of this body is 2500 metres.

6. DISCUSSION AND CONCLUSIONS

A recent paper by Cawthorn (1987) stated that the extent of the metamorphism of sediments in the Dullstroom - Lydenburg area is not consistent with the double metamorphism which one would expect from material sandwiched between two thick intrusions like the Wanhoop bodies. He concluded that the non-magnetic extension of the Wanhoop bodies must be quite thin and related it to known extensions of the Bushveld which do not have significant mineralization. However, Button (1976) stated that the sediments from the stratigraphic units of the Pretoria group above the Magaliesberg Quartzite, which contain the Wanhoop bodies, are metamorphosed both through the agency of mafic sills and the main body of the Bushveld Complex, which would obscure the double metamorphism suggested by Cawthorn.

When looking at the distribution of mafic sills in the floor of the eastern Bushveld Complex it might be suggested that the Wanhoop bodies are caused by a group of sills, as concluded by Cawthorn (1987). However, Sharpe (1982) stated that the most abundant sill-forming liquid was of upper-critical zone parentage, which would relate them in time to the normal polarity zone MPZA of the Rustenburg Layered Suite (Hattingh, 1983). This model is incompatible with the model deduced from the quantitative interpretation of the Wanhoop anomalies which revealed the following:

1. On all the east-west profiles the body consists of a major westward dipping sheet-like unit, 200-500 metres deep and approximately 1000 metres thick.
2. A second thinner sheet underlies the former one and extends approximately 7,0 km further east from the former main sheet, but terminates at a much greater depth (> 1000 metres).
3. The direction of magnetization of these bodies is $D = 30^\circ$; $I = +58^\circ$ and the intensity of magnetization is of the order of $4000 \times 10^{-3} \text{ Am}^{-1}$.

4. The depth to the non-magnetic body, which extends beyond the Wanhoop magnetic bodies towards Dullstroom, is approximately 1000 metres and it has a maximum thickness of 500 metres.
5. A density of 3100 kg/m³ for the Wanhoop bodies was used in the two-dimensional gravity modelling process.

From the above-mentioned geophysical data it is evident that the Wanhoop bodies cooled through the Curie point at the same time as the main zone of the Rustenburg Layered Suite, thereby attaining the direction of magnetization of the reversed polarity zone which has a positive inclination. The intensity of magnetization of the Wanhoop bodies is many times greater than that of the main zone rocks in the Draaikraal - Roossenekal area, in fact it can be compositionally related to the black magnetite gabbro of the main zone further south which originates from a more iron-rich magma (Von Gruenewaldt, 1973).

The quantitative interpretation of the Mooiland anomalies revealed the following:

1. The Mooiland magnetic anomaly is caused by an inducedly magnetized, sill-like body, 1400 metres deep, which has a susceptibility of 0,25 SI units and a thickness of approximately 500 metres.
2. The gravitational model consists of a 2500 metres thick sill-like body, dipping to the south, which has a density contrast of 410 kg/m³ with respect to the Archaean granites.

The high susceptibility used in the two-dimensional magnetic modelling process is indicative of a high percentage magnetite present in the body, similar to that of the upper zone of the Rustenburg Layered Suite. Another similarity between the Mooiland bodies and the Rustenburg Layered Suite is the fact that only the upper unit of the gravitational model is magnetic.

From the colour coded aeromagnetic map (in folder) and the Bouguer anomaly map (Fig. 4.6) it is evident that the Mooiland bodies are not linked to the main Bushveld body, but should rather be interpreted as an intrusive complex on its own.

It was previously mentioned, in section 2.3, that the calculated thickness of the Uitkomst Complex, which bears considerable resemblance to the Bushveld Complex (Kenyon et al., 1986) was much larger than the maximum thickness revealed by borehole data, which could possibly indicate that the complex extends westward under the cover of the rocks from the Transvaal Sequence. Another interpretation of this discrepancy is that the Mooiland complex, assuming its relation to the Rustenburg Layered Suite, acted as a feeder to the Uitkomst Complex.

ACKNOWLEDGEMENTS

The author would like to express her gratitude to all the institutions and persons who made this study possible.

1. The Foundation for Research Development of the CSIR for the post-graduate research award.
2. The Institute for Geological Research on the Bushveld Complex for additional financial support.
3. My supervisors Dr P.J. Hattingh* and Dr E.H. Stettler** for their guidance and helpful suggestions.
4. The Chief Director of the Geological Survey of South Africa for permission to use the palaeomagnetic laboratory facilities as well as unpublished data and maps.
5. My colleagues, friends and family for their interest and support.

* University of Pretoria

**Geological Survey of South Africa

REFERENCES

- ANHAEUSSER, C.R., ROBB, L.J. and VILJOEN, M.J., 1983. Notes on the provisional geological map of the Barberton greenstone belt and surrounding granitic terrane, Eastern Transvaal and Swaziland (1:250 000 colour map). Spec. Publ. geol. Soc. S.Afr., v. 9, 221-223.
- BATH, G.C., 1962. Magnetic Anomalies and Magnetizations of the Biwabik Iron-Formation, Mesabi Area, Minnesota: Geophysics, v. 27, 627-650.
- BOOKS, K.G., 1962. Remanent Magnetism as a Contributor to Some Aeromagnetic Anomalies: Geophysics, v. 27, 359-375.
- BRIDEN, J.C., 1972. A stability index of remanent magnetization. J. Geophys. Res., v. 77, 1401-1404.
- _____, 1976. Application of paleomagnetism to Proterozoic tectonics. Phil. Trans. Roy.Soc. Lond.A., v. 280, 405-416.
- BUTTON, A., 1976. Stratigraphy and relations of the Bushveld floor in the Eastern Transvaal. Trans. geol. Soc. S.Afr., 79, 3-12.
- _____, 1986. The Transvaal Sub-Basin of the Transvaal Sequence. (Anhaeusser, C.R. and Maske, S. (Eds) (1986)). In: Mineral Deposits of Southern Africa, Vol II, 811-817.
- CAWTHORN, R.G., 1987. Extensions to the platinum resources of the Bushveld Complex. Suid-Afrikaanse Tydskrif vir Wetenskap, v. 83, No. 2, 69-71.
- COERTZE, F.J., 1969. The geology of the western part of the Bushveld Igneous Complex. In: Symposium on the Bushveld Igneous Complex and other layered intrusions. Geol. Soc. S.Afr. Spec. Publ. 1, 5-22.

- CREER, K.M. and SANVER, M., 1967. The use of the sun compass, 11-16. In: Collinson, D.W., Creer, K.M. and Runcorn, S.K. (ed). *Methods in Palaeomagnetism. Developments in solid Earth Geophysics, 3*, Elsevier Publishing Company, Amsterdam.
- DE BEER, J.H., MEYER, R. and HATTINGH, P.J., 1987. Geoelectrical and palaeomagnetic studies on the Bushveld Complex. In: A.Kröner, ed., *Proterozoic Lithospheric Evolution, Geodynamics Series, v. 17*.
- DE BEER, J.H., STETTLER, E.H., DU PLESSIS, J.G. and BLUME, J., 1988. The deep structure of the Barberton Greenstone Belt: A Geophysical study. *S. Afr. J. Geol.* (in press).
- DUNLOP, D.J., 1979. On the use of Zijderveld vector diagrams in multicomponent Paleomagnetic studies. *Physics of the Earth and Planetary Interiors, v. 20*, 12-24.
- DU PLESSIS, A. and KLEYWEGT, R.J., 1987, A dipping sheet model for the mafic lobes of the Bushveld Complex. *S.Afr. J.Geol.*, v. 90, 1-6.
- DU PLESSIS, A. and LEVITT, J.G., 1987. On the structure of the Rustenburg Layered Suite - Insight from seismic reflection data. In: *Abstracts of the Indaba on the tectonic setting of layered intrusives*, 14-15.
- FISHER, R., 1953. Dispersion on a sphere. *Proc. R. Soc. Lond.A.*, v. 217, 295-305.
- FLINN, D., 1962. On folding during three-dimensional progressive deformation. *Q.J. Geol. Soc. London*, v. 118, 385-433.
- FULLER, M.D., 1963. Magnetic Anisotropy and Paleomagnetism. *J. Geophys. Res.*, v. 68, 293-309.

- FULLER, M.D., 1967. The A.C. bridge method, 403-408. In: Collinson, D.W., Creer, K.M. and Runcorn, S.K. (eds). Methods in Palaeomagnetism. Developments in solid Earth geophysics, 3, Elsevier Publishing Company, Amsterdam.
- GIRDLER, R.W. and PETER, G., 1960. An example of the Importance of Natural Remanent Magnetization in the interpretation of Magnetic Anomalies, Geophys. Prosp., v. 8, 474-483.
- GIRDLER, R.W., 1961. Some Preliminary measurements of Anisotropy of Magnetic Susceptibility of Rocks. Geophys. J.R. Astr. Soc., v. 5, 197-206.
- GOUGH, D.I., 1967. Notes on rock sampling for palaeomagnetic research, 3-7. In: Collinson, D.W., Creer, K.M. and Runcorn, S.K. (eds). Methods in Palaeomagnetism. Developments in solid Earth geophysics, 3, Elsevier Publishing Company, Amsterdam.
- GRAHAM, K.W.T., 1961. The remagnetisation of a surface outcrop by lightning currents. Geophys. J.R. Astr. Soc., v. 6, 85-102.
- GREEN, R., 1960. Remanent Magnetization and the Interpretation of Magnetic Anomalies. Geophys. Prosp., v. 8, 98-110.
- HAMMER, S., 1939. Terrain corrections for gravimeter stations. Geophysics, v. 4, 184-194.
- HARMER, R.E. and SHARPE, M.R., 1985. Field Relations and Strontium Isotope Systematics of the Marginal Rocks of the Eastern Bushveld Complex. Econ. Geol., v. 80, 813-837.

- HATTINGH, P.J., 1980. The structure of the Bushveld Complex in the Groblersdal-Lydenburg-Belfast area of the eastern Transvaal as interpreted from a regional gravity survey. *Trans. geol. Soc. S. Afr.*, v. 83, 125-133.
- _____, 1983. A palaeomagnetic investigation of the Layered Mafic Sequence of the Bushveld Complex. Unpub. D.Sc. thesis, Univ. of Pretoria, 177 pp.
- HAYS, W.W. and SCHARON, L., 1963. An example of the influence of remanent magnetization on magnetic intensity measurements. *Geophysics*, v. 28, 1037-1048.
- HENDERSON, R.G. and CORDELL, L., 1971. Reduction of unevenly spaced potential field data to a horizontal plane by means of finite harmonic series. *Geophysics*, v. 36, 856-866.
- HILLHOUSE, J.W., 1977. A method for the removal of rotational remanent magnetization acquired during alternating field demagnetization. *Geophys. J.R. astr. Soc.* v. 50, 29-34.
- HOOD, P., 1963. Remanent Magnetism - A Neglected Factor in Aeromagnetic Interpretation. *Canadian Mining Journal*, v. 84, 76-79.
- HUNTER, D.R., 1975. The Regional Setting of the Bushveld Complex. An adjunct to the provisional tectonic map of the Bushveld Complex. *Econ. geol. Rs. Unit, Univ. Witwatersrand*, 18pp.
- IRVING, E., 1964. Palaeomagnetism and its application to geological and geophysical problems. John Wiley and Sons, New York, 399pp.
- KANE, M.F., 1962. A comprehensive system of terrain corrections using a digital computer. *Geophysics*, v. 27, 455-462.

- KENYON, A.K., ATTRIDGE, R.L. and COETZEE, G.L., 1986. The Uitkomst Nickel-Copper Deposits Eastern Transvaal. In: Mineral Deposits of Southern Africa, Vol I, Geol. Soc. S. Afr., 1009-1017.
- KLEYWEGT, R.J., 1986. Isostatic anomaly map of the Republics of South Africa, Transkei, Bophuthatswana, Venda and Ciskei and the Kingdoms of Lesotho and Swaziland. Ex. Abstracts Geocongress 1986, geol. Soc. S.Afr., 1013-1016.
- KLIGFIELD, R., LOWRIE, W. and DALZIEL I.W.D., 1977. Magnetic susceptibility anisotropy as a strain indicator in the Sudbury Basin, Ontario. Tectonophysics, v. 40, 287-308.
- LAYER, P.W., 1986. Archean Paleomagnetism of Southern Africa. Unpub. Ph.D. thesis, Stanford University.
- McELHINNY, R.W., 1964. An improved method for demagnetising rocks in alternating magnetic fields. Geophys. J.R. Astr. Soc., v. 10, 369-374.
- _____, 1973. Palaeomagnetism and plate tectonics. Cambridge Univ. Press, 358 pp.
- MEYER, R. and DE BEER, J.H., 1987. The structure of the Bushveld Complex from resistivity measurements. Nature, v. 325, 610-612.
- MOLYNEUX, T.G. and KLINKERT, P.S., 1978. A structural interpretation of part of the eastern mafic lobe of the Bushveld Complex and its surrounds. Trans. geol. Soc. S. Afr., v. 81, 359-368.
- MORELLI, C., GANTER, C., HONKASALO, T., McCONNEL, R.K., SZABO, B., TANNER, J.G., VOTILA, U., and WHALEN, C.T., 1974. The international gravity standardization net, 1971. Spec. Publ. Int. Assoc. Geod. Paris., 4, 194pp.

- MORRIS, W.A., 1982. A palaeomagnetic investigation of the Sudbury Basin offsets, Ontario, Canada. *Tectonophysics*, 85, no. v. 3-4, 291-312.
- NAGATA, T., 1953. *Rock magnetism*. Maruzen Company, Tokyo, 225 pp.
- NOLTIMIER, H.C., 1967. Use of the spinner magnetometer for anisotropy measurements, 400-402. In: Collinson, D-W., Creer, L.M. and Runcorn, S.K., (eds). *Methods in Palaeomagnetism. Developments in solid Earth geophysics*, 3, Elsevier Publishing Company, Amsterdam.
- PALMER, J.E., 1979. Myntcorr- A Fortran IV program for the calculation of terrain corrections to gravity data. *Geol. Surv. S.A. Int. Rep.*, 1979-0018, 15pp.
- ROBERTSON, I.D.M. and VAN BREEMEN, O., 1969. The southern satellite dykes of the Great Dyke, Rhodesia. In: *Symposium on the Bushveld Igneous Complex and other layered intrusions*. *Geol. Soc. S. Afr. Spec. Publ.* 1, 621-644.
- RUNCORN, S.K., 1967. Statistical discussion of magnetization of rock samples 329-339. In: Collinson, D.W. Creer, K.M. and Runcorn, S.K. (eds). *Methods in Palaeomagnetism. Developments in solid Earth geophysics*, 3, Elsevier Publishing Company, Amsterdam.
- SHARPE, M.R., 1982. Distribution of mafic sills in the floor of the Bushveld Complex. *Res. Rep. Inst. Geol. Res. Bushveld Complex, Univ. Pretoria*, 35, 25pp.
- _____, 1984. Petrography, classification and chronology of mafic sill intrusions beneath the eastern Bushveld Complex. *Bull. Geol. Surv. S. Afr.*, 77, 40p.
- _____, 1986. Eastern Bushveld Sills - A progress Report. *An. Rep. Inst. Geol. Res. Bushveld Complex, Univ. Pretoria*, 116pp.

- SHARPE, M.R., 1986. REE and Isotopic Evidence for Multiple Parental Magmas to the Bushveld Complex. An. Rep. Inst. Geol. Res. Bushveld Complex, Univ. Pretoria, 116p.
- SMIT, P.J. and MAREE, B.D., 1966. Densities of South African rocks for the interpretation of gravity anomalies. Geol. Surv. S. Afr. Bull., 48, 37pp.
- SOUTH AFRICAN COMMITTEE FOR STRATIGRAPHY (SACS), 1980. Stratigraphy of South Africa. Part 1 (Comp. L.E. Kent). Lithostratigraphy of the Republic of South Africa, South West Africa/Namibia, and the Republics of Bophuthatswana, Transkei and Venda : Handb. geol. Surv.S.Afr. 8, 690pp.
- SPECTOR, A. and GRANT, F.S., 1970. Statistical models for interpreting aeromagnetic data. Geophysics, v. 35, 293-302.
- TALWANI, M., and HEIRTZLER, J.R., 1964. Computation of magnetic anomaly caused by two-dimensional structures of arbitrary shapes. Stanford Univ. Publs. geol. Sci., v. 9, No. 1, 464-480.
- _____, WORZEL, J.L., and LANDISMAN, M., 1959. Rapid gravity computations for two-dimensional bodies with application to the Mendocino submarine fracture zone. J. Geophys. Res., v. 64, 49-50.
- VON GRUENEWALDT, G., 1973. The main and upper zones of the Bushveld Complex in the Roossenekal area, eastern Transvaal. Trans. geol. Soc. S.Afr., v. 76, 207-227.
- _____, COERTZE, F.J., HUNTER, D.R., VERMAAK, C.F. and WALMER, F., 1980. Lithostratigraphy of the Bushveld Complex. In: Kent, L.E. (Compiler). The Lithostratigraphy of South Africa. Spec. Pub. geol. Surv. South Afr. Handbook 8, 690pp.

VON GRUENEWALDT, G., SHARPE, M.R., and HATTON, C.J., 1985. The Bushveld Complex: Introduction and Review. *Econ. Geol.*, v. 80, 803-812.

WALRAVEN, F., 1987. Geochronological and isotopic studies of Bushveld Complex rocks from the Fairfield borehole at Moloto, Northeast of Pretoria. In: Abstracts of the Indaba on the tectonic setting of layered intrusives, 8-13.

WATSON, G.S.A., 1956. A test for randomness of directions. *Mon. Not. R. Astr. Soc. Geophys. Suppl.*, v. 7, 153-159.

ZIJDERVELD, J.D.A., 1967. A.C. Demagnetization of rocks : Analysis of results, 254-286. In: Collinson, D.W., Creer, K.M. and Runcorn S.K. (eds). *Methods in Palaeomagnetism, Developments in solid Earth geophysics*, 3, Elsevier Publishing Company, Amsterdam.